Study on the Effect of Hydrometeors on the Track and Intensity of Tropical Cyclone using WRF-ARW Model

M. Phil. Thesis

By

Md: Jakir Hossain

Roll No: 1055551

Session: July 2010

A thesis submitted in partial fulfillment of the requirements for the degree of Master of Philosophy in the Department of Physics, Khulna University of Engineering & Technology, Khulna-9203.
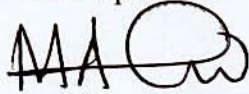
Khulna University of Engineering & Technology (KUET)

Khulna 9203, Bangladesh

December 2015

DECLARATION

This is to certify that the thesis work entitled "Study on the effect of hydrometeors on the track and intensity of tropical cyclone using WRF-ARW model" has been carried out by Md. Jakir Hossain in the department of Physics, Khulna University of Engineering & Technology, Khulna, Bangladesh. The above thesis work or any part of this work has not been submitted anywhere for the award of any degree or diploma.

Signature of Supervisor

....
(Prof. Dr. Md. Mahbub Alam)

Signature of Candidate

....
(Md. Jakir Hossain)

KHULNA UNIVERSITY OF ENGINEERING & TECHNOLOGY
DEPARTMENT OF PHYSICS

Approval

This is to certify that the thesis work submitted by *Md. Jakir Hossain* entitled *"Study on the Effect of Hydrometeors on the Track and Intensity of Tropical Cyclone using WRF-ARW Model"* has been accepted by the board of examiners for the partial fulfillment of the requirements for the degree of Master of Philosophy in the Department of Physics, Khulna University of Engineering & Technology, Khulna, Bangladesh on 11 December 2015.
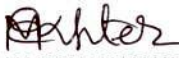
Board of Examiners

Sl. No.	Name, Designation & Address	
1.	Prof. Dr. Md. Mahbub Alam Department of Physics Khulna University of Engineering & Technology	Chairman & Supervisor
2.	Prof. Dr. Md. Abdullah Elias Akhter Department of Physics Khulna University of Engineering & Technology	Co-Supervisor
3.	Head Department of Physics Khulna University of Engineering & Technology Khulna 9203	Member
4.	Prof. Dr. Shibendra Shekher Sikder Department of Physics Khulna University of Engineering & Technology Khulna 9203	Member
5.	Dr. Samarendra Karmakar Director (Rtd), BMD 63 Jafrabad, 2nd floor, Dhaka-1206	Member (External)

To

My Parents, Wife and Md. Humayun Kabir

Acknowledgements

CONTENTS

Chapter III

Model Description and Methodology

Chapter IV

Results and Discussions

Chapter V

Summary & Conclusions **113**

Nomenclature:

BoB	Bay of Bengal
TC	Tropical cyclones
MSLP	Mean Sea level Pressure
NCAR	National Center for Atmospheric Research
NCEP	National Centers for Environmental Prediction
FSL	Forecast Systems Laboratory
AFWA	Air Force Weather Agency
WRF	Weather Research and Forecasting
YSU	Yonsei University scheme
NIO	North Indian Ocean
IC	Initial Condition
VSCS	Very Severe Cyclonic Storms
MP	Microphysics
CP	Cumulus Parameterization
KF	Kain-Fritch
MY	Mellor Yamada
PBL	Planetary Boundary Layer
MM5	Fifth generation non-hydrostatic Mesoscale Model
NCAR	National Center for Atmospheric Research
NWP	Numerical Weather Prediction
IWV	Integrated Water Vapor
WVMR	Water Vapor Mixing Ratio
CGMR	Cloud Graupel Mixing Ratio

CSMR	Cloud Snow Mixing Ratio
CIMR	Cloud Ice Mixing Ratio
RWMR	Rain Water Mixing Ratio
CWMR	Cloud Water Mixing Ratio
RH	Relative Humidity
FAA	Federal Aviation Administration
RRTM	Rapid Radiative Transfer Model
IMD	Indian Meteorological Department
JTWC	Joint Typhoon Warning Center
CSLP	Central Sea Level Pressure
UTC	Universal Time Co-ordinate
ARW	Advanced Research WRF
NMM	Non hydrostatic Mesoscale Model
WSM6	WRF Single-moment 6-class
LES	large eddy simulation
BMJ	Betts-Miller-Janjic
YSU	Yonsei University
FNL	Final Reanalysis
LBC	Lateral Boundary Conditions
GrADS	Grid Analysis and Display System
CS	Cyclonic Storm
DD	Deep Depression
SCS	Severe Cyclonic Storm
MWS	Maximum Wind Speed

ABSTRACT

In this research microphysical and cumulus parameterization schemes on Weather Research and Forecasting (WRF-ARW core) model have been used to study the effects of hydrometeors on the prediction of track and intensity of tropical cyclones Mala (2006), Sidr (2007) and Phailin (2013) which formed over the Bay of Bengal and hit Myanmar, Bangladesh and eastern coast of India respectively. The hydrometeors are cloud water, rain water, graupel, snow, ice and water vapor mixing ratio. The initial and boundary conditions are drawn from the global operational analysis and forecast products of National Center for Environmental Prediction (NCEP-GFS) available for the public at $1°×1°$ resolution. The model was run by using Kessler, Lin *et al.*, WSM 3-class simple ice, Ferrier (New Eta), WSM 6-class graupel and Thomson graupel microphysics (MP) coupling with different cumulus parameterization (CP) schemes. The CP schemes used to simulate the Tropical Cyclone are Kain-Fritsch (KF) and Betts-Miller-Janjic (BMJ). The model domain consists of 8-24°N and 77-96°E and has 12 km horizontal resolution with 28 vertical sigma levels. The model was run for 96 and 72-h using initial data at 0000 UTC of 26 and 27 April 2006 for TC Mala, at 0000 UTC of 8 and 9 October 2013 for TC Phailin and at 0000 UTC of 11 and 12 November 2007 for TC Sidr. In order to examine the effect of hydrometeors on the movement of tropical cyclones space-averaged vertical profiles of water vapor, cloud water, rain water, graupel, snow, ice mixing ratio (g kg^{-1}), vorticity and relative humidity have been calculated once every three hours. For the analysis of effects of cloud hydrometeors the model domain has been divided into 5 different regions. The different regions are D1 (22°N-26°N and 87°E-93°E), D2 (18°N-22°N and 81°E-87°E), D3 (14°N-18°N and 78-84°E), D4 (12°N-22°N and 84°E-94°E) and D5 (17°N-22°N and 94°E-97°E). The tracks and intensity are compared with those provided by the operational centers like JTWC and IMD.

The simulated result suggests that the hydrometeors and vorticity have impact on the track of tropical cyclones. The amount of hydrometeors are started to increase 2 to 3 days before in a direction where the tropical cyclone moves. In all combination of MP and CP the area and time average of water vapor mixing ratio (g/kg) provides similar results. Water vapor mixing ratio has not change significantly during the period of movement of tropical cyclones.

Chapter I

Introduction

Tropical cyclones that form over the Bay of Bengal (BoB) during pre-monsoon (March-May) and post-monsoon (October-November) seasons cause considerable damage and destruction to lives and property over the coast of India, Sri Lanka, Bangladesh and Myanmar surrounding the Bay of Bengal (BoB). The combination of a shallow coastal plain along with a thermodynamically favorable environment allows TCs to impart high surface winds, torrential rains and significant wave heights causing storm surges as these systems move inland. The destruction is due to strong gale winds, torrential rain and associated storm surge. It is now well known that the tropical cyclones form over warm tropical oceanic regions and intensify under favorable environmental conditions such as high sea surface temperatures ($\geq 26.5°C$), weak vertical wind shear, certain minimum Coriolis force and pre-existing low-pressure conditions (Anthes 1982; Gray 2000). Timely and reasonably accurate prediction of the tracks and intensities of such cyclones can minimize the loss of human lives and damage to properties. Though the general movement of the tropical cyclones is well known, it is desirable to have as much as accurate landfall prediction as possible for effective implementation of disaster mitigation. There have been considerable improvements in the development of numerical models with increasing computer resources during recent decades. However, application of numerical models for tropical cyclone prediction necessitates a study of suitable physics. Tropical cyclones originate over the ocean, where conventional meteorological observations tend to be sparse on a daily routine basis. Due to lack of data, deficiencies in model initial conditions lead to inaccurate forecasts of tropical cyclones (Lorenz, 1963; Mullen, 1989; Pielke, 2006). Knowledge of the physical processes that control tropical cyclone evolution is also limited.

The sensitivity of different microphysical schemes and processes on cumulus parameterization were investigated by many authors. Thus, the forecasting of tropical cyclone track and intensity remains a challenging problem to the modeling community. As suggested by White *et al.* (1999) and Cacciamani *et al.* (2000) insufficient model resolution, inadequate physical

1

parameterization, lack of sufficient detail or accuracy in the initial and boundary conditions (IBCs) or any combination of three may be the possible reasons for the poor forecast. It is therefore, the prediction of movement and intensity of tropical cyclone is very much essential. The performance of a numerical weather prediction (NWP) model greatly depends on the initial and boundary conditions and physical parameterizations employed in the model. Further, the NWP model performance is very sensitive to grid sizes and the geographical region of interest. The best set of schemes for one region may not be suitable for some other regions. The horizontal and vertical resolutions are also very important factors, since different parameterization schemes can give different results for different model resolutions. Sensitivity experiments are the only logical way to identifying the best set of physics schemes for a particular region. Srinivas *et al.* (2007) conducted a sensitivity study of the Andhra severe cyclone (2003) by using the National Center for Atmospheric Research (NCAR) fifth generation non-hydrostatic mesoscale model (MM5). They reported that the Planetary Boundary Layer (PBL) schemes and convective parameterization schemes play an important role in predicting both the intensity and movement of the model simulated storms. They also conducted that the combination of Mellor Yamada scheme for PBL parameterization and Kain-Fritch (KF) scheme as the CP give the best results in terms of intensity and track. A sensitivity study of the Orissa super cyclone by Rao and Prasad (2007) also indicates that a combination of the MY scheme from the PBL and KF from CP gives better results in terms of cyclone track and intensity prediction.

A number of cumulus parameterization schemes (CP) have been developed and their role with PBL and microphysics parameterization (MP) in the simulation of tropical cyclone (TC) using different mesoscale models are also studied by many researchers. Hill and Lackmann (2009) studied the sensitivity to PBL parameterization (MYJ and YSU) and horizontal grid spacing (36, 12, 4 km) for a wide variety of idealized vortices, ranging from an unbalanced warm bubble to fully balanced vortices with KF as CP & Lin schemes as MP for all the experiments. They found that YSU scheme with horizontal grid spacing of 4 km incorporates values of exchange coefficient for moisture more consistently with the observations and leads to simulated TC intensity comparable to empirical estimates of maximum intensity. Bhaskar Rao *et al.* (2006, 2007) and Srinivas *et al.* (2007) examined the role of CP, PBL and MP on track

2

& intensity of tropical cyclone using MM5. These studies indicate that convective processes control the movement of the model storm while PBL processes are crucial in determining the intensity of cyclone. Some of the studies (Li and Pu, 2008; Mukhopadhyay et al., 2011; Tao et al., 2011; Efstathiou et al., 2012) suggested the combination WSM6-YSU as MP and PBL schemes works better for different weather systems. Srinivas and Bhaskar Rao (2014) studied the sensitivity for Orissa Super cyclone and found that KF, MYJ (Efstathiou et al., 2013) and Lin cloud microphysics has performed better for the track and intensity simulation. Raju et al. (2011) reported slightly higher better track errors of TC Nargis as 136, 252 and 381 km at 24, 48 and 72 hrs respectively with MYJ PBL scheme. Very recent study by Hariprasad et al. (2014) examined the sensitivity of different PBL schemes at Kalpakkam and demonstrated that YSU scheme simulated various PBL quantities are in better agreement with the observations. Thus, there are different opinions of PBL schemes as well as MP schemes for different intense events. Therefore, MYJ and YSU as PBL schemes and Ferrier and WSM6 as MP schemes are not yet tested for relatively weak intensity cyclones over NIO.

Several simulation studies have been conducted to understand the TCs over the NIO using high resolution mesoscale models (Trivedi et al., 2006; Li and Pu, 2008; Pattanayak and Mohanty, 2008; Bhaskar Rao et al., 2009; Deshpande et al., 2010, 2012; Srinivas et al., 2010; Mukhopadhyay et al., 2011; Raju et al., 2011; Tao et al., 2011; Efstathiou et al., 2012; Osuri et al., (2012). These studies are based on evaluating the model performance with respect to physics sensitivity, resolution, initial conditions and impact of data assimilation on the track and intensity forecast of very severe cyclones. Few studies have focused on simulating the less intensity storms (Osuri et al., 2013; Srinivas et al., 2013), but the detailed evolutions behind the success or failure of physical parameterization is hardly addressed. Kanase and Salvekar (2014), Yesubabu et al. (2014) have worked on the numerical study of cyclone Laila by studying its vertical structure as well as role of nudging factor respectively.

In mesoscale models, large scale global analyses provide the initial condition to the mesoscale models. So the initial conditions may not be able to capture the intensity and location of the initial vortex to give correct forecast of TCs. Importance of accurate initial conditions is studied by Arpe et al. (1985), Sanders (1987), Kuo and Reed (1988), Mohanty et al. (2010). NWP being an initial value problem, Lorenz (1963) and Pielke (2006) have shown that even a

3

small error in the initial condition (IC) may lead to a large error in the subsequent forecast. Effect of initial condition from different data sources on the numerical simulation of Orissa Super Cyclone is studied by Trivedi *et al.* (2002) by generating the synthetic vortex data using empirical relation. Pattanaik and Rama Rao (2009) studied the case of very severe cyclonic storm with core of hurricane wind 'Nargis' with four different initial conditions (28, 291, 30 April and 1st May) after the formation of depression with the combination of YSU as PBL, Grell-Devenyi as CP and WSM 3 simple ice as MP using WRF model. They concluded that 30 April and 01 May initial conditions give less landfall errors of 85 km and 50 km. For a numerical modeler, it is required to know the intensity of the initial vortex that can give better prediction of TCs. To our knowledge, there is hardly any work available in the literature to examine the role of initial condition starting from different initial states of the system. Basically, these initial conditions are very useful for timely warning as well as effective implementation of disaster mitigation. Thus the main objective of the present study is to evaluate the influence of the choice of physical parameterization and also to study the impact of initial conditions on simulating track and intensity of the cyclone.

Alam *et al.* (2013) has shown the impact of cloud microphysics and cumulus parameterization on meso-scale simulation of TC by using WRF Model. Pattnaik and Krishnamurti have suggested that the production and distribution of graupel hydrometeors within the eye-wall significantly influences the intensity of the hurricane. However, their study has shown that the microphysical parameters of hydrometeors significantly modulate the intensity forecast of the hurricane. Tao *et al.* (2011) showed that the dominant microphysical processes were quite different between the convective and stratiform regions and between the mature and decaying stages. Willoghby *et al.*, and Lord *et al.* (1984) studied the impact of cloud microphysics on tropical cyclone structure and intensity using 2D axi-symmetric non-hydrostatic model. Their results show that the ice-phase microphysical scheme can produce a lower MSLP than the case without the ice-phase. Wang (2001) demonstrated that the intensification rate and intensity are not sensitive to the cloud microphysical parameterizations. However, he noted that cloud structures and aerial coverage of and the peak precipitation in the tropical cyclone were quite sensitive to details of the cloud microphysical parameterization in their TCM3 model.

Davis and Bosart (2002) considered the effects of cumulus parameterization on tropical storm track. They found that the BMJ and Grill schemes produced more westward deviated track than KF scheme. The KF scheme tended to intensify the storm too rapidly but produced the best track compared with observations. Fovell and Su (2007) simulate Hurricane Rita (2005) and compared the effects of Kessler, Lin *et al.* and WSM3 microphysics schemes, coupled with the effects of KF, GD, and BMJ schemes. The hurricane Rita's track was simulated best when the WSM3 scheme was paired with BMJ convection. The worst simulated track was when Kessler was paired with KF convection, which produced a weaker storm that tracked well west of the actual storm. Rosenfeld *et al.* (2007) noted in their simulations that the suppression of warm rain through the addition of large amounts of aerosols will cause the tropical cyclone to divert eastward. Zhu and Zhang (2006) informed that the hurricane track was not sensitive to cloud microphysical processes except for very weak storms. Alam *et al.* (2013) suggested that Lin *et al.* and WSM6 schemes in combination with KF scheme have simulated the analogous wind speed and pressure fall with the observed wind speed and pressure fall. Also Lin-KF and Lin-BMJ combinations provide the most precise intensity and track respectively of TC Sidr. Akhter *et al.* (2010) proposed that the microphysical parameterization would be desirable to make sensitivity experiments with all possible combinations of the schemes of the physical processes.

In this research many experiments have been conducted by using six different (Kessler, Lin *et al.*, WSM3, Ferrier, WSM6 and Thompson) MP schemes in combination with two different (KF and BMJ) CP schemes considering different initial conditions for the tropical cyclone of Mala (2006), Phailin (2013) and Sidr (2007) that formed in the BoB and crossed Myanmar, eastern coast of India, and Bangladesh. The aim of this research is to investigate the effects of hydrometeors e.g. cloud water, rain water, ice, snow, graupel and water vapor mixing ratio, relative humidity and vorticity for the movements and intensification of TCs in the BoB. The destruction of properties and loss of lives can be minimized by knowing the accurate intensity, time of landfall and track of tropical cyclones.

After introduction (Chapter I) brief description of tropical cyclone has given in Chapter II, followed by the experimental design in Chapter III. The details results are discussed in Chapter IV and the conclusions of this research in Chapter V.

Chapter II

Literature Review

2.1   Tropical Cyclone

In meteorology, a cyclone is an area of closed, circular fluid motion rotating in the same direction as the Earth. This is usually characterized by inward spiralling winds that rotate anti-clockwise direction in the Northern Hemisphere and clockwise direction in the Southern Hemisphere of the Earth. Most large-scale cyclonic circulations are cantered on areas of low atmospheric pressure. The largest low-pressure systems are cold-core polar cyclones and extratropical cyclones which lie on the synoptic scale. According to the NHC glossary, warm-core cyclones such as tropical cyclones and subtropical cyclones also lie within the synoptic scale. Meso cyclones, tornadoes and dust devils lie within the smaller mesoscale. Upper level cyclones can exist without the presence of a surface low, and can pinch off from the base of the Tropical Upper Tropospheric Trough during the summer months in the Northern Hemisphere. Cyclones have also been seen on extra terrestrial planets, such as Mars and Neptune. Cyclogenesis describes the process of cyclone formation and intensification. Extratropical cyclones form as waves in large regions of enhanced mid-latitude temperature contrasts called baroclinic zones. These zones contract to form weather fronts as the cyclonic circulation closes and intensifies. Later in their life cycle, cyclones occlude as cold core systems. A cyclone's track is guided over the course of its 2 to 6-day life cycle by the steering flow of the cancer or subtropical jet stream.

2.2   Classification of Tropical Cyclones

Cyclonic disturbances in the North Indian Ocean are classified according to their intensity. The following nomenclature is in use by IMD (2003):

Type of System		Wind Speed (km/hr)	Pressure fall (hPa)
Low	:	< 31	------
Well marked low	:	31-40	------
Depression	:	41 - 51	2-3

6

Deep Depression	:	52 - 61	4-5
Cyclonic Storm	:	62 - 88	6-14
Severe Cyclonic Storm	:	89 - 117	15-28
SCS with a core of hurricane intensity	:	118 - 221	29-75
Super cyclone	:	≥ 222	>76

2.3 Life Cycle of Tropical Cyclones

The life span of tropical cyclones with full cyclonic intensity averages at about 6 days from the time they form until the time they enter land or recurve into the Temperate Zone. Some storms last only a few hours; a few as long as two weeks. The evolution of the average storm from birth to death has been divided into four stages.

- **Formative Stage:** Tropical storms form only in near pre-existing weather systems. Deepening can be a slow process, requiring days for the organization of a large area with diffuse winds. It can also produce a well-formed eye within 12 hours. Wind speed usually remains below hurricane force in the formative stage. Unusual fall of pressure over 24 hours by 2 - 3 hPa or more takes place in the center of the vorticity concentration.

- **Immature Stage:** A large number of formative cyclones die within 24 hours. Others travel long distances as shallow depressions. Wind of cyclonic force forms a tight band around the center. The cloud and rain pattern changes from disorganized squalls to narrow organized bands, spiraling inward. Only a small area is as yet involved, though there may be a large outer envelope. The eye is usually visible but ragged and irregular in shape.

- **Mature Stage:** The force of cyclonic winds may blow within a 30 - 50 km radius during immature stage. This radius can increase to over 300 km in mature storms. On the average, the mature stage occupies the longest part of the cycle and most often lasts several days. The eye is prominent and circular and the cloud pattern is almost circular and smooth. The surface pressure at the center is no longer falling and the maximum wind speeds no longer increasing. At this stage, heating from convective clouds furnishes the largest amount of energy for cyclone maintenance. Pressure gradient is largest at the surface. Wind speed range is between 128 - 322 km/hr.

- **Terminal Stage:** Nearly, all cyclones weaken substantially upon entering land, because they lose the energy source furnished by the underlying ocean surface. The decay is especially rapid where the land is mountainous. Movement of a cyclone over land cuts off the surface energy source and increases the surface friction, especially when the land is mountainous. Some cyclones die out over sea and this event can be related to their moving over a cold ocean current or being invaded by a surface cold air mass behind a cold front or by a cold center at high levels moving over their top.

2.3.1   Surface Pressure

Mature storms have very low central pressures dropping below 900 hPa at times although 920 to 930 hPa are more typical and some quite intense hurricanes may have central pressures around 950 hPa. Note the diurnal variation prior to the main pressure fall which takes place over a period less than 12 hours. Pressure falls prior to this were not particularly significant, thus demonstrating the limited value of pressure tendency as a long term forecasting aid. Once pressure falls are noticed it is likely that the ship or station is already well within the tropical cyclone circulation.

2.4   Hydrometeors

Any product of condensation or sublimation of atmospheric vapor, whether formed in free atmosphere or at the earth's surface; also any water particles blown by the wind from the earth's surface is called hydrometeor. Hydrometeors consist of liquid or solid water particles that are either falling through or suspended in the atmosphere, blown from the surface by wind, or deposited on objects. Hydrometeors comprise all forms of precipitation, such as rain, drizzle, snow, and hail, and such elements as clouds, fog, blowing snow, dew, frost, tornadoes and waterspouts. A general term for atmospheric water in any of its forms, i.e. clouds, fog, hail, ice crystals, rain are known as hydrometeors. Any form of atmospheric water vapor, including those blown by the wind off the earth's surface also known as hydrometeors. Liquid or solid water formation that is suspended in the air includes clouds, fog, ice fog, and mist. Drizzle and rain are examples of liquid precipitation, while freezing drizzle and freezing rain are examples of freezing precipitation. Solid or frozen precipitation includes ice pellets, hail, snow, snow pellets, snow grains, and ice crystals. Water vapor that evaporates before reaching

8

the ground is virga. Examples of liquid or solid water particles that are lifted off the earth's surface by the wind include drifting and blowing snow and blowing spray. Dew, frost, rime and glaze are examples of liquid or solid water deposits on exposed objects. A precipitation product, such as rain, snow, fog, or clouds, formed from the condensation of water vapor in the atmosphere is called hydrometeor. The typical configuration of a cloud microphysics parameterization includes three classes of hydrometeors: the source class (e.g., water vapor and cloud condensation nuclei), the cloud class (e.g., cloud water and cloud ice), and the precipitation class (e.g., rain, snow, graupel). The total budget of phase changes among hydrometeors in these three classes determines the heating rate, which feeds back to dynamical processes.
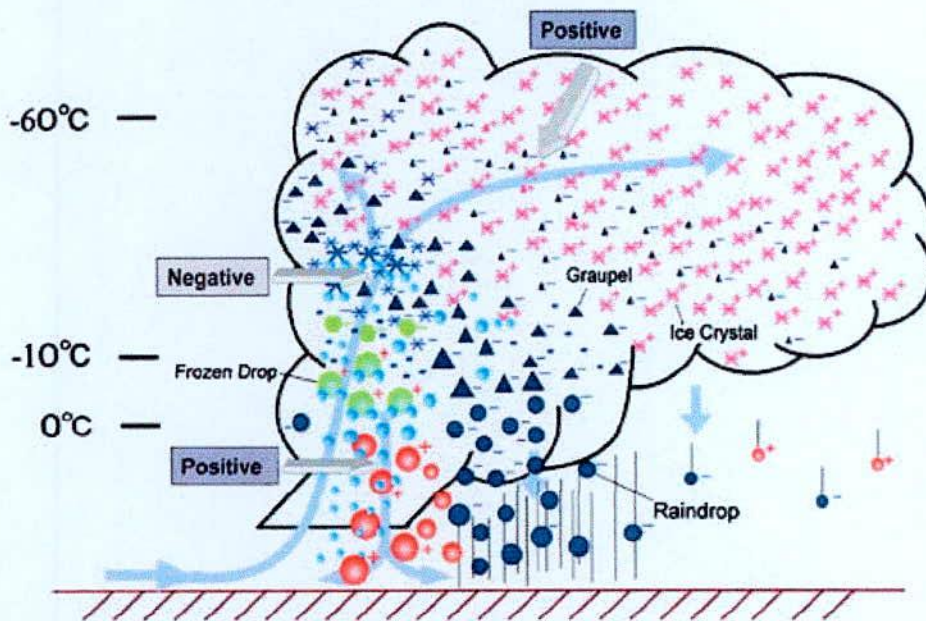
Figure 2.1: Conceptual model of hydrometeor growth and space charge. Red circles are for raindrops originating on frozen drops. Blue circles are for raindrops, originating on graupel. Green circles are frozen drops, blue triangles are graupel, and red crosses are ice crystals. A two-step growth process is suggested by warm rain-frozen in front and graupel growth in the upper level.

The generation of source-class materials is related to the hydrological and vegetational evaporative conditions of the atmosphere. These source-class materials are then redistributed

9

by the large--scale dynamical processes (e.g., atmospheric transport and convergence/ divergence associated with a weather system). In state-of-the-art microphysics modeling's, the distributions of atmospheric aerosols and cloud condensation nuclei are not simulated (at least in a numerical weather forecast model) but are assumed to be abundant in the atmosphere and to have a uniform distribution. Water vapor is explicitly modeled and serves as the sole and deterministic source materials for the ensuing microphysical processes to occur. Whenever water vapor exceeds its saturation values (with respect to water or ice), condensation or deposition occurs.
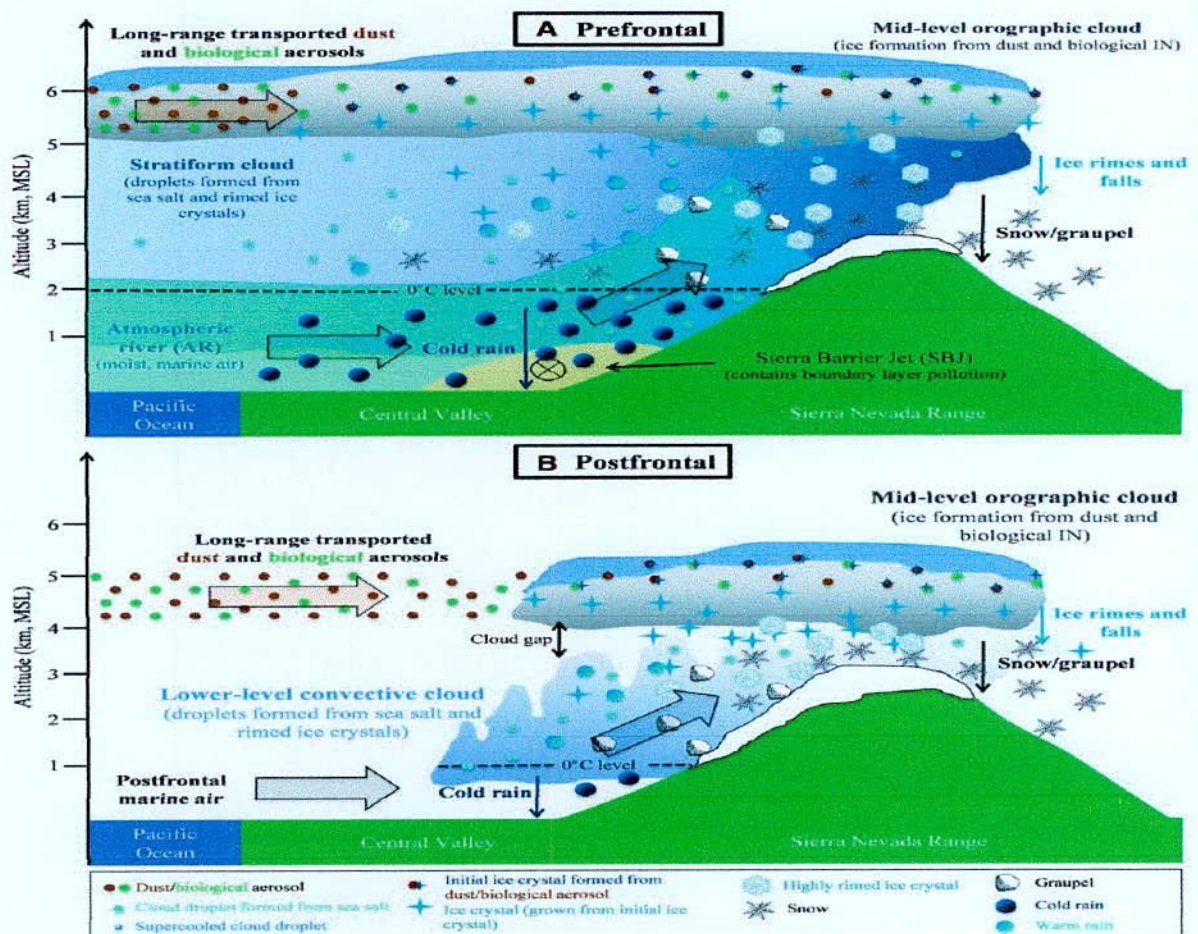
Figure 2.2: Formation of Different Hydrometeors

Cloud water and cloud ice are the basic substances that form the cloud class, i.e., definable clouds (both in visual and physical definitions). They are the intermediate class linking the source and precipitation classes. Under a sub-saturation condition, these cloud-class materials

10

can convert back to water vapor by evaporation or sublimation. Otherwise, they either remain in their forms as water droplets or small ice particles (for non precipitating clouds) or continuously grow and transform into the precipitation class through various growth mechanisms (for precipitating clouds) in a saturated or slightly supersaturated environment.

The precipitation fields (e.g., rain, snow, and graupel) form the final class in microphysical parameterization schemes. Either they fall out from clouds to complete the hydrological cycle, or parts of them evaporate or sublimate to convert back to the source class during their fallout. Obviously, incorrectly parameterizing and computing the production rates of this class directly affect the accuracy of precipitation forecasts. The total budget of phase changes among hydrometeors in these three classes determines the heating rate which feeds back to dynamical processes.

For the Kessler (1969) type of warm rain process, only three families of cloud materials are considered: water vapor, cloud water, and rain. Each of these species represents one of the functional classes discussed above. For mixed-phase clouds, a more comprehensive microphysics scheme typically includes five or six species of hydrometeors. There are both ice-phase and water-phase hydrometeors constituting the cloud and precipitation classes. McCumber et al. (1991) compared the performances of two- and three-class ice-phase microphysical parameterization schemes in numerical simulations. They found that the use of three ice classes produced better results in tropical squall line simulations than did two ice classes or ice-free conditions. Because the goal of this study is to analyze the currently existing microphysical parameterization schemes (e.g., a scheme used in Penn State/NCAR MM5 model) rather than to develop a new scheme, for simplicity of presentation, a cloud scheme with water vapor and four species of hydrometeors (including two classes of water-phase and two classes of ice-phase species) is analyzed. As shown in Fig. 1, these five families of cloud materials are: water vapor (the source class), cloud water and cloud ice (the cloud class), rain and snow (the precipitation class). In this scheme, snow can be treated as a category including all the precipitating ice. In a more complete microphysics scheme (three-class ice-phase microphysical parameterization), graupel/hail is separated from the general precipitating ice family. Again, this separation is neglected in the schemes under consideration.

11

In Fig. 2.1, the lines connecting two hydrometeor families represent the possible microphysical processes (conversions) between the two species. For example, water vapor can interact with all the other four species. When air is supersaturated with respect to water or ice, water vapor can condense into water-phase hydrometeors or deposit onto the ice-phase hydrometeors. When air is sub-saturated with respect to water or ice, the other four species can convert back to water vapor by evaporation or sublimation. If a conversion between two species is considered to be reversible, then eight different conversion processes would occur for water vapor. They are:

i.   water vapor $\rightleftharpoons$ cloud water,

ii.   vapor $\rightleftharpoons$ cloud ice,

iii.   vapor $\rightleftharpoons$ rain, and

iv.   vapor $\rightleftharpoons$ snow.

(Each pair of processes is not concurrent, meaning that the condition favored for one process to occur precludes the reversible process.) In nature, all these processes may exist. However, in most cloud microphysics schemes, the transformation from the source class directly to some precipitation class (excluding water vapor deposition on ice particles) is not modeled (but not vice versa); e.g., the growth of rain by consuming water vapor is essentially neglected. On the other hand, between two families of hydrometeors there may be more than one interaction mechanism transforming one species to the other. For example, cloud ice can be formed directly from water vapor by two different processes: water vapor deposition onto ice nuclei and homogeneous cloud ice initiation (e.g., at very cold temperatures).

2.4.1   Cloud Water Mixing Ratio

Water is the only naturally occurring substance that occurs in solid, liquid, and gaseous forms at the range of temperatures and pressures found in the Earth's atmosphere. This curious fact, plus the abundance of water and its importance for life, makes water one of the most important components of the atmosphere. It plays a crucial role in the weather, the transfer of energy on a wide range of scales from microclimates to the planetary, and of course is vital for the supply of moisture to plants and other living things. Atmospheric water is made visible in the form of clouds and precipitation (water droplets and ice crystals), but is also present in form of

12

gas or vapor. Clouds are among the most fascinating phenomena in atmosphere: clouds make visible the movement of the air, and can reveal much about the state of the atmosphere. To understand them, and larger-scale weather systems, we need to examine the behavior of water in the atmosphere. Clouds affect the radiation balance of the earth-atmosphere system by both reflecting a fraction of incoming solar radiation back to space (cooling the near surface) and blocking a fraction of the earth emitting long wave radiation from escaping to space (greenhouse warming). The net effect is either cooling or warming. Cloud macro-physical properties such as the amount of cloud cover, cloud top height, etc. and cloud microphysical properties such as cloud droplet size, liquid-ice phase, etc., play a key role in cloud-radiation interaction. For example, relatively shallow stratus clouds tend to cool the earth-atmosphere system (cooling dominates warming), whereas upper tropospheric thin cirrus clouds tend to warm the system (warming dominates cooling). Greenhouse warming is strongly related to high cloud amount, and cooling is more related to high cloud amount and cloud optical depth. The clouds can be composed of water droplets, ice crystals, or a mixture of the two. Water and ice clouds have distinctive appearances, so we can tell the difference from the ground. Ice clouds (such as cirrus) are fibrous in appearance, whereas water clouds (such as cumulus or ground fog) may vary in appearance from 'puffy' to 'misty'. Clouds are suspensions of water droplets or ice crystals. We have seen that clouds will form when the air is too cool to support the amount of water present in vapor form. In nature, clouds form in 3 basic situations: Cloud will form if a mass of air is chilled so that it can no longer support the water present as vapor. The most familiar cloud of this type is fog forming near the ground on a cold night. Because the mechanism of cooling is the loss of energy by long wave emission, this type of fog is termed radiative fog. Similarly, cloud will form if an air mass is uplifted to higher altitudes where the pressure drop causes cooling. Uplift may be due to winds blowing over high ground (orographic cloud), or by vertical motions in the free atmosphere (convection). Cloud may also form by the mixing of two unsaturated air masses in some circumstances. This may occur because of the non-linear form of the saturation vapor pressure/temperature curve.

2.4.2 Rain Water Mixing Ratio

Water droplets or ice crystals form precipitation when they fall through the atmosphere to reach the ground. This occurs when the fall velocity of the particle is greater than up draught

velocities. The likelihood that particles will form precipitation is thus a function of droplet size: small droplets will tend to be kept aloft, whereas large particles are more likely to fall to ground. Two main mechanisms have been identified to explain the growth of water droplets to form precipitation: (1) Activated nuclei or the growth of droplets by condensation from surrounding vapor; (2) Collision, or the growth of droplets by the combination of two colliding particles. For water droplets, both of these mechanisms are very slow: too slow to account for observed rates of cloud development and precipitation formation. Thus most precipitation is thought to develop as ice crystals at low temperatures, which may then defrost to form rain. This is known as the Bergeron-Findeisen mechanism, after two Norwegian meteorologists who first proposed the mechanism. Ice crystals grow more rapidly than water droplets, due to the lower saturation vapor pressure of air over ice, compared to water, but require very low temperatures. The formation of ice crystals in clouds is known as glaciations (not to be confused with terrestrial glaciation). This is probably the most important mechanism of precipitation formation in many parts of the world, even in the tropics (where low temperatures occur in high cumulus clouds). Ice crystal clouds have wispy, fibrous shapes, and allow us to see glaciations occurring in high clouds. An important type of ice clouds is known as cirrus, after the Latin word for hair. Types of precipitation include rain; snow (branching ice crystals or aggregates of crystals); sleet; hail, and graupel (conical pellets of spongy hail). The type that falls is dependent on the processes operating within clouds and the air temperature profile between there and ground (i.e. whether precipitation thaws or freezes en route to ground).

2.4.3   Cloud Ice Mixing Ratio

At low temperatures, ice crystals may form from water vapor in the atmosphere. This does not occur at 0^oC, because there is a need for freezing nuclei with suitable surface characteristics, which are less common than condensation nuclei. At temperatures $> -10^oC$, almost no ice will form; -10^oC to -20^oC increasing minority of ice crystals; -20^oC to -30^oC increasing majority of ice crystals; $< -30^oC$ mostly ice crystals. Cold air ($< 0^oC$) which contains liquid water droplets is referred to as super cooled. The water will tend to freeze as soon as it finds a suitable

surface where ice crystals can grow. An example of this process is the formation of rime ice on fence posts, clothing, hair and beards when cold, misty air blows past.

Figure: 2.3 Frozen Ice

2.4.4   Cloud Snow Mixing Ratio

Snow is precipitation in the form of flakes of crystalline water ice that falls from clouds. Since snow is composed of small ice particles, it is a granular material. It has an open and therefore soft, white, and fluffy structure, unless subjected to external pressure. Snowflakes come in a variety of sizes and shapes. Types that fall in the form of a ball due to melting and refreezing, rather than a flake, are hail, ice pellets or snow grains. The process of precipitating snow is called snowfall. Snowfall tends to form within regions of upward movement of air around a type of low-pressure system known as an extra tropical cyclone. Snow can fall pole ward of these systems' associated warm fronts and within their comma head precipitation patterns.

Figure: 2.4 Snow

Where relatively warm water bodies are present, for example because of water evaporation from lakes, lake-effect snowfall becomes a concern downwind of the warm lakes within the cold cyclonic flow around the backside of extra tropical cyclones. Lake-effect snowfall can be heavy locally. Thunder snow is possible within a cyclone's comma head and within lake effect precipitation bands. In mountainous areas, heavy snow is possible where upslope flow is maximized within windward sides of the terrain at elevation, if the atmosphere is cold enough. Snowfall amount and its related liquid equivalent precipitation amount are measured using a variety of different rain gauges. Extra tropical cyclones can bring cold and dangerous conditions with heavy rain and snow with winds exceeding 119 km/h. The band of precipitation that is associated with their warm front is often extensive, forced by weak upward vertical motion of air over the frontal boundary, which condenses as it cools off and produces precipitation within an elongated band, which is wide and stratiform, meaning falling out of nimbostratus clouds. When moist air tries to dislodge an arctic air mass, overrunning snow can result within the pole ward side of the elongated precipitation band. In the Northern Hemisphere, pole ward is towards the North Pole, or north. Within the Southern Hemisphere, pole ward is towards the South Pole, or south. Large water bodies such as lakes efficiently

store heat that results in significant temperature differences (larger than 13 °C) between the water surface and the air above. Because of this temperature difference, warmth and moisture are transported upward, condensing into vertically oriented clouds that produce snow showers. The temperature decrease with height and cloud depth is directly affected by both the water temperature and the large-scale environment. The stronger the temperature decrease with height, the deeper the clouds get, and the greater the precipitation rate becomes.

2.4.5   Cloud Graupel Mixing Ratio

Graupel is a German word for ice pellets which are crisp, opaque and easily compressible. Graupel forms when snow in the atmosphere encounters super cooled water. In a process known as accretion, ice crystals form instantly on the outside of the snow and accumulate until the original snowflake is no longer visible or distinguishable.

Figure: 2.5 Groupel

Snow pellets, Soft hail, Graupel precipitation of white and opaque ice particles, which fall from a cloud and which are generally conical or rounded, with diameters attaining as much as 2 to 5 mm, but some graupel can be the size of a quarter (coin). Graupel is sometimes

mistaken for hail. Graupel does not include other frozen precipitation such as snow or ice crystals with an experimental investigation of the heat and mass transfer of graupel. Graupel, heavily rimed snow, is an extreme product of this process. The coating of these ice crystals on the outside of the snow is called a rime coating. To tell the difference between graupel and hail, simply have to touch a graupel ball. Graupel pellets typically fall apart when touched or when they hit the ground. Hail is formed when layers of ice accumulate and are very hard as a result.

2.4.6   Cloud Water Vapor Mixing Ratio

Structures in atmospheric (vertically) Integrated Water Vapor (IWV) strongly reflect the dynamics of the atmosphere. Cold fronts are associated with a strong gradient (from high to low values) in IWV. These structures can also be seen in water (vapor) related variables, like cloud fields. This requires detailed measurements of IWV. Ideally, of course, the complete time evolution of the two-dimensional IWV field should be known. Satellites can measure water vapor from the top of the atmosphere in the 6.7 mm water vapor absorption channel. These measurement have good spatial resolution; however, the data only represent a measure of the water vapor content of the upper troposphere above (on average) 5 km, while most of the moisture is in the lower troposphere (with about 90% in the lower 5 km). Water vapor is a very important gas in the atmosphere and can influence many things like condensation and the formation of clouds and rain, as well as how hot or cold it feels at the surface. Different regions typically contain different amounts of water vapor and this can drastically affect the climate across these regions. Water vapor is also a necessary tool in forecasting; therefore the measurement of the amount of water vapor in the air is standard for most weather observation stations (along with temperature and wind properties). The different ways in which meteorologists express water vapor amounts as well as how to measure it. The mixing ratio is the ratio of the mass of water vapor in the air over the mass of dry air. This quantity is found by reading the mixing ratio line that goes through the dew point temperature at the pressure level of interest in the thermodynamic diagram. It can be expressed as the mixing ratio divided by the saturation mixing ratio or the vapor pressure divided by the saturation vapor pressure.

18

2.4.7　Relative Humidity

Relative Humidity is the most commonly used measurements of moisture content in the air. The Relative Humidity is the amount of water vapor (moisture) in the air compared to the maximum amount that the air could hold at a given temperature. The relative humidity is:

$$f = \frac{\omega}{\omega_s} \times 100 = \frac{\rho_w}{\rho_{ws}} \times 100 = \frac{q}{q_s} \times 100 = \frac{e}{e_s} \times 100$$

If the relative humidity is 100%, the air is saturated. If the relative humidity is 50%, the air contains half the water vapor required for it to be saturated. If the amount of water vapor in the air increases, the relative humidity increases, and if the amount of water vapor in the air decreases, the relative humidity decreases. However, relative humidity is dependent on air temperature, too. If the water vapor content remains the same and the temperature drops, the relative humidity increases. If the water vapor content remains the same and the temperature rises, the relative humidity decreases. This is because colder air doesn't require as much moisture to become saturated as warmer air. Warm air can hold more water vapor than cool air, so a particular amount of water vapor will yield a lower relative humidity in warm air than it does in cool air. If I watch the weather in the summer, you'll notice that the relative humidity is actually higher in the morning than in the afternoon. This is because the cooler morning air is closer to saturation than the hot afternoon air, even with the same amount of water vapor. Surprisingly, there is no significant difference in daily average relative humidity between summer and winter. Since warm air is less dense than cold air, there is more room for water vapor in warm summer air as compared with cold winter air. At a given vapor pressure (or mixing ratio), relative humidity with respect to ice is higher than that with respect to water. Water is known by different names in different states. If the maximum amount of water vapor has been reached and more water is introduced into the air, an equal amount of water must transform back to liquid or solid form through condensation. At this point, the air is said to be saturated with water, and the relative humidity is 100%. On the other end of the scale, when there is no water vapor in the air, the relative humidity is 0% whatever the temperature. In other words, relative humidity always lies between 0 and 100%. As

mentioned, the ability of air to hold water vapor is strongly dependent on temperature. This means that relative humidity is also strongly temperature dependent.

2.4.8   Vorticity

The vorticity is the microscopic measurement of the rotation of a small air parcel. Air parcel has vorticity when the parcel spins as it moves along its path. Although the axis of the rotation can extend in any direction, meteorologists are primarily concerned with the rotational motion about an axis that is perpendicular to the earth's surface. If it does not spin, it is said to have zero vorticity. In the Northern Hemisphere, the vorticity is positive when the parcel has a counterclockwise or cyclonic rotation. It is negative when the parcel has clockwise or anticyclonic rotation. For turning of the atmosphere, vorticity may be imbedded in the total flow and not readily identified by a flow pattern. The rotation of the Earth imparts vorticity to the atmosphere; absolute vorticity is the combined vorticity due to this rotation and vorticity due to circulation relative to the Earth (relative vorticity). The negative vorticity is caused by anticyclonic turning; it is associated with downward motion of the air. The positive vorticity is caused by cyclonic turning; it is associated with upward motion of the air. Also the relative vorticity is the air relative to the Earth, disregarding the component of vorticity resulting from Earth's rotation.

The absolute vorticity ω_a is given by the curl of the absolute velocity, while the relative vorticity ω is given by the curl of the relative velocity:

$$\omega_a \equiv \overline{\nabla} \times \overline{V}_a \qquad\qquad \omega \equiv \overline{\nabla} \times \overline{V}$$

In meteorology the general concerned only with the vertical components of absolute and relative vorticity:

$$\eta = \hat{k}.\left(\overline{\nabla} \times \overline{V}_a\right), \quad \zeta = \hat{k}.\left(\overline{\nabla} \times \overline{V}\right)$$

In particular, the vertical component of relative vorticity ζ is highly correlated with synoptic scale weather disturbances. Large positive ζ tends to occur in association with cyclonic storms in the Northern Hemisphere. Furthermore, η tends to be conserved following the motion in the middle troposphere. Thus, analysis of the η field and its evolution due to advection forms the basis for the simplest dynamical forecast scheme.

2.5 Weather Research & Forecasting Model

The Weather Research and Forecasting (WRF) Model is a next-generation mesoscale numerical weather prediction system designed to serve both atmospheric research and operational forecasting needs. It features two dynamical cores, a data assimilation system, and a software architecture facilitating parallel computation and system extensibility. The model serves a wide range of meteorological applications across scales from tens of meters to thousands of kilometers. The effort to develop WRF began in the later part of the 1990's and was a collaborative partnership principally among the National Center for Atmospheric Research (NCAR), the National Oceanic and Atmospheric Administration represented by the National Centers for Environmental Prediction (NCEP) and the Forecast Systems Laboratory (FSL), the Air Force Weather Agency (AFWA), the Naval Research Laboratory, the University of Oklahoma, and the Federal Aviation Administration (FAA). WRF offers two dynamical solvers for its computation of the atmospheric governing equations, and the variants of the model are known as WRF-ARW and WRF-NMM. The Advanced Research WRF (ARW) is supported to the community by the NCAR Mesoscale and Micro scale Meteorology Division. The WRF-NMM solver variant was based on the Eta Model, and later Non hydrostatic Mesoscale Model, developed at NCEP. The WRF-NMM is supported to the community by the Developmental Test bed Center.

2.5.1 Microphysics schemes in WRF-ARW Model

Microphysics includes explicitly resolved water vapor, cloud and precipitation processes. The model is general enough to accommodate any number of mass mixing-ratio variables, and other quantities such as number concentrations. Four-dimensional arrays with three spatial indices and one species index are used to carry such scalars. Memory, i.e., the size of the fourth dimension in these arrays, is allocated depending on the needs of the scheme chosen, and advection of the species also applies to all those required by the microphysics option. In the current version of the ARW, microphysics is carried out at the end of the time-step as an adjustment process, and so does not provide tendencies.

The rationale for this is that condensation adjustment should be at the end of the time-step to guarantee that the final saturation balance is accurate for the updated temperature and

21

moisture. However, it is also important to have the latent heating forcing for potential temperature during the dynamical sub-steps and this is done by saving the microphysical heating as an approximation for the next time-step as described.

2.5.1.1 Kessler Scheme

The Kessler scheme is a simple warm cloud scheme that includes water vapor, cloud water and rain. The microphysical process consists of the production, fall and evaporation of rain, the accumulation and auto conversion of cloud water and the production of cloud water from condensation. A warm-rain scheme has been used commonly in idealized cloud modeling studies. Kessler scheme is one moment scheme. The purpose of the scheme is to increase understanding of the roles of cloud conversion, accretion, evaporation, and entrainment processes in shaping the distributions of water vapor, cloud, and precipitation associated with tropical circulations. This scheme is idealized microphysics process without the consideration of ice phase and melting zone. Kessler scheme has been used widely in cloud modeling studies due to its simplicity. The equation represented the processes between cloud, vapor and rain are also much simplified compared with other scheme. Kessler scheme produced much heavier precipitation and can show unrealistic precipitation profiles in some studies.

2.5.1.2 Lin *et al.* Scheme

A sophisticated scheme that has ice, snow and graupel processes, suitable for real-data high-resolution simulations. Lin *et al.* (1983) scheme includes six classes of hydrometeors are included: water vapor, cloud water, rain, cloud ice, snow, and graupel. All parameterization production terms are based on Lin *et al.* This is a relatively sophisticated microphysics scheme in WRF, and it is more suitable for use in research studies. The scheme is taken from Purdue cloud model and the details can be found in Lin *et al.* 2-D microphysics scheme. This is one of the first schemes to parameterize snow, graupel, and mixed-phase processes. It has been used extensively in research studies and in mesoscale NWP Model. The scheme includes ice sedimentation and time- split fall terms.

2.5.1.3 WSM 3-class scheme

The WSM3 microphysics scheme includes ice sedimentation and other new ice-phase parameterizations. In this scheme an analytical relation is used for ice number concentration

that is based on ice mass content rather than temperature. The WSM3 scheme predicts three categories of hydrometers: water vapor, cloud water and rain water mixing ratio, which is a so-called simple-ice scheme. This scheme is computationally efficient for the inclusion of ice processes, but lacks super cooled water and gradual melting rates.

2.5.1.4 Ferrier scheme

Ferrier scheme predicts changes in water vapor and condensate in the forms of cloud water, rain, cloud ice, and precipitation ice. Local storage arrays retain first-guess information that extract contributions of cloud water, rain, cloud ice, and precipitation ice of variable density in the form of snow, graupel, or sleet. The density of precipitation ice is expected from a local array that stores information on the total growth of ice by vapor deposition and accretion of liquid water. Sedimentation is treated by partitioning the time averaged flux of precipitation into a grid box between local storage in the box and fall out through the bottom of the box. Advection only of total condensate and vapor diagnostic cloud water, rain and ice from storage arrays assumes fractions of water and ice within the column are fixed during advection super cooled liquid water and ice melt.

2.5.1.5 WRF Single-moment 6-class (WSM6) microphysics scheme

The WRF-single-moment-6-class (WSM6) microphysics scheme has been one of the options of microphysical process in the WRF model since August 2004. This scheme predicts the mixing ratios for water vapor, cloud water, cloud ice, snow, rain, and graupel. The characteristics of the cold rain process in the WSM6 scheme follow the revised ice microphysics process (Hong *et al.*, 2004), whereas the warm rain processes are primarily based on the works of Lin *et al.* (1983) and the auto conversion process from Tropoli and Cotton (1980). The daily forecasts at NCAR have shown that the WSM6 scheme works successfully in predicting mesoscale convective systems, but it sometimes overestimates the peak intensity and underestimates the areas of anvil clouds. Attempt has been made to improve such existing deficiencies in the WSM6 scheme by incorporating the prediction of number concentrations for warm rain species. This new method uses a large eddy simulation (LES)-based approach (Khairoutdinov and Kogan 2000) to determine the auto conversion rates and allow for a more sophisticated coupling between cloud field and number

concentrations of warm species. Double-moment prediction for the warm species in WSM6 scheme will allow more flexibility of the size distribution enabling the mean diameter to evolve in contrast to the one-moment scheme. WSM6 scheme includes vapor, rain, snow, cloud ice, cloud water and graupel in six different arrays. A new method for representing mixed-phase particle fall speeds for the snow and graupel by assigning a single fall speed to both that is weighted by the mixing ratios, and applying that fall speed to both sedimentation and accumulation processes is introduced. Of the three WSM schemes, the WSM6 scheme is the most suitable for cloud-resolving grids, considering the efficiency and theoretical backgrounds. A new method for representing mixed-phase particle fall speeds for the snow and a scheme with ice, snow and graupel processes suitable for high-resolution simulations. The WSM6 scheme has been developed by adding additional process related to graupel to the WSM5 scheme.

2.5.1.6 Thompson Scheme

A bulk microphysical parameterization (BMP) was developed for use with WRF or other mesoscale models. The snow size distribution depends on both ice water content and temperature and is represented as a sum of exponential and gamma distributions. Furthermore, snow assumes a non-spherical shape with a bulk density that varies inversely with diameter as found in observations. A new scheme with ice, snow and graupel are processes suitable for high-resolution simulations. This adds rain number of concentrations and updates the scheme from the one in Version 3.0 New Thompson *et al.* scheme in V3.1. Replacement of Thompson *et al.* scheme that was option 8 in V3.0 6-class microphysics with graupel, ice and rain number concentrations also predicted.

2.5.2 Cumulus Parameterization

These schemes are responsible for the sub-grid-scale effects of convective and/or shallow clouds. The schemes are intended to represent vertical fluxes due to unresolved up drafts and down drafts and compensating motion outside the clouds. They operate only on individual columns where the scheme is triggered and provides vertical heating and moistening profiles. Some schemes provide cloud and precipitation field tendencies in the column, and future schemes may provide momentum tendencies due to convective transport of momentum. The

24

schemes provide the convective component of surface rainfall. Cumulus parameterizations are theoretically only valid for coarser grid sizes (e.g., > 10 km), where they released latent heat on a realistic time scale in the convective columns. Where the assumptions about the convective eddies being entirely sub-grid-scale break down for finer grid sizes, sometimes these schemes have been found to be helpful in triggering convection in 5-10 km grid applications. Generally they should not be used when the model can resolve the convective eddies itself. One of the main options which could potentially affect precipitation severely is the cumulus parameterization. It accounts for unresolved cloud formation. Depending on the grid resolution, convective clouds could be resolved by the explicit scheme, but with the resolution used here (15 km) it still seems necessary to take into account the unresolved scales. The feedback from these parameterizations to the larger–scale equations of the model is the profile of latent heat release and moistening caused by convection. Two different schemes were used. Even though the efficiency of a given parameterization depends on the concrete event, other cumulus parameterizations have been proved to have less accuracy, e.g. the Anthes–Kuo (Pan *et al.* 1996, Ferretti et al. 2000) or Betts–Miller schemes (Cohen 2002). The Kain–Fritsch scheme has demonstrated good performance on several situations and regions (Wang and Seaman 1997, Kotroni and Lagouvardos 2001, Cohen 2002). In the study by Ferretti *et al.* (2000) in the Alpine region, the Grell scheme was better than the Kain–Fritsch scheme for some concrete events.

These schemes are responsible for the sub-grid-scale effects of convective and shallow clouds. The schemes are intended to represent vertical fluxes due to unresolved updrafts and downdrafts and compensating motion outside the clouds. The cumulus parameterization are theoretically only valid for coarser grid sizes, (e.g., > 10km), where they are necessary to properly release latent heat on a realistic time scale in the convective columns.

2.5.2.1 Kain-Fritsch (KF) scheme

In the KF scheme the condensates in the updraft are converted into precipitation when their amount exceeds threshold value. In this scheme, the convection consumes the convective available potential energy in a certain time scale. The KF scheme also includes the shallow convection other than deep convection. The shallow convection creates non-precipitable condensates and the shallowness of the convection is determined by a vertical extent of the

25

cloud layer that is known by a function of temperature at LCL of rising air parcel. The KF scheme was derived from the Fritsch–Chappell, and its fundamental framework and closure assumptions are described by Fritsch and Chappell. KF90 modified the updraft model in the scheme and later introduced numerous other changes, so that it eventually became distinctly different from the Fritsch–Chappell scheme. It was distinguished from its parent algorithm by referring to the more elaborate code as the KF scheme, beginning in the early 1990s. This is also deep and shallow convection sub-grid scheme using a mass flux approach with downdrafts and CAPE removal time scale.

Updraft generates condensate and dump condensate into environment downdraft evaporates condensate at a rate that depends on RH and depth of downdraft leftover condensate accumulates at surface as precipitation. The Regional Atmospheric Modeling System, version 4.4, is used to simulate this event.

2.5.2.2 Betts-Miller-Janjic (BMJ) scheme

The BMJ cumulus parameterization scheme is a nudging type adjustment of temperature and humidity in grid scale. The scheme adjusts the sounding towards a pre-determined, post convective profile derived from climatology. This post convective profile has been defined by points at the cloud base, cloud top and freezing level. In this scheme there is no explicit updraft or downdraft and no cloud detrainment occur. Convection is initiated when soundings are moist through a deep layer and when CAPE and convective cloud depth thresholds are exceeded. Betts and Miller proposed a convective adjustment scheme that includes both deep and shallow convection. The deep convection in the Betts–Miller scheme is similar to the other adjustment schemes except that it uses empirically based quasi-equilibrium thermodynamic profiles as a reference state rather than a moist adiabatic. The basic shape of these quasi-equilibrium reference profiles is based on the numerous observations. The construction of the reference profiles and the specification of the relaxation timescale are two major components of the Betts–Miller scheme.

These points and thresholds can vary by season and between the tropics and extra tropics. Compared with the original sounding, the sounding modified to the post convective profile will note a net change in perceptible water as well as changes in net heating and cooling.

Convection is initiated when soundings are moist through a deep layer and when CAPE and convective cloud depth thresholds are exceeded. Important vertical structures may be eliminated since the reference profiles are based on climatology. Convection is only initiated for soundings with deep moisture profile. When convection is initiated the scheme often rains out to much water. This is because the reference profile is too dry for the forecast scenario or the transition to the reference profile was too rapid. Scheme does not account for the strength of CAPE inhibiting convective development. Scheme does not account for any changes below the cloud base.

2.5.3 Planetary Boundary Layer (PBL) Parameterizations

The planetary boundary layer (PBL) is the layer in the lower part of the troposphere with thickness ranging from a few hundred meters to a few kilometers within which the effects of the Earth's surface are felt by the atmosphere. The PBL processes represent a consequence of interaction between the lowest layer of air and the underlying surface. The interactions can significant impact on the dynamics of the upper air flows. The influence of the small-scale eddies on large scale atmospheric circulations may be included in the model equations. Accurate depiction of meteorological conditions, especially within the PBL, is important for air pollution modeling, and PBL parameterization schemes play a critical role in simulating the boundary layer. This study examines the sensitivity of the performance of the WRF model to the use of six different PBL schemes. It is a very important portion of the atmosphere to correctly model to provide accurate forecasts, e.g., air pollution forecasts (Deardorff 1972; Pleim 2007). As important as the PBL is, it has one basic property whose accurate and realistic prediction is paramount to its correct modeling: its height. After all, the height of the top of the PBL defines its upper boundary. This is critical since PBL parameterizations schemes in WRF-ARW models need to know the extent through which to mix properties such as heavy rainfall, relative humidity, outgoing long wave flux, downward long wave flux. PBL schemes were developed to help resolve the turbulent fluxes of heat, moisture, and momentum in the boundary layer. Another important issue is the interaction between the atmosphere and the surface. The PBL schemes handle the latent and sensible heat fluxes into the atmosphere, the frictional effects with the surface and the strong sub–grid–scale mixing which takes place in the lower levels due to these processes. In this case, both schemes were used complex, but

27

with quite a different computing efficiency. No other PBL schemes are compatible with the selected 5–layer soil scheme. Besides, these are the best performing parameterizations according to previous short–range studies (Cassano *et al.* 2000, Bright and Mullen 2002).

2.5.3.1 Yonsei University (YSU) scheme

The Yonsei University (YSU) PBL is the next generation of the MRF, Non local-K scheme with explicit entrainment layer and parabolic K profile in unstable mixed layer. The YSU scheme is a bulk scheme that expresses non-local mixing by convective large eddies. Non-local mixing is achieved by adding a non-local gradient adjustment term to the local gradient. At the top of the PBL, the YSU scheme uses explicit treatment of the entrainment layer, which is proportional to the surface layer flux (Hu *et al.* 2010, Shin and Hong 2011, Hong *et al.* 2006).

Chapter III

Model Description and Methodology

3.1   Model Description

In the present study the Weather Research and Forecast (WRF-ARW Version 3.2.1) model consists of fully compressible non-hydrostatic equations and different prognostic variables is utilized. The model vertical coordinate is terrain following hydrostatic pressure and the horizontal grid is Arakawa C-grid staggering. Third-order Runge-Kutta time integration is used in the model. The model is configured in single domain, 12 km horizontal grid spacing with 186×196 grids in the west-east and north-south directions and 28 vertical levels. The six different microphysics schemes used are Kessler, Lin *et al.*, WSM3 for explicit moisture processes, Eta (Ferrier), WSM 6-class graupel and Thompson graupel schemes. The Lin *et al.*, WSM6 and Thompson MP schemes contain prognostic equations for cloud water, rainwater, cloud ice, snow, and graupel mixing ratio. The Kessler, WSM3 and Ferrier MP schemes contain prognostic equations for cloud water and rainwater mixing ratios. The Ferrier scheme also contains prognostic equations for cloud water, rainwater and snow mixing ratio. Dudhia simple five-layer soil thermal diffusion scheme for soil processes, Rapid Radiative Transfer Model (RRTM) for long wave scheme for shortwave radiation and Yonsei University scheme planetary boundary layer (PBL) have been used for the simulation of TC Mala, Phailin and Sidr. Two different cumulus parameterization (CP) schemes have been used in WRF model are Kain-Fritsch (KF) (Kain and Fritsch, 1990, 1993; Kain, 2004) and Betts-Miller-Janjic (BMJ) (Janjic, 1994, 2000). The 5-layer thermal diffusion option with prognostic soil temperature and land-use-dependent soil-moisture availability represented the land surface. The RRTM scheme has been chosen for long-wave radiation with the Dudhia scheme for short wave radiation. The model domain is given in Fig.3.1. The detail of the model and domain configuration is given in Table 1.

3.2   Model configuration

In this study, the WRF–ARW model has been configured with single domain. For the analysis of cloud hydrometeors, the model domain has been divided into 5 different regions.
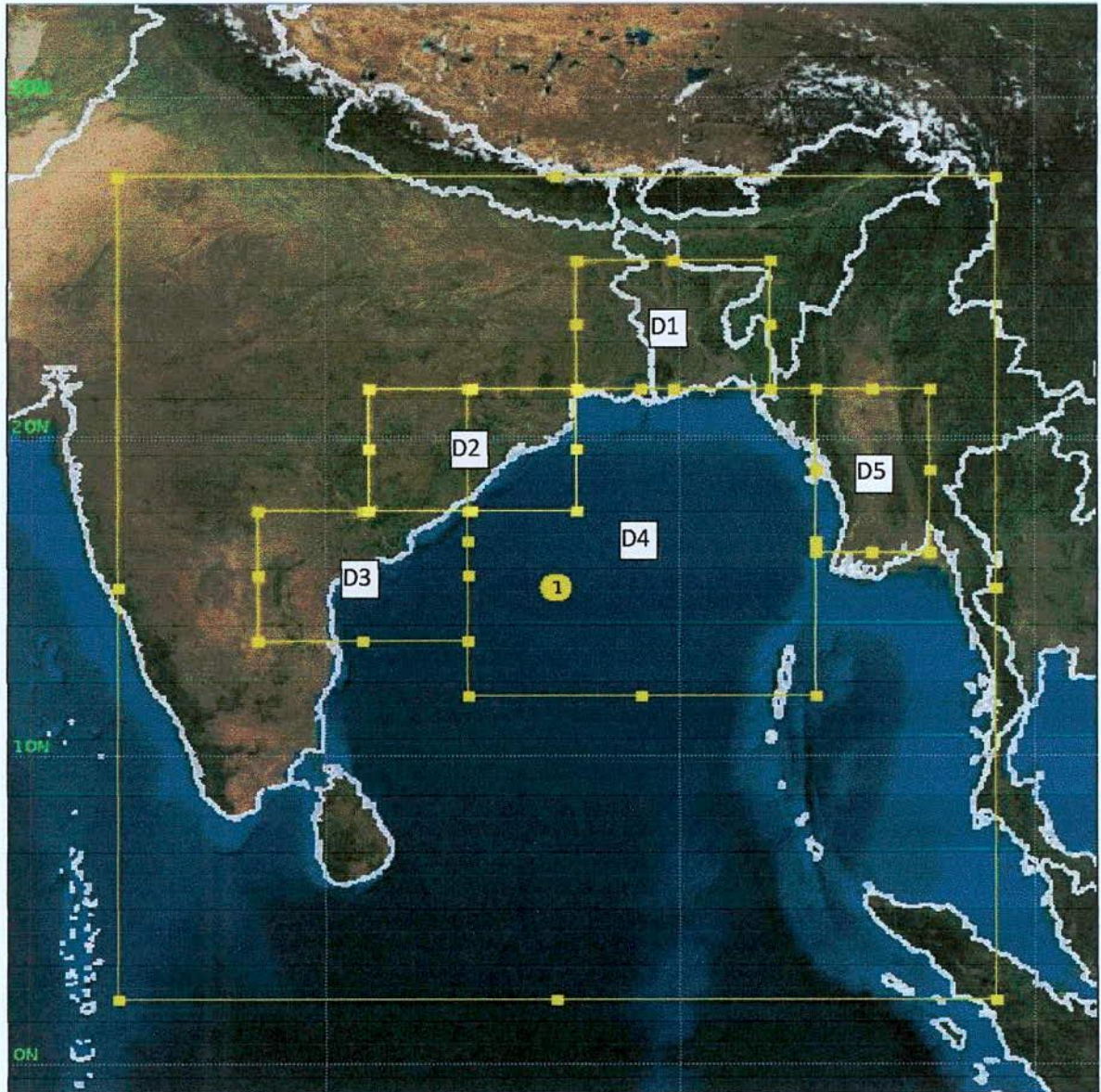
Figure 3.1: The WRF–ARW domain set up for the study.

We have divided the model domain into different regions D1 (22-26°N and 87-93°E), D2 (18-22°N and 81-87°E), D3 (14-18°N and 78-84°E), D4 (12-22°N and 84-94°E) and D5 (17-22°N and 94-97°E) (Fig. 3.1).

3.3 Data and Methodology

Final Reanalysis (FNL) data (1° x1°) collected from National Centre for Environment Prediction (NCEP) is used as initial and lateral boundary Conditions (LBCs) which is updated

Table 1: WRF Model and Domain Configurations

Dynamics	Non-hydrostatic
Number of domain	1
Central points of the domain	Central Lat.: 16.5°N, Central Lon.: 86.5°E
Horizontal grid distance	12 km
Integration time step	60 s
Number of grid points	X-direction 186 points, Y-direction 196 points
Map projection	Mercator
Horizontal grid distribution	Arakawa C-grid
Nesting	One way
Vertical co-ordinate	Terrain-following hydrostatic-pressure co-ordinate (28 sigma levels up to 100 hPa)
Time integration	3rd order Runge-Kutta
Spatial differencing scheme	6th order centered differencing
Initial conditions	Three-dimensional real-data (FNL: $1° \times 1°$)
Lateral boundary condition	Specified options for real-data
Top boundary condition	Gravity wave absorbing (diffusion or Rayleigh damping)
Bottom boundary condition	Physical or free-slip
Diffusion and Damping	Simple Diffusion
Microphysics	(1) Kessler, (2) Lin *et al.* (1983) scheme (3) WSM3-class scheme (Hong *et al.*, 2004) (4) Eta (Ferrier) scheme (5) WSM 6-class graupel sch. (Hong and Lim, 2006) and (6) Thompson graupel scheme.
Radiation scheme	Dudhia (1989) for short wave radiation/ RRTM long wave Mlawer *et al.* (1997)
Surface layer	Monin-Obukhov similarity theory scheme (Hong and Pan, 1996)
Land surface parameterization	5 Layer Thermal diffusion scheme (Ek *et al.*, 2003)
Cumulus parameterization schemes	1) Kain-Fritsch (KF) scheme, (Kain and Fritsch, 1990, 1993; Kain, 2004) 2) Betts-Miller-Janjic (BMJ), (Janjic, 1994, 2000)
PBL parameterization	Yonsei University Scheme (YSU) (Hong *et al.*, 2006)

at six hours interval i.e. the model is initialized with 0000, 0600, 1200 and 1800UTC initial field of corresponding date. The NCEP FNL data is interpolated to the model horizontal and vertical grids and the model was integrated for 96 and 72-h period for tropical cyclone (TC) Mala, Sidr and Phailin. 24 experiments have been conducted in each case by using different microphysics schemes (e.g., Kessler, Lin *et al.*, WSM3-class simple ice scheme, Ferrier, WSM 6-class graupel scheme and Thompson graupel) in combinations with Kain-Fritsch (KF) and Betts-Miller-Janjic (BMJ) CP schemes with different initial conditions. In this regard, the initial conditions of 0000 UTC of 26 and 27 April 2006 have been considered for TC Mala, initial conditions at 0000 UTC of 8 and 9 October 2013 have been considered for TC Phailin and initial conditions at 0000 UTC of 11 and 12 November 2007 have been considered for TC Sidr. The different periods for different cyclones were characterized by the formation of tropical cyclone until dissipation. The model simulated MSLP, maximum wind at 10 m level, track, Cloud Water Mixing Ratio (CWMR), Cloud Ice Mixing Ratio (CIMR), Cloud Graupel Mixing Ratio (CGMR), Cloud Snow Mixing Ratio (CSMR), Rain Water Mixing Ratio (RWMR), Cloud Vapor Mixing Ratio (CVMR), Relative Humidity (RH) and Vorticity have been analyzed. Simulated track and intensity have also been compared with the IMD and JTWC observed results. We have divided the model domain into different regions D1 in the northern side of BoB, D2 in the northwestern side of BoB, D3 in the western side of BoB, D4 in the Oceanic area and D5 in the northeastern side of BoB.

We have calculated the average values of hydrometeors in different regions by using the software Grid Analysis and Display Systems (GrADS). The Grid Analysis and Display System (GrADS) is an interactive desktop tool that is used for easy access, manipulation, and visualization of earth science data. GrADS has two data models for handling gridded and station data. GrADS supports many data file formats, including binary (stream or sequential), GRIB (version 1 and 2), NetCDF, HDF (version 4 and 5), and BUFR (for station data). GrADS has been implemented worldwide on a variety of commonly used operating systems. GrADS uses a 5-Dimensional data environment: the four conventional dimensions (longitude, latitude, vertical level, and time) plus an optional 5th dimension for grids that is generally implemented but designed to be used for ensembles. Data sets are placed within the 5-D space by use of a data descriptor file. GrADS handles grids that are regular, non-linearly spaced,

gaussian, or of variable resolution. Data from different data sets may be graphically overlaid, with correct spatial and time registration. Operations are executed interactively by entering FORTRAN-like expressions at the command line. A rich set of built-in functions are provided, but users may also add their own functions as external routines written in any programming language. Data may be displayed using a variety of graphical techniques: line and bar graphs, scatter plots, smoothed contours, shaded contours, streamlines, wind vectors, grid boxes, shaded grid boxes, and station model plots. Graphics may be output in PostScript or image formats. GrADS provides geo physically intuitive defaults, but the user has the option to control all aspects of graphics output. After getting txt data from grads we converted it into Excel sheet and plotted graph using Excel. We have plotted the data on Excel at every 6 hourly intervals for observing the changing scenario of hydrometeors for the movement of TCs.

Paint (formerly Paintbrush for Windows) is a simple computer graphics program that has been included with all versions of Microsoft Windows. It is often referred to as MS Paint or Microsoft Paint. The program mainly opens and saves files as Windows bitmap (24-bit, 256 color, 16 color, and monochrome, all with the .bmp extension), JPEG, GIF. We have converted our Excel graph into Paint and then transferred to Word.

Chapter IV

Results and Discussion

In this research the hydrometeors have simulated of TC Mala (2006), TC Sidr (2007) and TC Phailin (2013) using WRF-ARW model and have been discussed in the following subsections. Cloud water mixing ratio, rain water mixing ratio, ice mixing ratio, snow mixing ratio, graupel mixing ratio, water vapor mixing ratio, relative humidity and vorticity simulated by six MPs coupling with two CPs are plotted and discussed. In order to examine the differences in the simulated track and intensity of tropical cyclones, space averaged and time averaged vertical profiles of cloud water, rain water, graupel, snow ice and water vapor mixing ratio (g/kg), relative humidity and vorticity were calculated once every three hours but plotted once every six hours for the TCs Mala, TC Phailin and TC Sidr.

4.1   Tropical Cyclone Mala

4.1.1   Synoptic situation of Tropical Cyclone Mala

A low pressure area formed over Southeast Bay of Bengal and adjoining south Andaman Sea on 23 April 2006. It moved west-northwesterly direction initially and intensified into a well-marked low over the same area. It intensified further into a depression at 0300 UTC of 24 April 2006 over Southeast Bay when its central location was at about 9.5°N and 90.5°E. The system moved slightly westwards and intensified into a deep depression (DD) at 0900 UTC of 24 April 2006 over Southeast Bay and adjoining areas and located at about 9.5°N and 90.0°E. The DD then moved slightly northwestwards and intensified into a cyclonic storm (CS) 'Mala' at 1200 UTC of 25 April 2006 over Southeast Bay and adjoining areas. At this stage, the estimated central mean sea level pressure (MSLP) of the system was about 996 hPa, the maximum estimated wind speed was about 18 m/s and the central location was at about 10.0°N and 89.5°E. The CS 'Mala' then moved further north-northwestwards, intensified further and its central MSLP lowered to 994 hPa, the maximum wind speed increased to 23 m/s and the centre located to about 11.0°N and 89.0°E at 0000 UTC of 26 April. Then, it moved north-northeastwards and intensified into a severe cyclonic storm (SCS) 'Mala' at 0300 UTC of 27 April over East-central Bay and adjoining areas with the central MSLP of 990 hPa

34

and the maximum wind speed of 28 m/s. At 1200 UTC of 27 April, the system attained the strength of a very severe cyclonic storm (VSCS) with the central MSLP of 984 hPa, the MWS of 33 m/s and the central location at about 13.0°N and 90.5°E. The VSCS 'Mala' moved in the same direction and intensified further and at 0900 UTC of 28 April its central MSLP lowered to 954 hPa, the MWS increased to 51 m/s when its central location was at about 15.0°N and 92.3°E. Then, the VSCS 'Mala' moved continuously northeastwards afterwards without changing intensification and finally crossed Arakan coast of Myanmar about 100 km south of Sandoway near to 19.0°N and 96.0°E at 0700 UTC of 29 April. After landfall the system weakened gradually by giving precipitation over Arakan coast and adjoining land areas of Myanmar. The IMD and JTWC tracks are depicted in Figure 4.1.2.

4.1.2 Intensity of TC Mala

Figure 4.1.1 (a-d) represents the simulated intensity of TC Mala considering 3-hourly central sea level pressure (CSLP) and associated maximum wind speed (m s^{-1}) at 10 m level using different MP schemes coupling with CP schemes. Figure 4.1.1 (a-b) shows that the simulated CSLP for six different MP schemes in combination with two different CP schemes and two different initial conditions at 0000 UTC of 26 and 27 April 2006. The simulated intensity in terms of CSLP for all MP schemes in combination with KF scheme are much higher than that of BMJ scheme with the initial condition at 0000 UTC of 26 and 27 April. IMD observed intensity (954 hPa, 51.44 m s^{-1}) is much lower than that of JTWC intensity (922 hPa, 61.73 m s^{-1}) in terms of pressure fall and 10 m level sustained wind. The simulated pressure fall with the 0000 UTC on 26 April initial condition for all MP schemes in combination with KF scheme are close to JTWC observed results but higher than that of IMD observed results. The simulated CSLP for all MP schemes in combination with KF scheme lies between IMD and JTWC observed results with the initial conditions 0000 UTC of 27 April. BMJ scheme simulated pressure drop and wind speed in combination with all MP schemes are much lower than that of IMD and JTWC observed pressure and maximum wind speed with the initial condition of 0000 UTC of 26 & 27 April. The wind speed simulated at 10 m level for all MP schemes coupling with KF scheme with the initial condition of 0000 UTC of 26 and 27 April are lower than that of JTWC observed wind speed and higher than that of IMD observed wind speed. BMJ scheme coupling with all MP schemes have simulated wind speed at 10 m level

are much lower than that of IMD and JTWC observed wind with the initial condition at 0000 UTC of 26 and 27 April. The simulated wind speeds for all MP schemes in combination of KF scheme at 10 m level are almost equal to IMD observed wind speed.
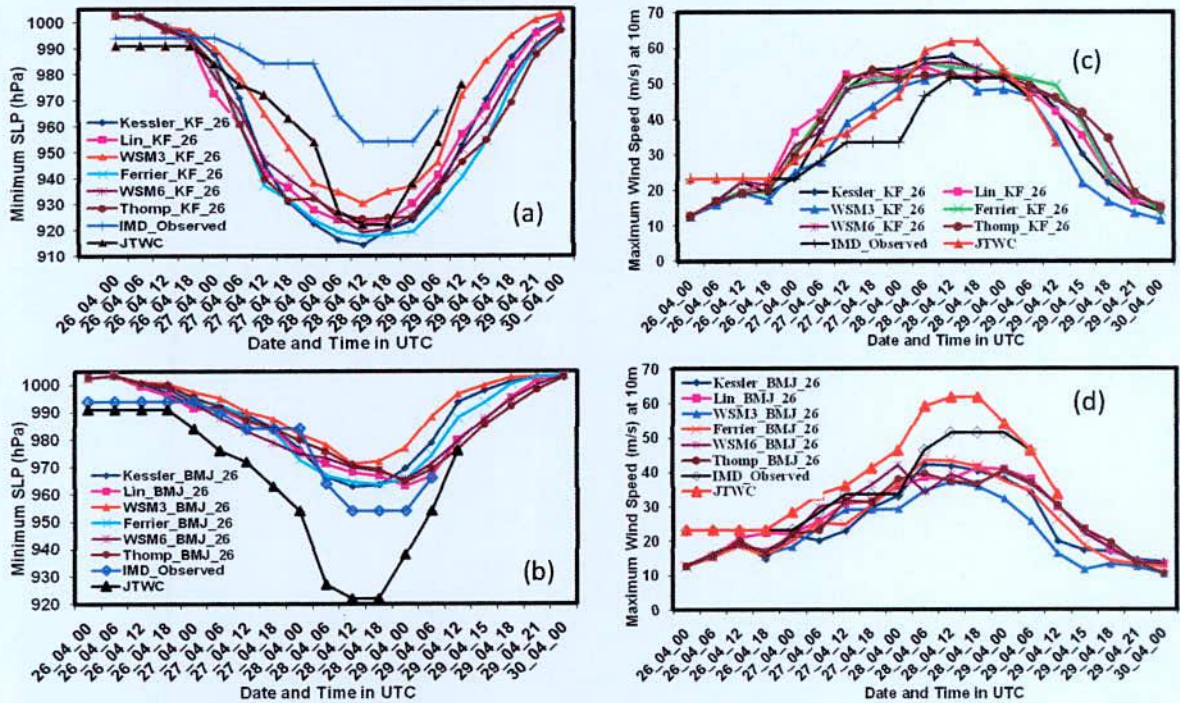
Figure 4.1.1: Model simulated (a-b) minimum central pressure (hPa) and (c-d) maximum sustained wind at 10m level of TC Mala using six different MP schemes coupling with KF and BMJ schemes with 0000 UTC of 26 April 2006 initial conditions.

4.1.3 Track of TC Mala

The observed and simulated track for the period of 96-h and 72-h of TC Mala for different MP schemes are displayed in Figure 4.1.2 (a-d). The track forecasts have shown reasonably accurate for different experiments i.e., up to the landfall time (landfall time of 0700 UTC of 29 April 2006). For all combination of MP and CP schemes, the model captured the north-northeastward movement with the initial condition at 0000 UTC of 26 and 27 April 2006. The significant deviations in tracks are observed among different microphysical schemes in combination with KF scheme with the initial condition of 0000 UTC of 26 April. Kessler and WSM3 schemes in combination with KF and BMJ schemes provide most deviated track with

the initial condition of 0000 UTC of 26 April. Kessler scheme deviated towards left and WSM3 deviated towards right from the IMD and JTWC track. At the time of landfall Ferrier and Thompson schemes in combination with KF scheme and Lin *et al.* and WSM6 scheme in combination with BMJ schemes simulate less deviated track with the initial condition of 0000 UTC of 27 April.
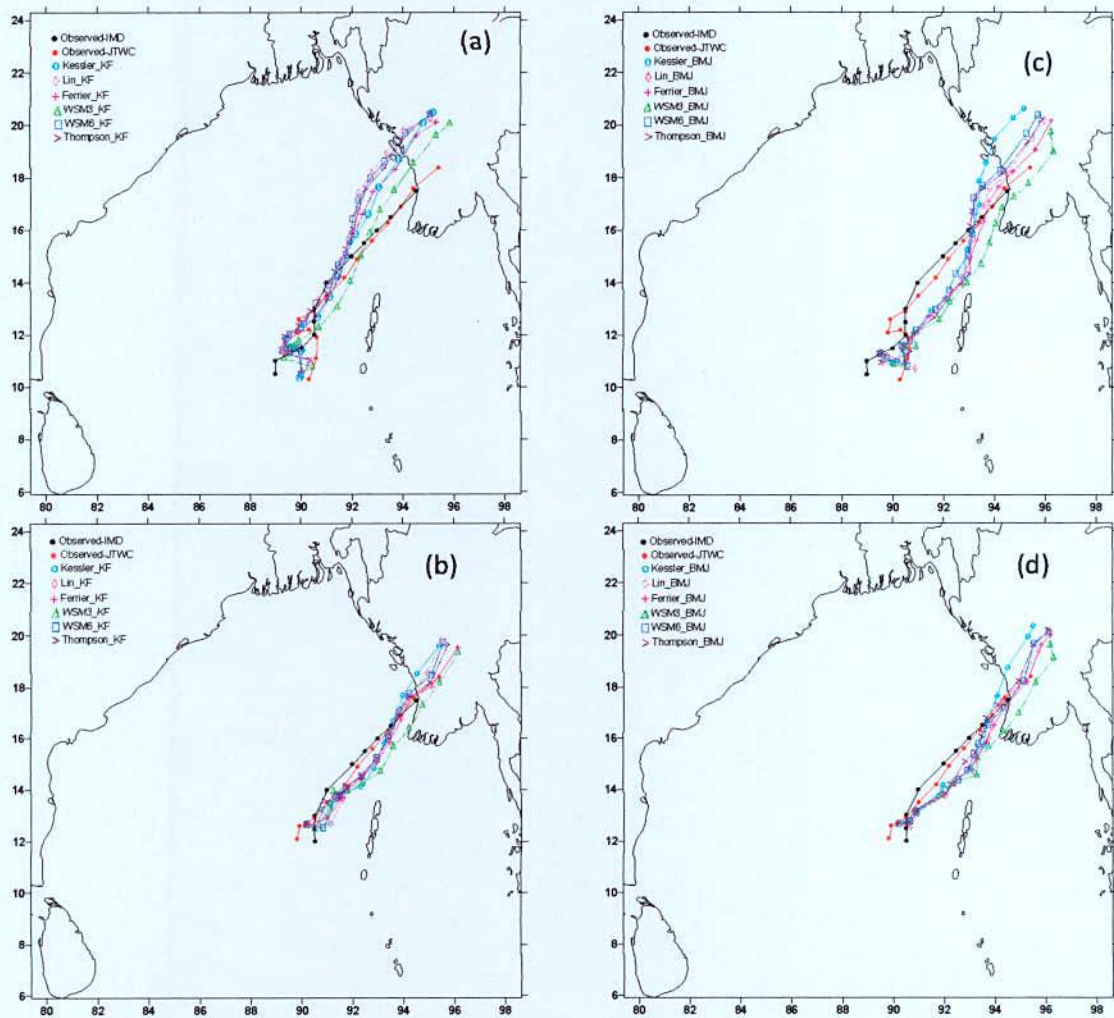
Figure 4.1.2: Simulated, IMD and JTWC observed track of tropical cyclone 'Mala' using six different MP schemes coupling with (a-b) KF scheme and (c-d) BMJ scheme with the initial conditions of 0000 UTC of 26 and 27 April 2006.

All microphysics coupling with KF and BMJ schemes captured the northeastward movement of TC Mala for the initial conditions of 0000 UTC of 27 April. The landfall time was delayed

by 4–9 h by using the initial conditions of 0000 UTC 26 April. The simulated landfall time by using six different MP schemes coupling with KF scheme are 1200, 1300, 1000, 1300, 1400 and 1500 UTC respectively but when coupling with BMJ scheme are 0700, 1000, 0300, 0900, 1200 and 1200 UTC respectively. The observed landfall time almost match with the model simulated landfall time with the initial condition at 0000 UTC of 27 April. Simulated landfall time by using Kessler, Lin *et al.*, WSM3, Ferrier, WSM6 and Thompson schemes coupling with KF scheme are 0900, 0700, 0400, 0700, 0700 and 0900 UTC respectively. But when these MP schemes are coupled with BMJ scheme, the landfall time are 0900, 0900, 0000, 0600, 0700 and 0900 UTC respectively. It suggests that the model simulated landfall times are close to the observation with the delayed initial condition.

4.1.4 Cloud Water Mixing Ratio (CWMR)

The vertical profiles of area averaged CWMR (gm/kg) at different times 0000 UTC of 27, 28, 29 and 1200 UTC of 26, 27, 28 and 29 April 2006 has been analyzed in region D4 by using six different MP schemes coupling with KF and BMJ schemes as shown in Figure 4.1.3 (a-l). Kessler and WSM3 schemes coupling with KF and BMJ schemes have simulated CWMR up to 100 hPa. All other MPs coupling with KF and BMJ schemes have simulated CWMR up to 350 hPa level. Kessler and WSM3 schemes coupling with KF and BMJ schemes have simulated two maxima of CWMR one at 500 & 600 hPa and another one at 150 & 250 hPa levels respectively. The CWMR have simulated maximum at 650–550 hPa level for Lin, Ferrier, WSM6 and Thompson schemes in combination with KF and BMJ schemes. Vertical profiles of area averaged profiles of CWMR for all MP schemes coupling with KF and BMJ schemes are almost constant and zero from 250-100 hPa level. The intensity of TC has changed continuously from CS to VSCS since 1200 UTC of 26 April to 0000 UTC of 29 April the CWMR has also increased significantly during this time at 900-400 hPa level by KS, Lin, WSM6 and Thompson schemes coupling with KF scheme. The CWMR decreased after 1200 UTC of 28 April by using WSM3-KF and Ferrier-KF combinations and 0000 UTC of 29 April all other MP schemes coupling with KF scheme. Due to the decreased of CWMR earlier the intensity of TC also decreased significantly by WSM3-KF combination earlier that of the other schemes. It has been observed that the CWMR increased up to 0000 UTC of 28 April and 1200 UTC of 28 April by Lin, Ferrier, WSM6 scheme and Kessler, Thompson scheme

respectively coupling with BMJ scheme after that the CWMR decreased significantly in region D4. Since the intensity of TC has also not increased significantly the CWMR has not increased sufficient time for different MP schemes in combination with BMJ scheme of TC Mala. The CWMR has decreased since 1200 UTC of 27 April by WSM3-BMJ combination the MSLP simulated values and MWS at 10 m level also simulated lower out of all combinations. As the track of the TC Mala deviated towards right from the observed track, the WSM3-BMJ combination simulated minimum CWMR out of all combinations.

Figure 4.1.3: Simulated CWMR with the progression of time using different MP schemes coupling with KF and BMJ schemes of TC 'Mala' at region D4.
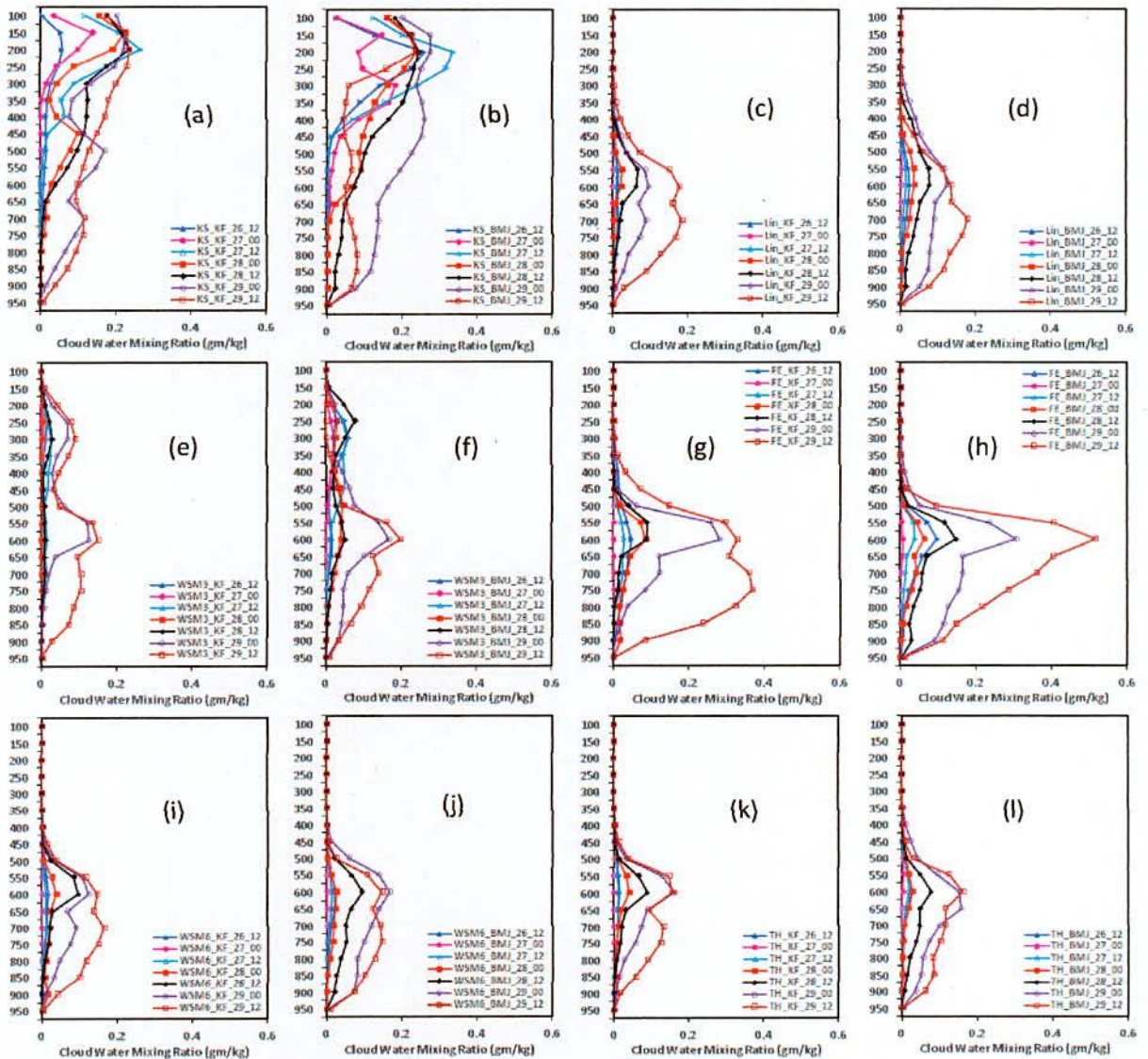
Figure 4.1.4: Simulated CWMR with the progression of time using different MP schemes coupling with KF and BMJ schemes of TC 'Mala' at region D5.

Vertical profiles of area averaged CWMR (gm/kg) at different times 0000 UTC of 27, 28, 29 and 1200 UTC of 26, 27, 28 and 29 April 2006 has been analyzed in region D5 by using six different MP schemes coupling with KF and BMJ schemes as shown in Figure 4.1.4 (a-l). Kessler and WSM3 schemes coupling with KF and BMJ schemes have simulated CWMR up to 100 hPa. All other MPs coupling with KF and BMJ schemes have simulated CWMR up to 400 hPa level. Kessler and WSM3 schemes coupling with KF and BMJ schemes have simulated two maxima of CWMR one at 500 & 600 hPa and another one at 200 & 250 hPa

respectively. Lin, Ferrier, WSM6 and Thompson schemes in combination with KF and BMJ schemes has simulated maximum CWMR at 750–600 hPa levels. Vertical profiles of area averaged profiles of CWMR for all MP schemes coupling with KF and BMJ schemes are almost constant and zero from 350-100 hPa level. The CWMR decreased in region D5 on 0000 UTC of 27 with respect to that of 1200 UTC of 26 April after that it has increased continuously up to the landfall time. The intensity of TC has changed continuously from CS to VSCS since 0000 UTC of 27 April to 1200 UTC of 28 April; the CWMR has also increased significantly during this time at 900-400 hPa level. It is observed that the CWMR has increased in region D5 as the TC moves towards that region. The CWMR increased up to 1200 UTC 29 April in region D5 i.e. also after the landfall. Ferrier scheme has simulated maximum CWMR and Thompson scheme has simulated minimum CWMR at mid troposphere. BMJ scheme has simulated much higher CWMR than that of KF scheme in combination with different MP schemes in region D1, but their magnitude is not significant (Figure not shown). As the time progress, the TC moves towards northeast direction and the CWMR has decreased in region D1. It indicates that the cyclone has not moved in this direction. Except Kessler, all MPs coupling with KF and BMJ schemes have simulated small peak of CWMR at around 550 hPa levels but at the other level the CWMR shows zero value in regions D2 and D3. BMJ scheme has simulated higher CWMR than that of KF scheme in combination with different MP schemes in regions D2 and D3, but their magnitude is not significant (Figure not shown). Since almost there is no change of CWMR, the cyclone has not moved in those directions.

4.1.5 Cloud Rain Water Mixing Ratio (RWMR)

The vertical profiles of area averaged RWMR (gm/kg) at different times 0000 UTC of 27, 28, 29 and 1200 UTC of 26, 27, 28 and 29 April 2006 has been analyzed in region D4 by using six different MP schemes coupling with KF and BMJ schemes as shown in Figure 4.1.5 (a-l). Kessler and WSM3 schemes has simulated RWMR up to 150 and 100 hPa respectively and the other MPs has simulated up to 500 hPa level coupling with KF and BMJ schemes. The maximum RWMR has been simulated at 450 hPa level by WSM3 scheme coupling with KF and BMJ scheme. The intensity of TC has changed continuously from CS to VSCS since 1200 UTC of 26 April to 0000 UTC of 29 April; the RWMR has also increased significantly during

41

this time at 900-500 hPa level by Lin, WSM6 and Thompson schemes coupling with KF scheme. The patterns of rain water profile are similar up to 500 hPa levels with Lin, FE, WSM6 and Thompson schemes coupling with KF and BMJ schemes. The RWMR decreased after 1200 UTC of 28 April by using KS-KF, WSM3-KF and Ferrier-KF combinations. Due to the significant increase of pressure fall and wind speed up to 1200 UTC of 28 April by KS, WSM3, Ferrier schemes and 0000 UTC of 29 April by Lin, WSM6 and Thompson the RWMR has increased.
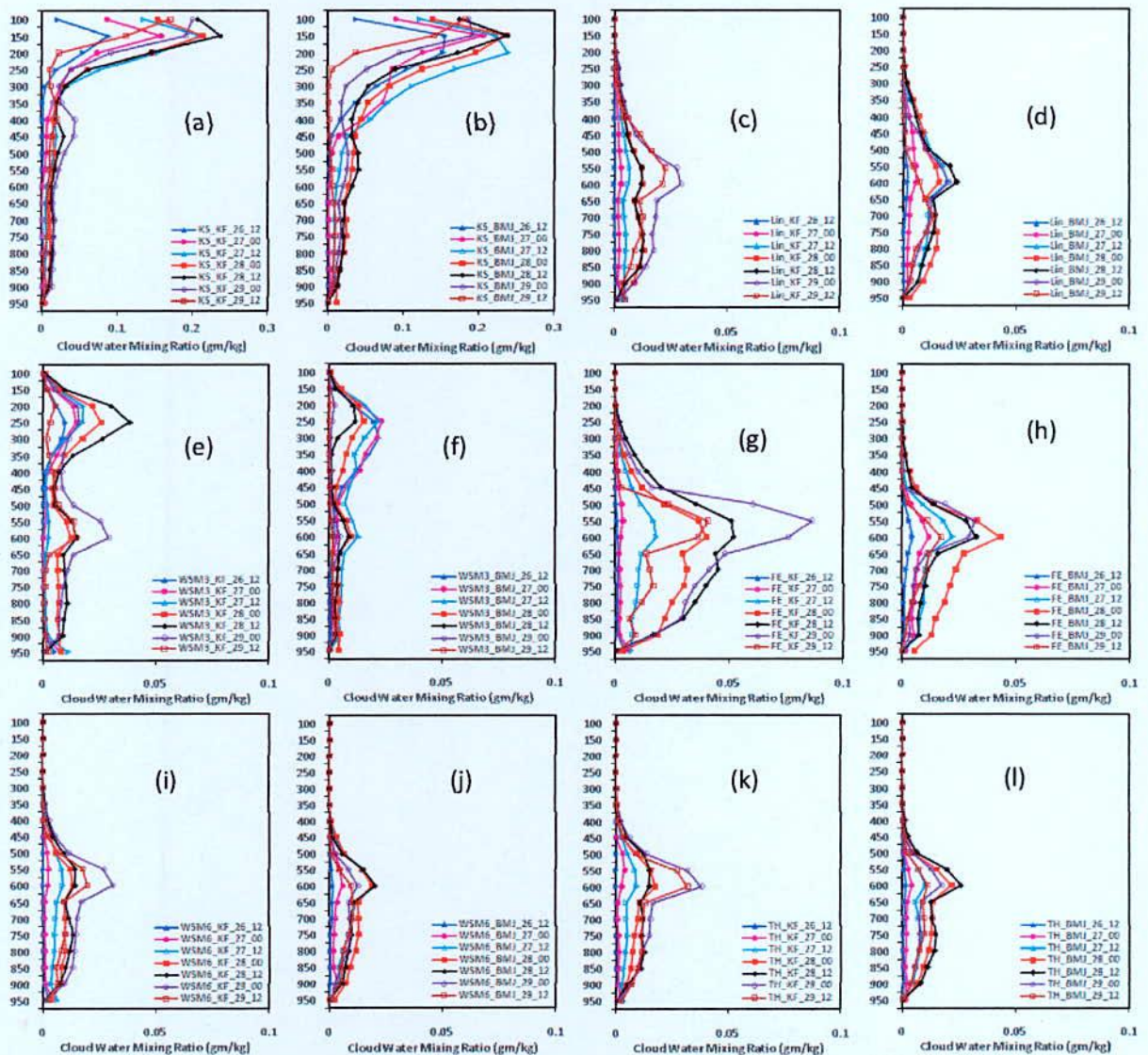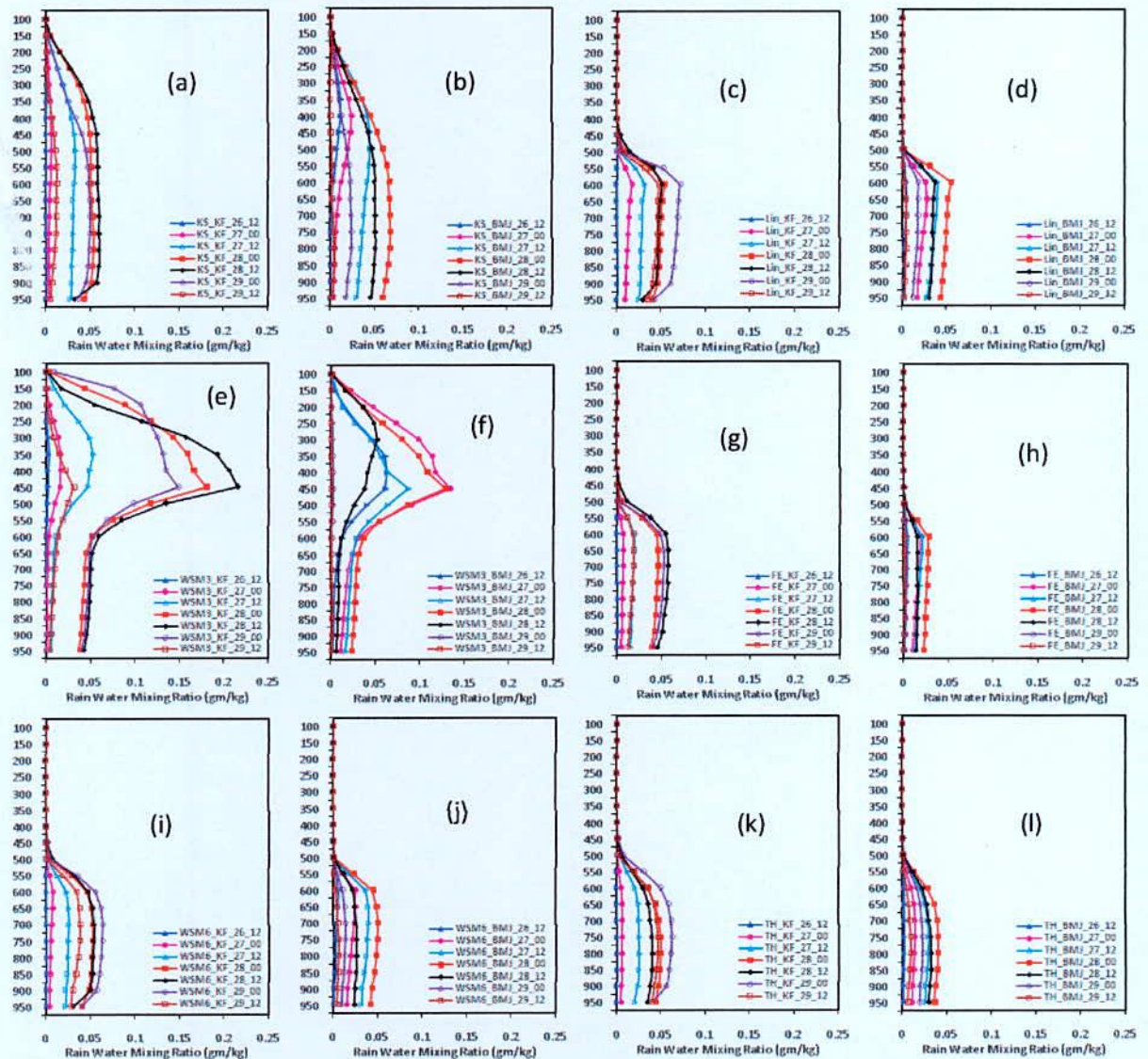

Figure 4.1.5: Simulated RWMR with the progression of time using different MP schemes coupling with KF and BMJ schemes of TC 'Mala' at region D4.
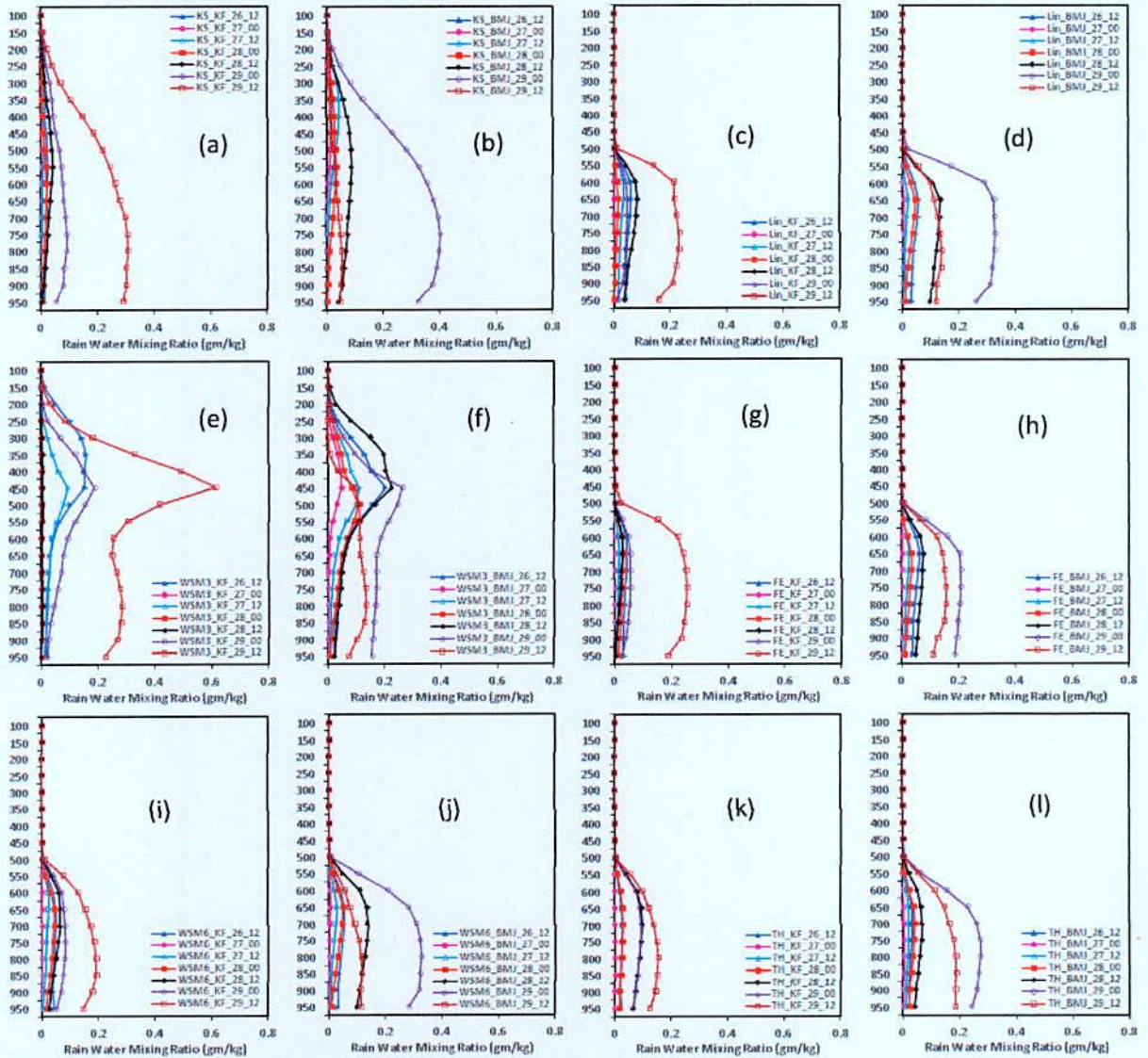
Figure 4.1.6: Simulated RWMR with the progression of time using different MP schemes coupling with KF and BMJ schemes of TC 'Mala' at region D5.

The RWMR has decreased since 0000 UTC of 28 April by all MPs coupling with BMJ scheme. Since TC Mala could not intensify similarly as observed by using all MPs coupling with BMJ scheme the RWMR decreased earlier. In this respect, the simulated MSLP and MWS at 10 m level have minimum values. The average maximum RWMR have been simulated by Kessler-BMJ, WSM3-KF, WSM3-BMJ, WSM6-KF and Lin-KF at 800, 450, 450, 700 and 600 hPa level are 0.06, 2.2, 1.5, 0.06 and 0.07 gm/kg (Fig. 4.1.5) respectively. WSM3-KF combination has simulated maximum and FE-BMJ combination has simulated

minimum area averaged RWMR from 950–500 hPa level. Vertical profiles of area averaged profiles of RWMR for Lin, Ferrier,WSM6 and Thompson schemes coupling with KF and BMJ schemes are almost constant and zero from 500-100 hPa level.

Vertical profiles of area averaged RWMR (gm/kg) at different times 0000 UTC of 27, 28, 29 and 1200 UTC of 26, 27, 28 and 29 April 2006 has been analyzed in region D5 by using six different MP schemes coupling with KF and BMJ schemes as shown in Figure 4.1.6 (a-l). RWMR simulated by Kessler and WSM3 schemes coupling with KF and BMJ schemes up to 150 hPa. All other MPs coupling with KF and BMJ schemes have simulated RWMR up to 500 hPa level. The maximum RWMR has simulated at 450 hPa level by WSM3 scheme coupling with KF and BMJ schemes. After decreasing the RWMR in region D5 on 0000 UTC of 27 with respect to that of 1200 UTC of 26 April by all MPs coupling with KF scheme then the RWMR has increased up to 1200 UTC of 29 April i.e. after the landfall also. Vertical profiles of area averaged profiles of RWMR for Lin, Ferrier, WSM6 and Thompson schemes coupling with KF and BMJ schemes are almost constant and zero from 500-100 hPa level. For BMJ scheme it increased up to 0000 UTC of 29 April and decreased at 1200 UTC of 29 April. As the time progress the RWMR has increased in region D5 for all MP schemes coupling with KF and BMJ schemes the TC Mala moves towards region D5 i.e. in Myanmar coast. This indicates that the RWMR has increased in a region where the TC moves.

BMJ scheme has simulated higher RWMR than that of KF scheme in combination with different MP schemes in region D1, D2 and D3 but their magnitude is not significant (Figure not shown). All MPs coupling with KF and BMJ schemes have simulated small peak of RWMR at around 650 hPa but at the other levels the vertical profiles of RWMR shows zero value in regions D1, D2 and D3. The RWMR has not been simulated so much in region D1, D2 and D3 but as the progression of time it has decreased. Due to the decrease of RWMR in region D1, D2 and D3 the TC Mala has not moved in those regions.

4.1.6 Cloud Ice Mixing Ratio

In regions D4 and D5, the vertical profiles of area averaged CIMR (gm/kg) at different times 0000 UTC of 27, 28, 29 and 1200 UTC of 26, 27, 28 and 29 April 2006 has been simulated by Lin et al., WSM6 and Thompson schemes coupling with KF and BMJ schemes are presented

in Figure 4.1.7 (a-d) and Figure 4.1.7 (e-h) respectively. Lin *et al.* and WSM6 schemes have simulated maximum cloud ice mixing ratio around at 250 hPa and Thompson scheme has simulated maximum cloud ice mixing ratio at 150 hPa. WSM6 profile exhibits a prominent spike containing much larger cloud ice mixing ratio values between 550 to 100 hPa and Thompson scheme has simulated less cloud ice mixing ratio than that of other schemes.

Figure 4.1.7: Simulated CIMR with the progression of time using different MP schemes coupling with KF and BMJ schemes of TC 'Mala' at region (a-d) D4 & (e-h) D5 respectively.

Thompson scheme in combination with KF and BMJ schemes have simulated much smaller amount of ice, concentrated at 250–100 hPa. Lin scheme has simulated cloud ice between 350–100 hPa levels. The area averaged profiles of CIMR for Lin, WSM6 and Thompson schemes coupling with KF and BMJ schemes are almost constant and zero from 950-400, 950-600 and 950-250 hPa level respectively. As the intensity of TC has increased continuously from CS to VSCS the CIMR has also increased significantly during 0000 UTC of 26 April to 1200 UTC of 28 April by Lin, WSM6 and Thompson schemes coupling with KF scheme. The CIMR decreased after 1200 UTC of 28 and 27 April by using Lin, WSM6 and Thompson

schemes coupling with KF and BMJ schemes respectively. As the intensity of TC Mala has increased with time progression, the vertical profiles of CIMR has also increased up to 1200 UTC of 28 April by Lin-KF, WSM6-KF and Thompson-KF combinations. Since for BMJ combination TC Mala could not intensify properly the CIMR has also decreased earlier. Lin *et al.* and WSM6 schemes have simulated maximum cloud ice around 300 hPa and Thompson scheme has simulated maximum ice at 150 hPa level. Lin *et al.*, WSM6 and Thompson schemes exhibit a prominent spike containing much larger cloud ice mixing ratio values between 400-100 hPa, 600-100 hPa and 300–100 hPa respectively. Thompson scheme has simulated less cloud ice mixing ratio than that of other schemes. The CIMR has increased at day and decreased at night for Lin, WSM6 and Thompson schemes coupling with KF and BMJ schemes except at 0000 UTC of 29 April when CIMR has increased by using BMJ scheme. CIMR has changed in region D5 as the propagation of TC in that direction.

The minimum CIMR has been simulated in regions D1, D2 and D3 by Lin *et al.*, WSM6 and Thompson schemes coupling with KF and BMJ schemes (Figure not shown) respectively. WSM6 scheme has simulated higher CIMR than that of Lin and Thompson scheme coupling with KF and BMJ schemes in region D1, D2 and D3. Lin *et al.*, WSM6 and Thompson schemes coupling with KF and BMJ schemes have simulated small peak of CIMR at around 200 hPa but at the other levels the CIMR shows zero value in regions D1, D2 and D3. With the progression of time the CIMR has decreased in region D1, D2 and D3 and TC Mala moves towards region D5. It indicates that the CIMR has increased in that direction where the cyclone moves.

4.1.7 Cloud Snow Mixing Ratio

In region D4 (i.e. in the oceanic region), the vertical profiles of area averaged CSMR (gm/kg) at different times i.e. 0000 UTC of 27, 28, 29 and 1200 UTC of 26, 27, 28 and 29 April 2006 has been simulated by Lin, Ferrier, WSM6 and Thompson schemes coupling with KF and BMJ schemes are presented in Figure 4.1.8 (a-h). It is seen from the figure that the vertical structure and magnitude of these profiles vary greatly. Ferrier, WSM6 and Thompson schemes have simulated maximum cloud snow around 350 hPa. Generally, the Thompson scheme has generated the highest amount of cloud snow between 600 to 100 hPa as compared to that of

other schemes. Lin scheme has simulated almost no CSMR. The abundance of snow in the mid troposphere (below 400 hPa) may be due to the improved ice content in the upper troposphere. The vertical profiles of area averaged profiles of CSMR for Ferrier, WSM6 and Thompson schemes coupling with KF and BMJ schemes are almost constant and zero at 600 hPa level. The intensity of TC has changed continuously from CS to VSCS since 1200 UTC of 26 to 29 April and the CSMR has also increased significantly during this time by Ferrier, WSM6 and Thompson schemes coupling with KF and BMJ schemes in region D4. The patterns of cloud snow profile are similar to upper level with Ferrier, WSM6 and Thompson schemes coupling with KF and BMJ schemes. The CSMR is found to decrease after 1200 UTC of 28 April by using Ferrier-KF, WSM6-KF and Thompson-KF combinations. Since the intensity of TC Mala has increased significantly in terms of pressure fall and wind speed, the CSMR has increased up to 1200 UTC of 28 April by Ferrier-KF, WSM6-KF and Thompson-KF combinations. The CSMR has decreased since 0000 UTC of 28 April by all MPs coupling with BMJ scheme.
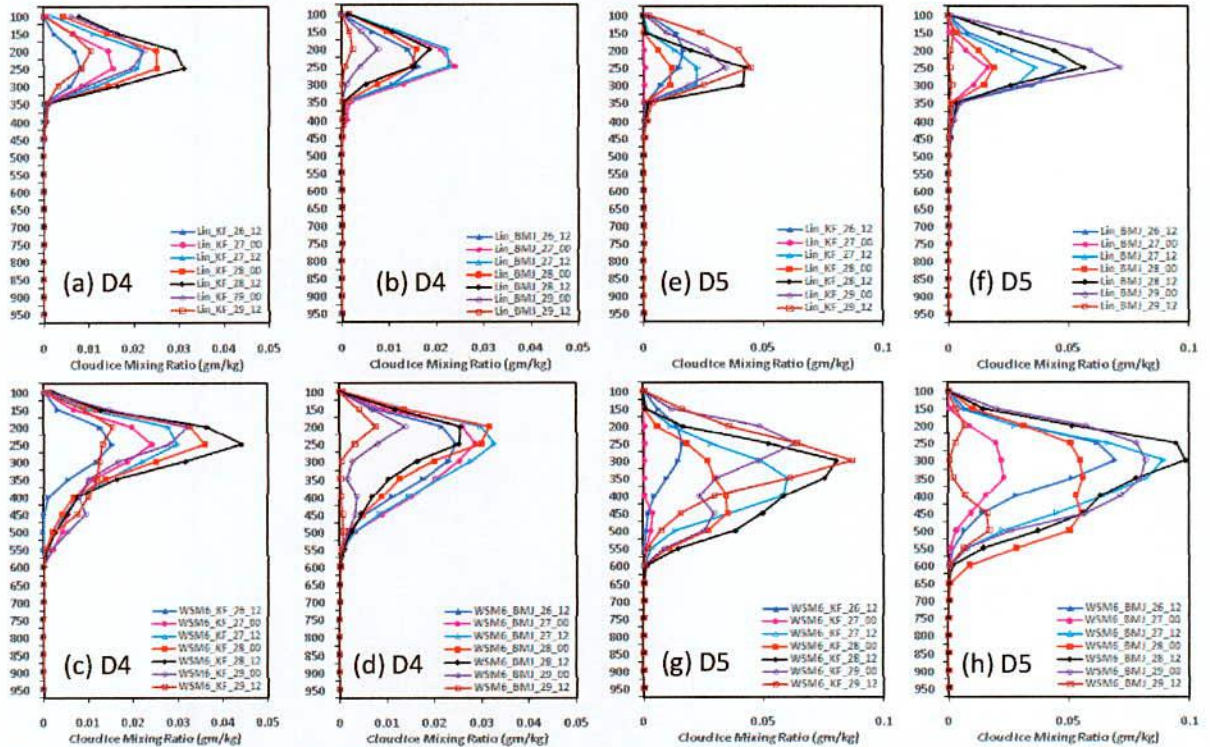

Figure 4.1.8: Simulated CSMR with the progression of time using different MP schemes coupling with KF and BMJ schemes of TC 'Mala' at region D4.

As the TC Mala could not intensify similarly as observed the CSMR decreased early in BMJ combination. In this respect, the terms of pressure fall and MWS at 10 m level have simulated minimum CSMR. In region D5 (i.e. Myanmar), the vertical profiles of area averaged CSMR (gm/kg) at different times i.e. 0000 UTC of 27, 28, 29 and 1200 UTC of 26, 27, 28 and 29 April 2006 has been simulated by Lin, Ferrier, WSM6 and Thompson schemes coupling with KF and BMJ schemes are presented in Figure 4.1.9 (a-h). It is marked from the figure that the vertical structure and magnitude of these profiles differ significantly. Overall, the Thompson scheme has generated the maximum amount of snow between 650 to 100 hPa.

Figure 4.1.9: Simulated CSMR with the progression of time using different MP schemes coupling with KF and BMJ schemes of TC 'Mala' at region D5.

Vertical profiles of area averaged profiles of CSMR for above mentioned combinations are almost zero from surface to 650 hPa level. BMJ scheme has simulated greater snow than that of KF scheme in combination with Lin, Ferrier, WSM6 and Thompson schemes. The plethora of snow in the mid troposphere (below 400 hPa) may be due to the improved ice content in the higher troposphere. The CSMR has increased continuously in region D5 since 0000 UTC of

27 to 0000 UTC of 29 April (i.e. before the landfall) by Lin, Ferrier, WSM6 and Thompson scheme coupling with KF and BMJ schemes and TC Mala also moves towards this region. This indicates that the TC moves in a region where the CSMR has increased.

The CSMR has simulated for Lin *et al.*, Ferrier, WSM6 and Thompson schemes coupling with KF and BMJ schemes. BMJ scheme has simulated higher CSMR than that of KF scheme in combination with different MP schemes in region D1, D2 and D3 but their magnitude is not significant (Figure not shown). With the progress of time the TC moves towards region D5 and the CSMR has decreased in region D1, D2 and D3. Lin, Ferrier, WSM6 and Thompson schemes coupling with KF and BMJ schemes have simulated small peak of CSMR at around 650-300 hPa but the other level the CSMR shows zero value in regions D1, D2 and D3. Since there is no change of CSMR in the mid troposphere of region D1, D2 and D3, the cyclone has not moved in those directions.

4.1.8 Cloud Graupel Mixing Ratio

In region D4, the vertical profiles of area averaged CGMR (gm/kg) at different times 0000 UTC of 27, 28, 29 and 1200 UTC of 26, 27, 28 and 29 April 2006 by Lin *et al.*, WSM6 and Thompson schemes coupling with KF and BMJ schemes has presented in Figure 4.1.10 (a-d). Lin *et al.*, WSM6 and Thompson schemes have produced the maximum amount of CGMR at around 500 hPa levels. It is evident from the figure that the vertical structure and magnitude of these profiles vary greatly. The WSM6 scheme has simulated higher CGMR and Thompson scheme has simulated lower but insignificant amount of CGMR than that of Lin *et al.* scheme. Graupel starts to produce at 650 hPa and sharp spike are found at 500 hPa levels in case of Lin *et al.* and WSM6 and then decreases to minimum at 100 hPa. KF scheme coupling with all MP schemes has simulated larger CGMR than that of BMJ scheme. The intensity of TC has changed continuously from CS to VSCS since 1200 UTC of 26 April to 0000 UTC of 29 April the CGMR has also increased significantly during this time by Lin and WSM6 schemes coupling with KF scheme. The patterns of cloud graupel profile are similar to upper level with Lin and WSM6 schemes coupling with KF and BMJ schemes. Due to the progression of time the intensity of TC Mala has increased in terms of pressure fall and wind speed, the vertical profiles of CGMR has also increased up to 0000 UTC of 29 April by Lin-KF and WSM6-KF

49

combinations. But in BMJ combinations (Lin *et al.*, WSM6 and Thompson) the vertical profiles of CGMR has increased up to 0000 UTC of 28 April and after that it has decreased up to 1200 UTC of 29 April.
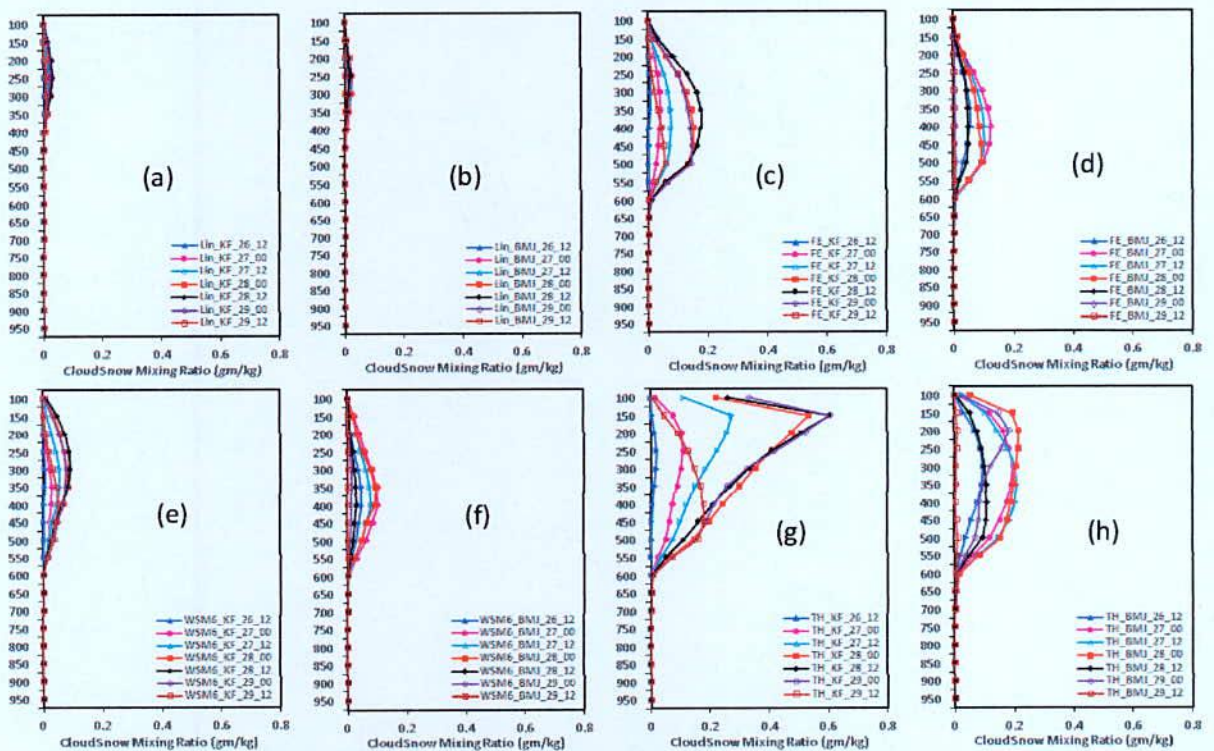

Figure 4.1.10: Simulated CGMR with the progression of time using different MP schemes coupling with KF and BMJ schemes of TC 'Mala' at region (a-d) D4 & (e-h) D5 respectively.

In region D5, the vertical profiles of area averaged CGMR (gm/kg) at different times 0000 UTC of 27, 28, 29 and 1200 UTC of 26, 27, 28 and 29 April 2006 by Lin *et al.*, WSM6 and Thompson schemes coupling with KF and BMJ schemes is presented in Figure 4.1.10 (e-h). Lin *et al.*, WSM6 and Thompson schemes have simulated maximum CGMR at around 500 hPa levels. The Lin and WSM6 scheme has simulated higher CGMR and Thompson scheme has simulated lower but insignificant CGMR. Graupel starts to produce at 650 hPa and sharp spike are found at 500 hPa levels in case of Lin *et al.* and WSM6 and then decreases to minimum at 100 hPa. BMJ scheme has simulated larger CGMR than that of KF scheme for Lin *et al.* and WSM6 schemes. After decreasing the CGMR in region D5 on 0000 UTC of 27 with respect to that of 1200 UTC of 26 April by Lin *et al.* and WSM6 coupling with KF and

BMJ schemes then the CGMR has increased up to 0000 UTC of 29 April i.e. before the landfall but in case of Lin-KF combination the CGMR has decreased at 0000 UTC of 27, 28 and 29 April than that of previous 1200 UTC. As the time progress the CGMR has increased in region D5 (i.e. Myanmar region) for Lin *et al.* and WSM6 schemes coupling with KF and BMJ schemes and also the TC Mala moves towards this region. It indicates that CGMR increased with the increase in intensity of TC and over the area where the TC Mala moves in region D5.

The simulated CGMR has not significant for Lin, WSM6 and Thompson schemes coupling with KF scheme in region D1, D2 and D3. BMJ scheme has simulated higher CGMR than that of KF scheme in combination with Lin, WSM6 and Thompson schemes in region D1, D2 and D3 but the amount is not significant (Figure not shown). As the progression of time the TC moves towards region D5 and the CGMR has decreased in region D1, D2 and D3. Lin, WSM6 and Thompson schemes coupling with KF and BMJ schemes have simulated small peak of GMR at around 700 to 300 hPa but the other level the CGMR has not shown any value in regions D1, D2 and D3. Since almost there is no change of CGMR, the cyclone was not moving in those directions.

4.1.9 Cloud Water Vapor Mixing Ratio

The vertical profiles of area averaged WVMR (gm/kg) at different times 0000 UTC of 27, 28, 29 and 1200 UTC of 26, 27, 28 and 29 April 2006 has been analyzed in region D4 by using six different MPs coupling with KF and BMJ schemes as shown in Figure 4.1.11 (a-l). The WVMR are similar up to 200 hPa levels with all MPs coupling with KF and BMJ schemes in this region. The maximum WVMR have been simulated and WVMR is approximately equal at the surface and decreased continuously with height for all MPs coupling with KF and BMJ schemes. It has been observed that the WVMR is almost constant but after 1200 UTC of 28 April simulated by all MPs coupling with KF and BMJ schemes the WVMR decreased significantly in region D4.

Vertical profiles of area averaged WVMR (gm/kg) at different times 0000 UTC of 27, 28, 29 and 1200 UTC of 26, 27, 28 and 29 April 2006 has been analyzed in region D5 by using six different MP schemes coupling with KF and BMJ schemes as shown in Figure 4.1.12 (a-l).

The patterns of WVMR are similar up to 200 hPa levels with all MPs coupling with KF and BMJ schemes. The WVMR has maximum at the surface and is found to decrease continuously with height for all MPs coupling with KF and BMJ schemes.
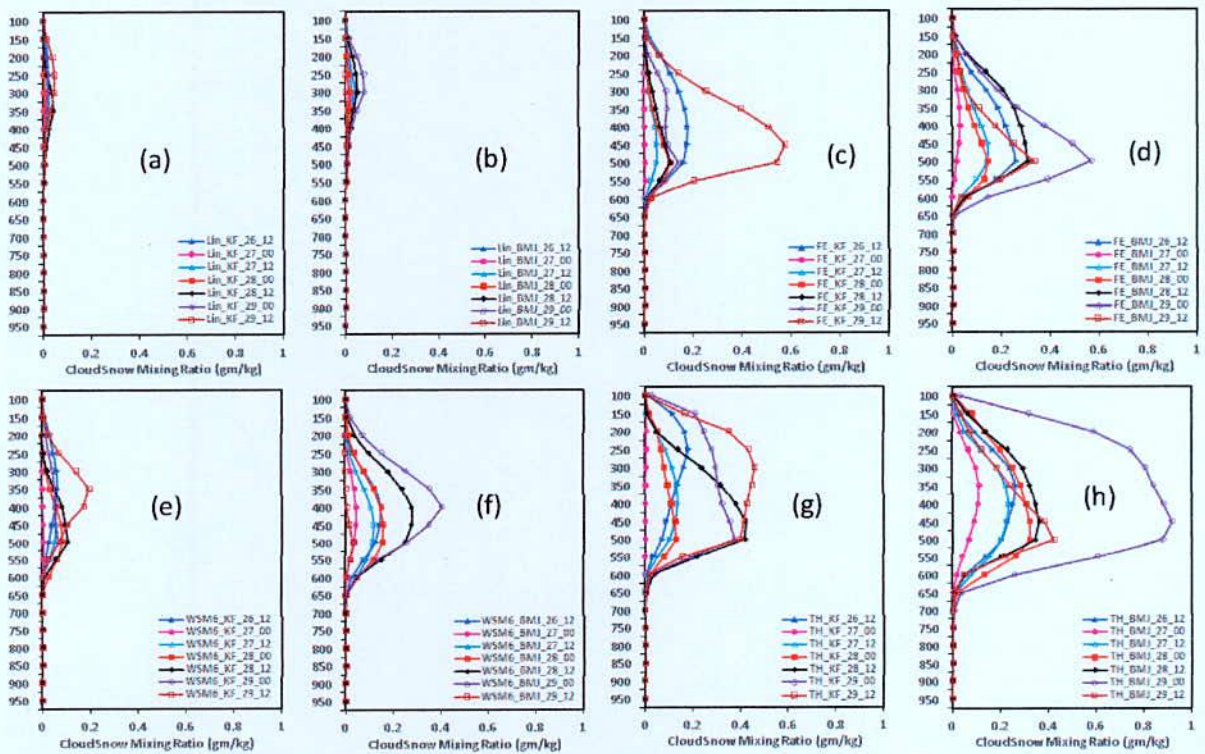

Figure 4.1.11: Simulated WVMR with the progression of time using different MP schemes coupling with KF and BMJ schemes of TC 'Mala' at region D4.

The intensity of TC has changed continuously from CS to VSCS since 0000 UTC of 27 April to 1200 UTC of 28 April and the WVMR has also increased significantly during this time. It is observed that the WVMR has increased in region D5 since 0000 UTC of 27 April to 1200

UTC of 29 April i.e. after the landfall also with respect to that of 1200 UTC of 26 April and TC Mala has moved towards region D5. This indicates that WVMR increased with the increase in intensity of TC Mala over the area where the TC moves.
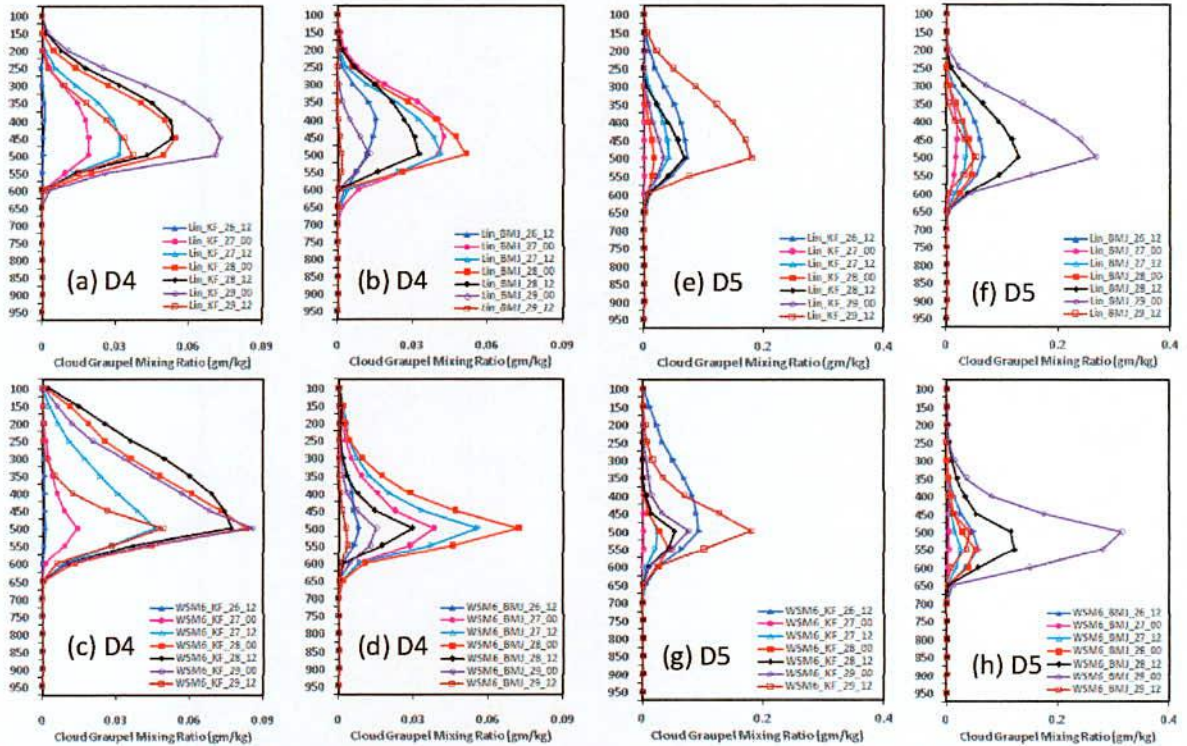

Figure 4.1.12: Simulated WVMR with the progression of time using different MP schemes coupling with KF and BMJ schemes of TC 'Mala' at region D5.

The simulated WVMR is maximum and approximately equal at the surface and decreases continuously with height for all MPs coupling with KF and BMJ schemes in regions D1, D2 and D3 (Figure not shown). It has been observed that the WVMR simulated is almost constant

and zero form 350 hPa to100 hPa and 400 hPa to100 hPa levels in regions D1 and region D2 and D3 respectively for all MPs coupling with KF and BMJ schemes. With the progression of time, the TC moves towards northeast direction and the WVMR has decreased significantly in regions D1 (north), D2 (northwest) and D3 (west).

4.1.10 Relative Humidity

In region D4, vertical profiles of area averaged RH (%) at different times 1200 UTC of 26, 0000 and 1200 UTC of 27, 28 and 29 April 2006 has been presented in Figure 4.1.13 (a-l) for six different MP schemes coupling with KF and BMJ schemes with 0000 UTC of 26 April initial condition. The simulated RH has been found below 80% from surface to 100 hPa levels for all MPs coupling with CP schemes on 28 and 29 April 2006. From figure 4.1.13, it is seen that the simulated RH is minimum at around 300 hPa. KS scheme coupling with KF and BMJ schemes has simulated more than 90% RH from 200 to 100 hPa levels [Figure no. 4.1.13 (a-b)]. It has found that the KS scheme coupling with KF and BMJ schemes have simulated CWMR, RWMR and RH up to 100 hPa level. From the Figure 4.1.13, it is observed that the simulated RH decreases continuously in region D4 from 1200 UTC of 26 April to 0000 UTC of 29 April i.e. before landfall of TC Mala on 0700 UTC of 29 April 2006. The figure also indicates that from the starting time of simulation the RH is found to decrease after the TC has deviated from region D4 to region D5 at Myanmar coast.

In region D5, the vertical profiles of area averaged RH (%) at different times 1200 UTC of 26, 0000 and 1200 UTC of 27, 28 and 29 April 2006 have been presented in Figure 4.1.14 (a-l) for six different MP schemes coupling with KF and BMJ schemes with 0000 UTC of 26 April initial condition. The simulated RH exceeds 80% from surface to 450 hPa levels for all MPs coupling with CP schemes on 28 and 29 April 2006. The sharp peak of RH has been found at 600-500 hPa level for all MPs except KS scheme coupling with CP schemes on 28 and 29 April 2006. KS scheme coupling with KF and BMJ schemes has simulated more than 90% RH from 850 to 100 hPa levels on 28 and 29 April. From Figs. 14 (a-l), it is observed that the simulated RH increases continuously in region 5 from 1200 UTC of 26 April to 0000 UTC of 29 April i.e. before landfall of TC Mala on 0700 UTC of 29 April 2006. The figure also indicates that the RH decreases after landfall of TC at Myanmar coast. This suggests that from

54

the starting time of simulation the RH continuously increases in region D5 and also TC crossed in that region.
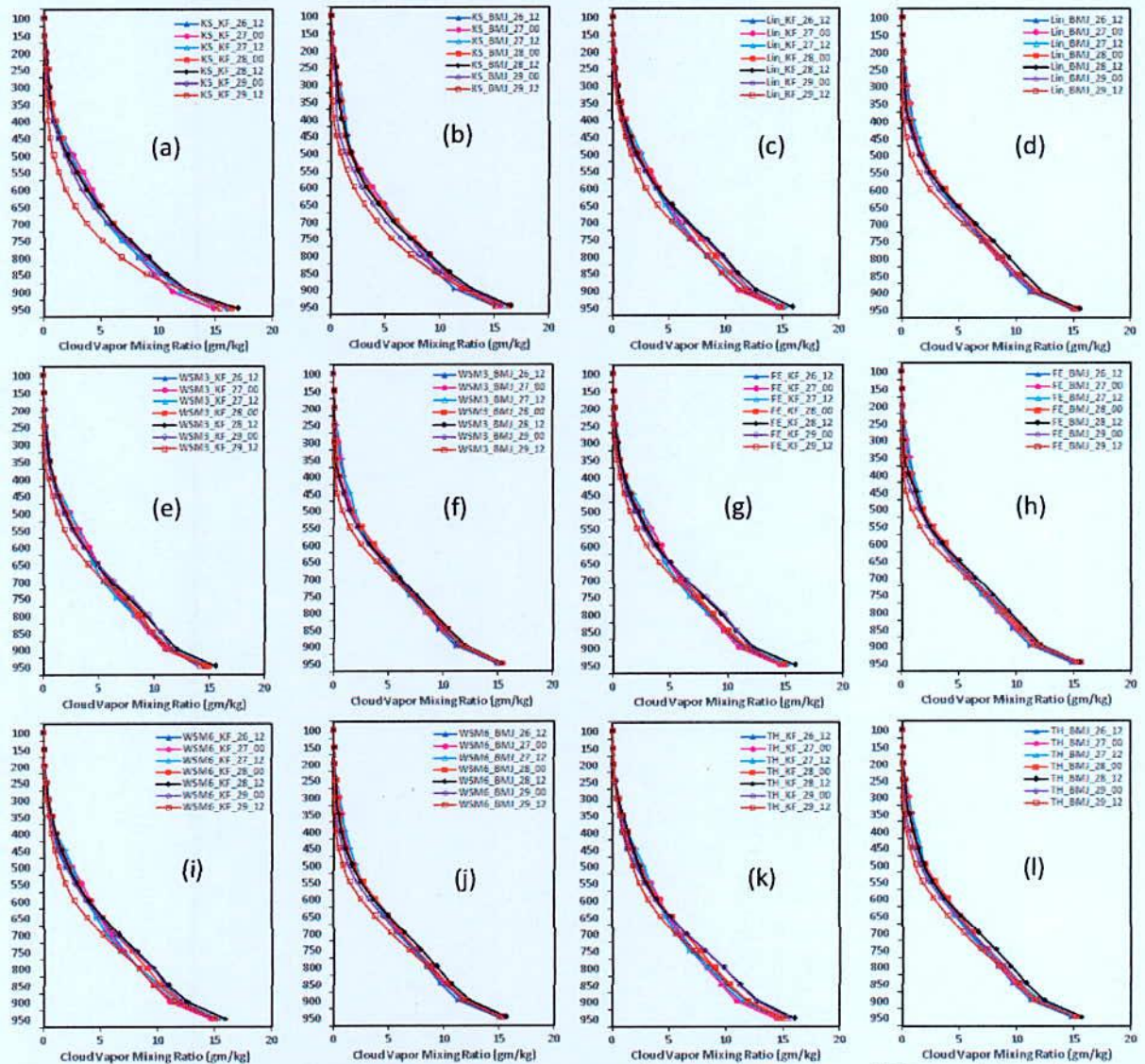

Figure 4.1.13: Simulated RH at region D4 with the progression of time using different MP schemes coupling with KF and BMJ schemes of TC 'Mala'.

The RH simulated has been maximum (above 80%) at the upper level (100 hPa) for Kessler scheme coupling with KF and BMJ schemes over regions D1, D2 and D3 but the simulated RH is below 60% for all MPs coupling with KF and BMJ schemes. It has been observed that the simulated RH is almost constant and is about zero to 10% from 550 hPa to 250 hPa level

55

for all MPs schemes coupling with KF and BMJ schemes over the regions D1, D2 and D3 (Figure not shown). In the upper troposphere the simulated RH has almost zero in regions D1, D2 & D3 (Figure not shown). As the time progresses, the TC moves towards northeast direction and the simulated RH has been minimum in regions D1, D2 and D3. It indicates that the cyclone was not moving in those directions.
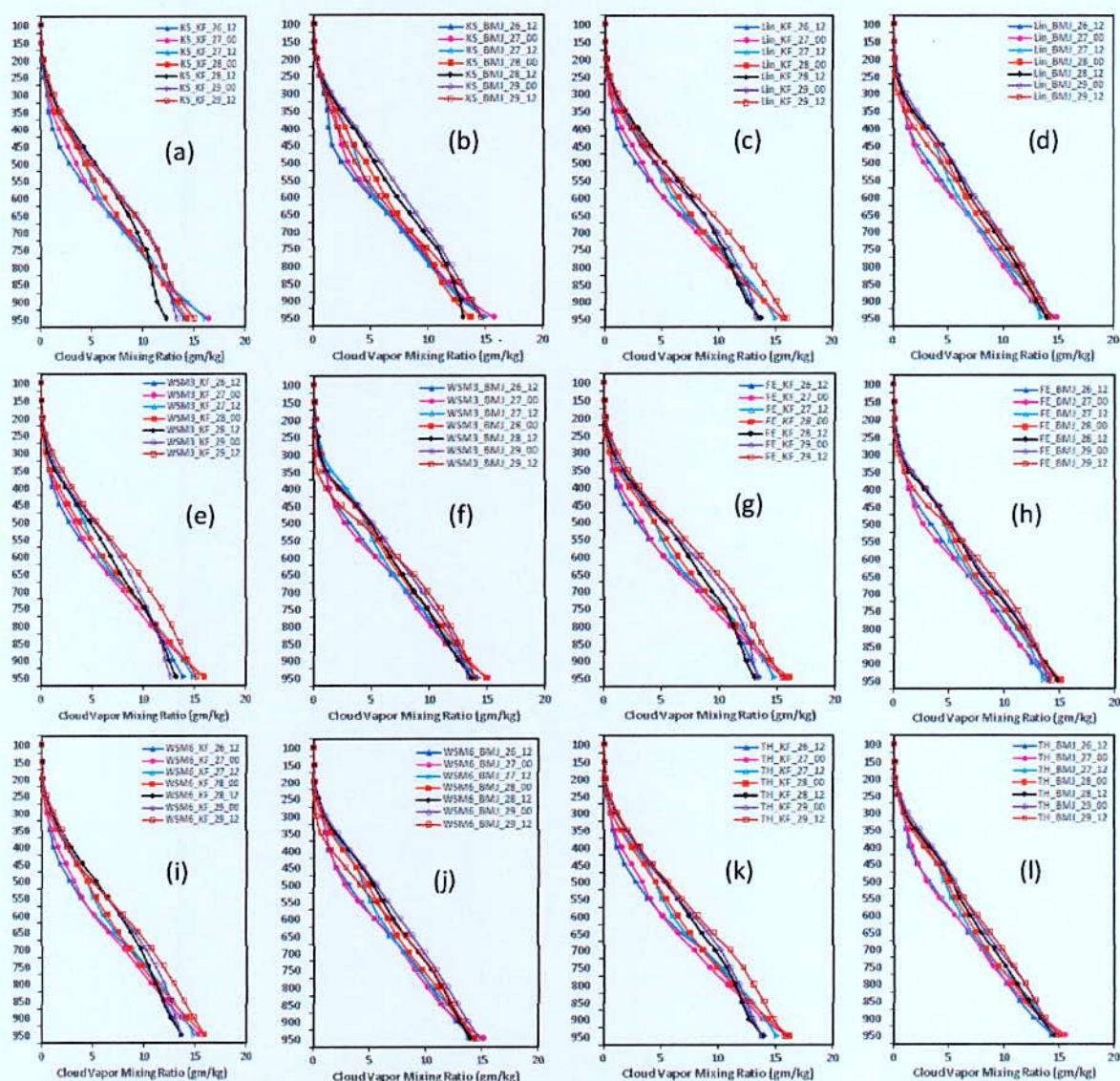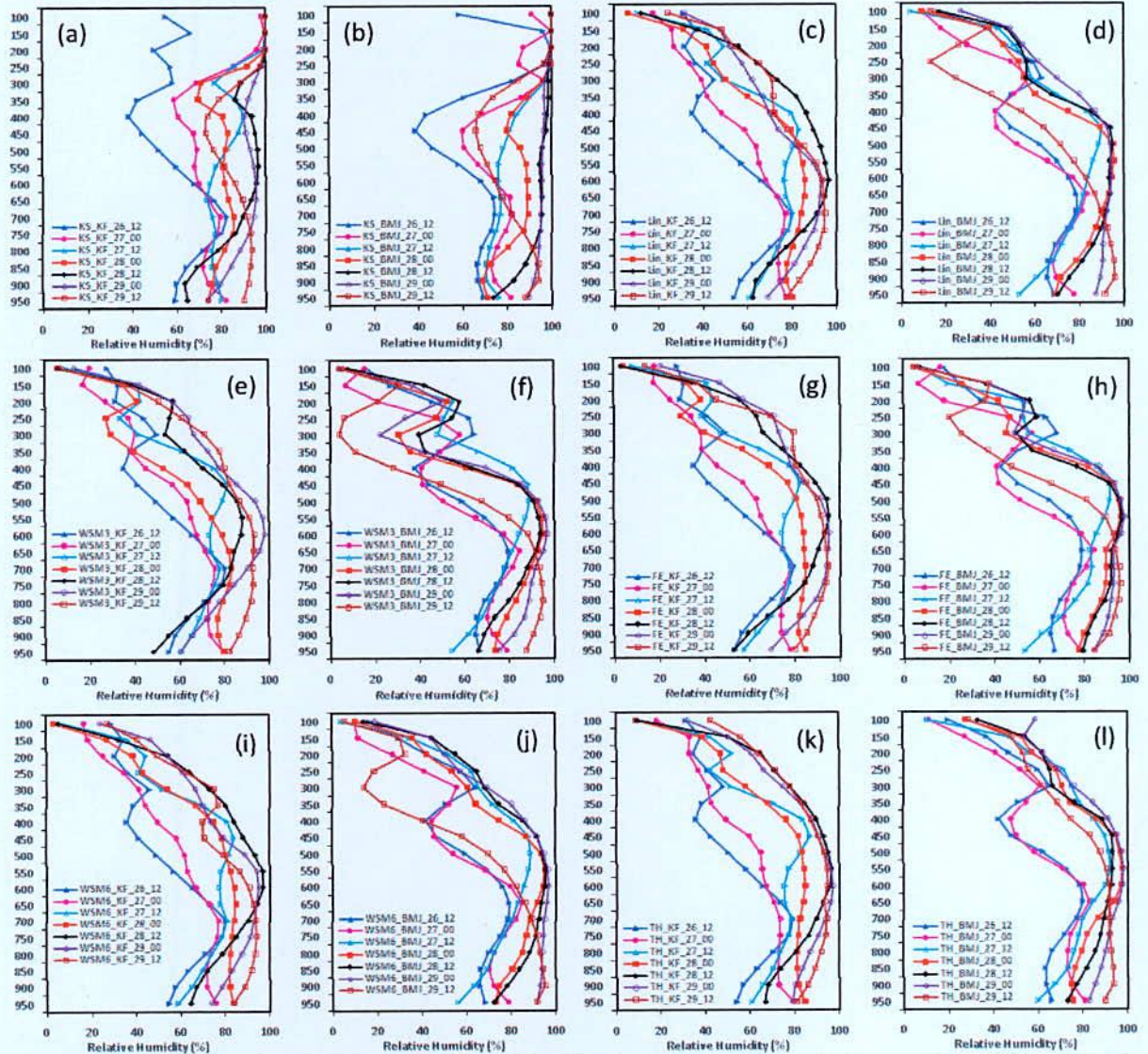

Figure 4.1.14: Simulated RH at region D5 with the progression of time using different MP schemes coupling with KF and BMJ schemes of TC 'Mala'.

4.1.11 Vorticity

The time variations of vertical profiles of space averaged vorticity ($\times 10^{-5}$/s) in region D4, simulated by six different MP schemes coupling with KF and BMJ schemes are presented in Figure 4.1.15 (a-l). The space averaged vorticity are almost constant during 0000–1200 UTC of 26 April for all MP schemes coupling with KF scheme. The positive vorticity has increased continuously since 1200 UTC of 26 April to 0000 UTC of 29 April and after that it has decreased significantly. It indicates that the cyclonic circulation has increased continuously with time and also height. The cyclonic circulation has extended from 950 hPa to 150 hPa levels for all MP schemes in combination with KF scheme during 1200 UTC of 26 April to 0000 UTC of 29 April. Due to significant enhancement of the cyclonic circulation in lower troposphere to upper troposphere, the intensity of TC Mala has increased from CS to VSCS during this time. All through the WSM3-KF has simulated minimum averaged vorticity and Thompson-KF has simulated maximum averaged vorticity. The cyclonic circulation has increased up to 300 hPa for BMJ combination during 1200 UTC of 26 April to 0000 UTC of 28 April and after that the positive vorticity has decreased significantly. Due to the insignificant increase of cyclonic circulation up to 0000 UTC of 28 April, the TC has not intensified so much during that time.

WSM3-BMJ combination has simulated minimum averaged vorticity and Kessler-BMJ has simulated maximum averaged vorticity during the period. After 0000 UTC of 29 April, the vorticity has decreased significantly for all MP schemes in coupling with KF scheme. The intensity of TC has changed continuously from CS to VSCS since 1200 UTC of 26 April to 0000 UTC of 29 April; the vorticity has also increased significantly during this time by all MPs coupling with KF scheme. All the figures show that in region D4, KF scheme has simulated higher vorticity than that of BMJ scheme. The positive vorticity has been simulated after 1200 UTC of 26 April from surface to 300 hPa for all MPs coupling with KF and BMJ schemes. The vorticity has simulated negative from 300 to 100 hPa for all MPs coupling with KF and BMJ schemes. This negative vorticity is due to the anticyclonic flow in the upper trophere. In region D5, the vertical profiles of area averaged (starting from 0000 UTC of 26 April to 1200 UTC of 29 April 2006) vorticity for six MP schemes coupling with KF and BMJ schemes is presented in Figure 4.1.16 (a-l). The negative vorticity has been simulated from

surface to 100 hPa by all MPs coupling with KF and BMJ schemes at 1200 UTC of 26 to 1200 UTC of 27 April. The simulated vorticity is positive and increases significantly on 0000 UTC of 28 April to 1200 UTC of 29 April for all MP schemes in coupling with BMJ scheme. For all MPs coupling with KF and BMJ schemes, the simulated vorticity has maximum at mid tropospheric level.
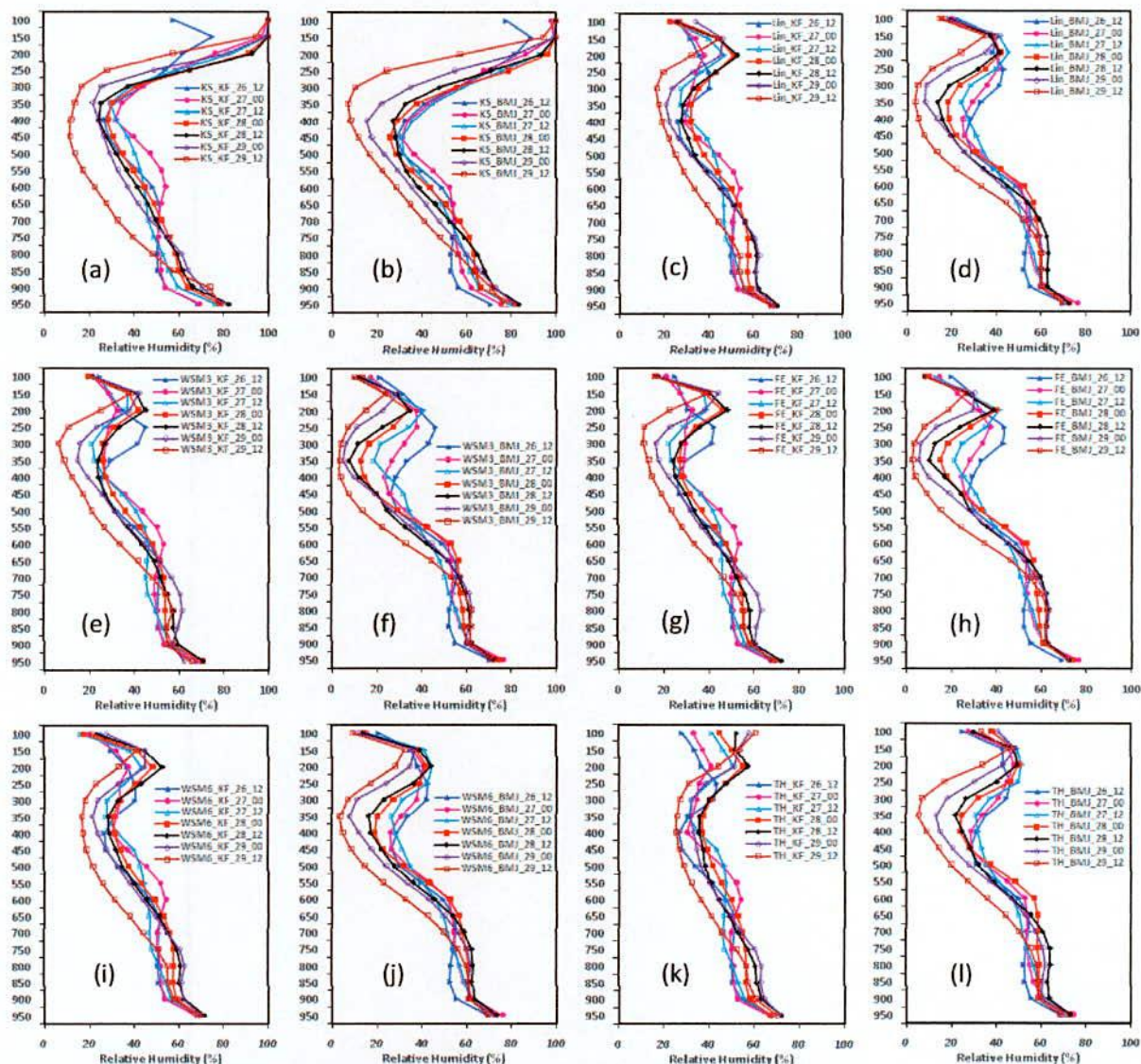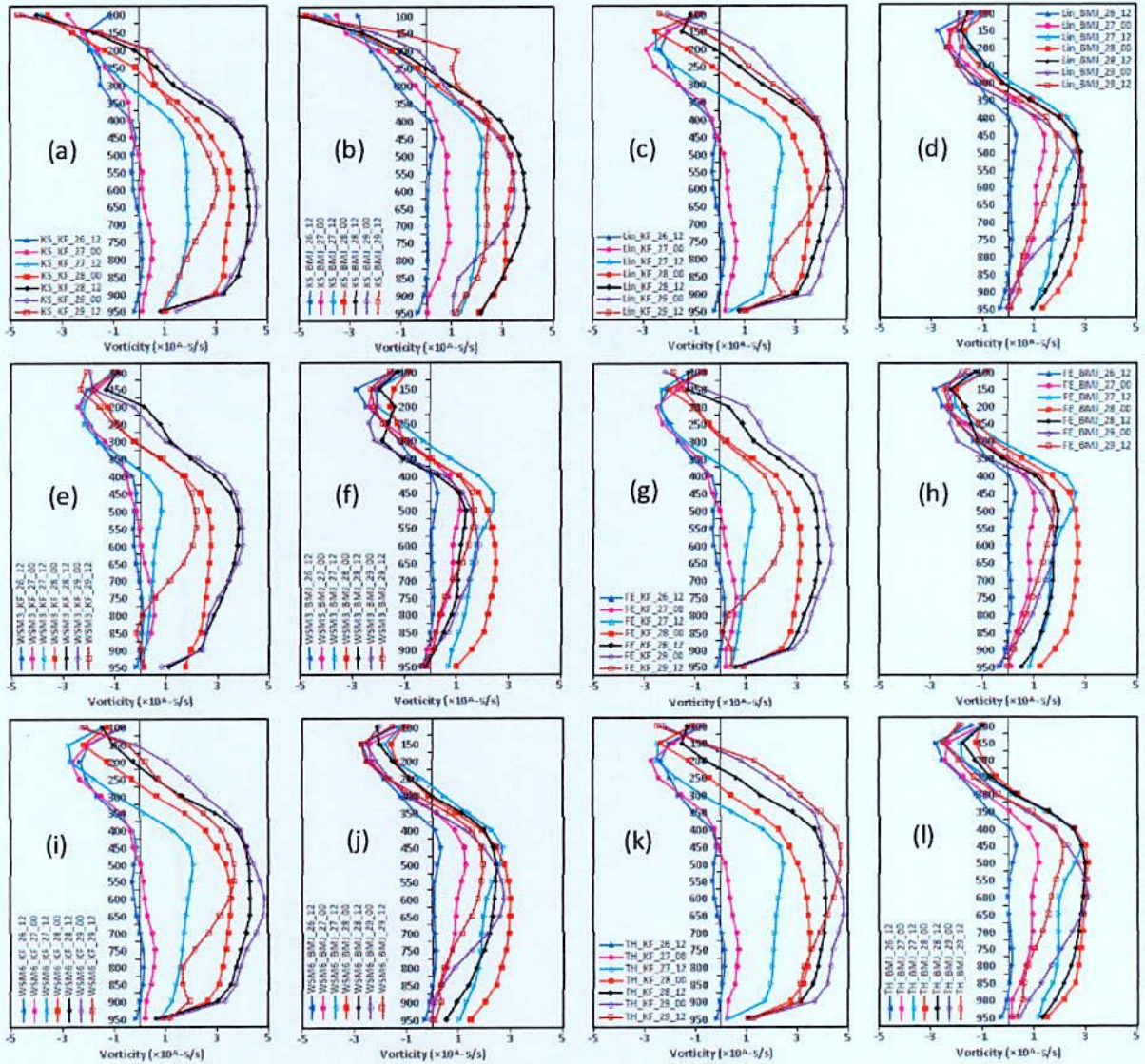

Figure 4.1.15: Simulated vorticity at region D4 with the progression of time using different MP schemes coupling with KF and BMJ schemes of TC 'Mala'.
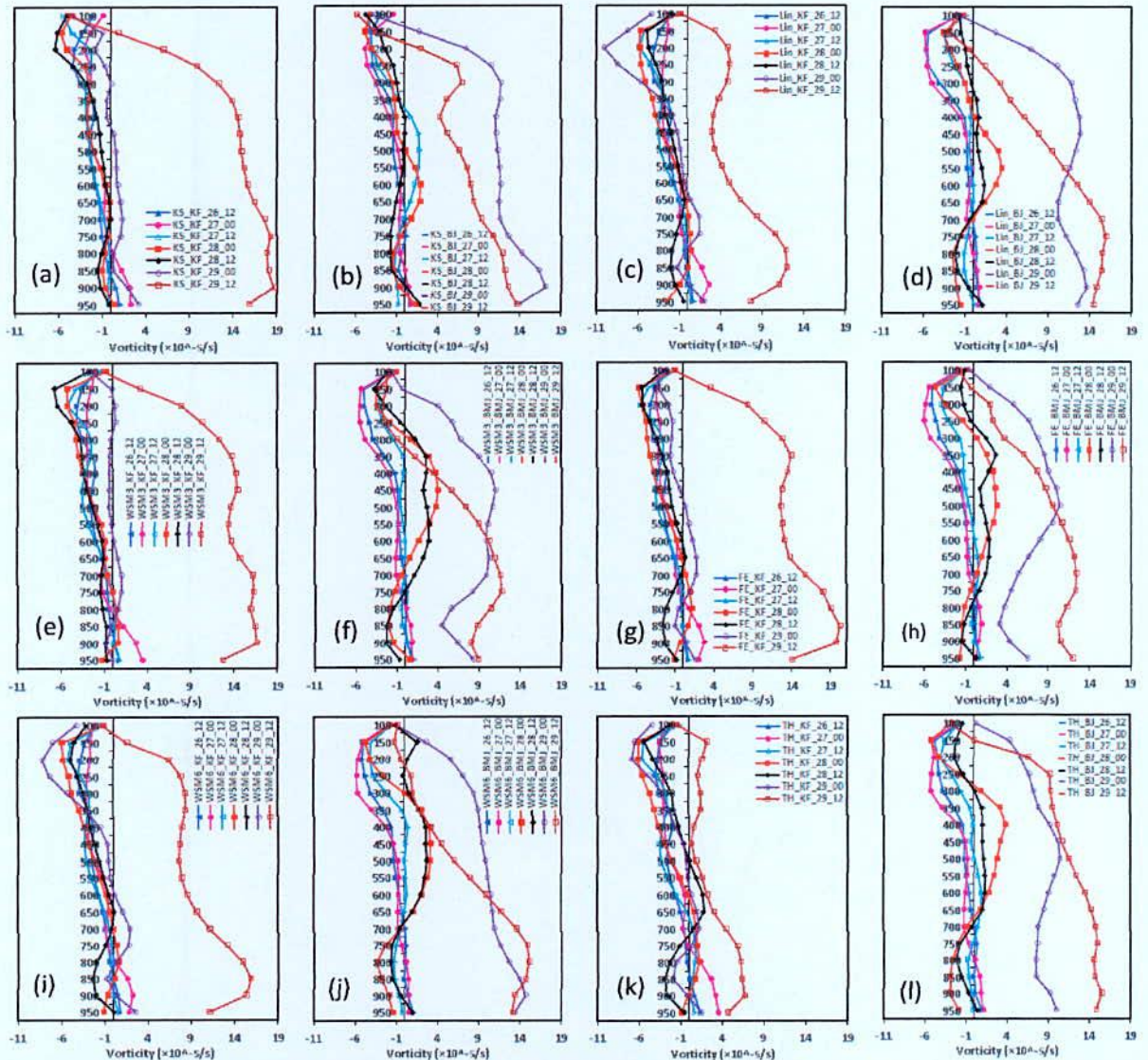
Figure 4.1.16: Simulated vorticity at region D5 with the progression of time using different MP schemes coupling with KF and BMJ schemes of TC 'Mala'.

All through the simulation Ferrier-KF has simulated maximum averaged vorticity and Thompson-KF has simulated minimum averaged vorticity and WSM3-BMJ combination has simulated minimum averaged vorticity and Kessler-BMJ has simulated maximum averaged vorticity during the period. But the general tendency of all the figures, the vorticity has increasing tendency with respect to the initial value. Due to the increasing tendency of vorticity in region D5, it is clear that the TC Mala has moved towards this region. The simulated vorticity in regions D2 and D3 is almost negative and has the same pattern for all

MPs coupling with KF and BMJ schemes (Figure not shown). The vorticity has increased in lower troposphere and decreased in mid to upper troposphere in region D1 for all MPs coupling with KF and BMJ schemes. For all MPs coupling with KF and BMJ schemes in region D2, the vorticity has decreased in lower level and increased in mid to upper level. In region D3, the vorticity shows positive value only at surface level and shows negative value with the very beginning of height but it has increased with respect to initial time. All MPs coupling with KF and BMJ schemes have simulated single peak of vorticity at around 400 hPa in regions D1, D2 and D3. The TC moves towards region D5 and the vorticity decreased in the lower troposphere in regions D2 and D3. It suggests that the cyclone has not moved in a direction where the vorticity has decreased in the lower troposphere.

4.2   Tropical Cyclone Phailin

4.2.1   Synoptic situation of Tropical Cyclone Phailin

A Very Severe Cyclonic Storm (VSCS) Phailin originated from a remnant cyclonic circulation and it lay as a low pressure over Tenasserim coast on 6 October 2013. The system lay over north Andaman Sea as a well marked low pressure area on 7 October. The well marked low pressure area transferred as a depression over the north Andaman Sea at 0000 UTC of 8 October with its centre near latitude 12^0 N and longitude 96^0 E. Maximum sustained surface wind speed was estimated to be about 25 knots gusting to 35 knots around the system centre. It moves west-northwestwards direction and intensified into a deep depression on 0000 UTC of 9 October and further moved into a cyclonic storm (CS), 'PHAILIN' at 1200 UTC of the same day. The CS moved further northwestwards and it intensified into a severe cyclonic storm (SCS) at 0300 UTC and into a VSCS at 0600 UTC of 10 October over east central Bay of Bengal. The VSCS crossed Odisha & adjoining north Andhra Pradesh coast near Gopalpur (19.2^0N and 84.9^0E) around 1700 UTC of 12 October 2013 with a sustained maximum surface wind speed of 200-210 kmph gusting to 220 kmph.

4.2.2 Intensity of TC Phailin

The 120 and 96-h (every 3 hourly) storm intensity forecasts in terms of minimum CSLP and maximum wind speed (m/s) at 10 m level using different MP schemes are presented in Figure 4.2.1 (a-h). The simulated CSLP and maximum wind speed (m/s) at 10 m level for six different MP schemes in combination with two different CP schemes and two different initial conditions at 0000 UTC of 8 and 9 October 2013 as presented in Figure 4.2.1 (a-d) and 4.2.1 (e-h) respectively. The simulated CSLP for all MP schemes in combination with KF scheme is much higher than that of BMJ scheme with the initial conditions at 0000 UTC of 8 and 9 October. IMD observed intensity is much lower than that of JTWC intensity in terms of pressure fall and 10 m level sustained wind. The IMD observed pressure fall are 22 hPa less than that of JTWC pressure fall and 10 m level wind is also less than that of JTWC wind speed by 12.7 m/s. The simulated pressure fall (10 m sustained wind) with the 0000 UTC of 8 and 9 October initial conditions for all combination of MP schemes in combination with KF scheme is much higher (lower) than that of IMD observed results. With the 0000 UTC of 8 initial conditions for all MP schemes in combination with BMJ scheme, the CSLP and 10 m level sustained wind is lower than that of IMD observed results. The simulated CSLP and 10 m level sustained wind for all MP schemes in combination with BMJ scheme are much lower than that of IMD observed results with the initial condition of 0000 UTC of 8 October. The model has simulated faster fall of CSLP up to 1800 UTC of 10 October for all MP schemes in combination with KF scheme with the 8 and 9 October initial conditions. The model also has simulated faster pressure drop for all MP schemes in combination with BMJ scheme up to 0300 UTC of 10 October and after that the observed pressure drop is much higher than that of simulated pressure drop for the initial condition of 8 October 2013. BMJ scheme has also simulated comparable pressure drop for all MP schemes up to 0600 UTC of 10 October but after that the model simulated pressure drop is seen to be much lower than that of observed pressure drop for 9 October initial condition. The simulated 10 m wind speed with the initial conditions at 0000 UTC of 8 and 9 October for all MP schemes coupling with KF and BMJ scheme are less than that of IMD and JTWC wind speed.

61
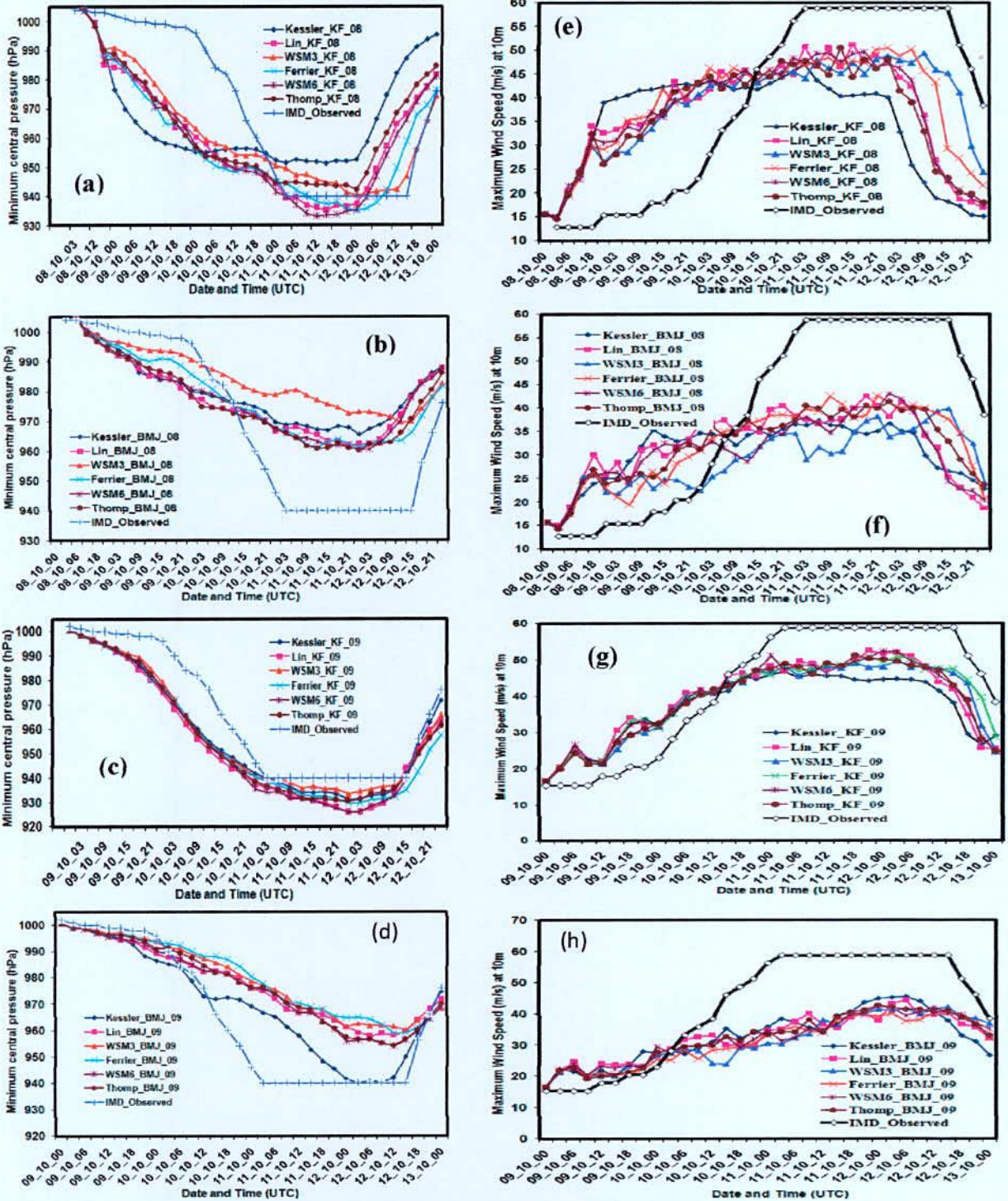
Figure 4.2.1: Model simulated and IMD observed (a-d) minimum CSLP and (e-h) maximum sustained wind at 10 m level of TC Phailin using six different MPs in combination with different CP schemes with the initial conditions of 0000 UTC of 8 and 9 October 2013.

4.2.3 Track of TC Phailin

The 120 and 96-h simulated and IMD observed track of TC Phailin for different cloud MP schemes are displayed in Fig.4.2.2 (a-d). It may be noted that roughly up to the landfall time (i.e., official landfall as on 1700 UTC of 12 October 2013), the track forecast for different sensitivity experiments have shown reasonably accurate prediction. All the simulations have captured the northwestward movement of tropical cyclone Phailin with the initial conditions at 0000 UTC of 8 and 9 October. The sensitivity test has shown significant difference in track among the different microphysical schemes in combination with KF and BMJ schemes with the initial conditions at 0000 UTC of 8 October.
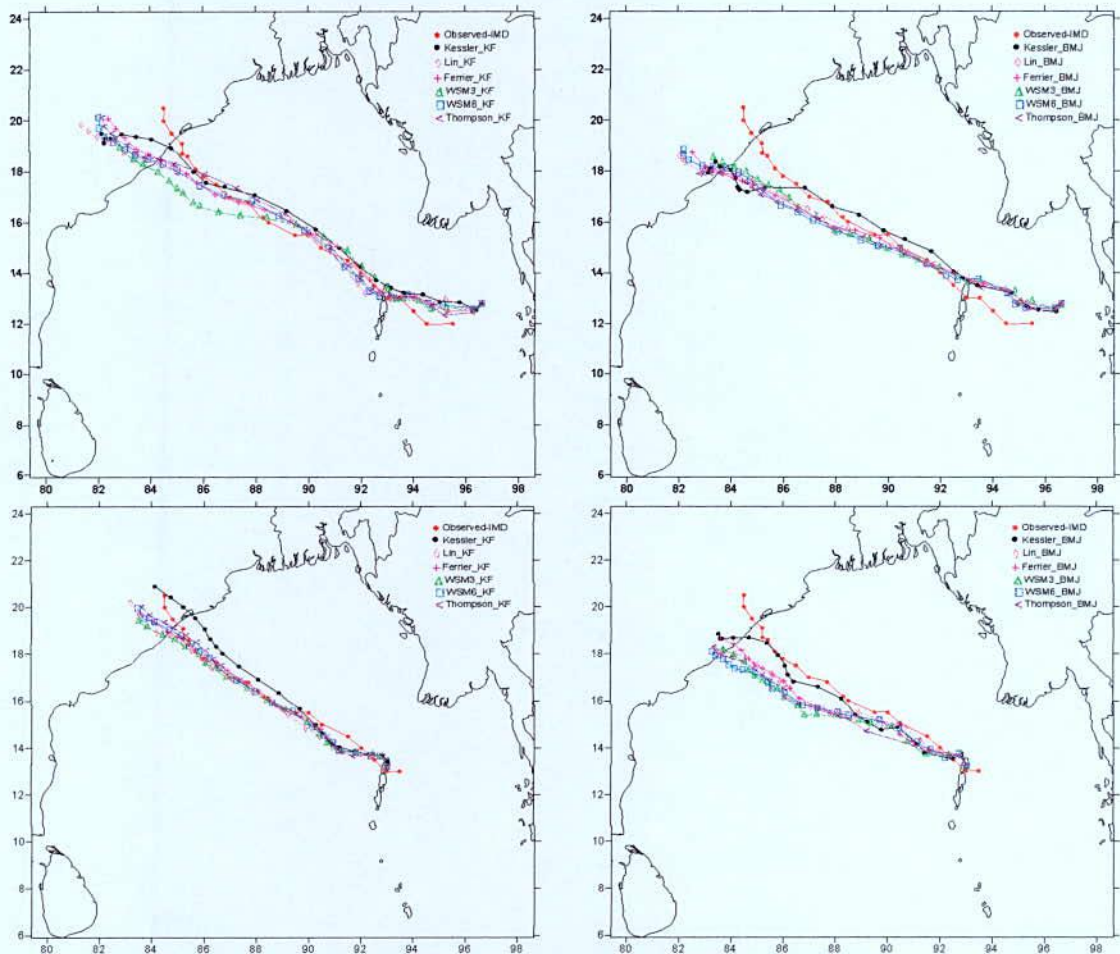
Figure 4.2.2: Model simulated and IMD Observed tracks of TC 'Phailin' using six different MP schemes coupling with (a-b) KF and (c-d) BMJ schemes with the initial conditions at 0000 UTC of 8 and 9 October.

WSM3-KF combinations have simulated most deviated track and Kessler-KF combinations have simulated less deviated track with the initial conditions at 0000 UTC of 8 October 2013. The simulated track for all MP schemes coupling with KF and BMJ schemes are found parallel to the observed track up to 0000 UTC of 12 October. After that the simulated track has followed the same path with the initial conditions at 0000 UTC of 8 October but the observed track has moved towards north. Due to this, the deviation is more on 12 October. The simulated track for Kessler-KF combination are shifted towards north from the observed track and for all other MP schemes in combination with KF scheme, the landfall position is very near to the observed landfall position with the initial conditions of 0000 UTC of 9 October. Out of all MP schemes, the Thompson-KF combination simulated less deviated track at crossing point. The track deviation has increased for all MP schemes coupling with BMJ scheme by using 9 October initial conditions. There is almost no time delay by WSM3, Ferrier, WSM6 and Thompson schemes in combination with KF scheme and Lin-BMJ and WSM6-BMJ combinations with the initial conditions of 0000 UTC of 9 October. The landfall time has delayed by maximum 2-h by using 0000 UTC 9 October initial conditions for Ferrier-BMJ and Thompson-BMJ combinations.

4.2.4 Cloud Water Mixing Ratio

Vertical profiles of area averaged CWMR (gm/kg) at different times 0000 UTC of 10, 11, 12 and 1200 UTC of 09, 10, 11 and 12 October 2013 has been analyzed in region D2 by using six different MP schemes coupling with KF and BMJ schemes and are presented in Figure 4.2.3 (a-l). Kessler and WSM3 schemes coupling with KF and BMJ schemes have simulated CWMR up to 100 hPa. All other MPs except Lin *et al.* scheme (up to 400 hPa level) coupling with KF and BMJ schemes have simulated CWMR up to 400 hPa level. Kessler and WSM3 schemes coupling with KF and BMJ schemes have simulated two maxima of CWMR one at 800 & 150 hPa and another one at 600 & 800 hPa respectively.

The simulated CWMR have maximum at 850–550 hPa level for Lin, Ferrier, WSM6 and Thompson schemes in combination with KF and BMJ schemes. Vertical profiles of area averaged vertical profiles of CWMR for Lin, Ferrier, WSM6 and Thompson schemes coupling with KF and BMJ schemes are almost constant and zero from 350-100 hPa level. The CWMR

has decreased in region D2 at 0000 UTC of 11 October with respect to that of 1200 UTC of 09 October after that it has increased continuously up to the landfall time. The intensity of TC has changed continuously from CS to VSCS since 1200 UTC of 09 October to 0600 UTC of 10 October and the CWMR has also increased significantly during this time at 900-400 hPa level. It is observed that the CWMR has increased in region D2 as the TC moves towards in that region. This indicates that the CWMR increases with the increase in intensity of TC and over the area where the TC moves.
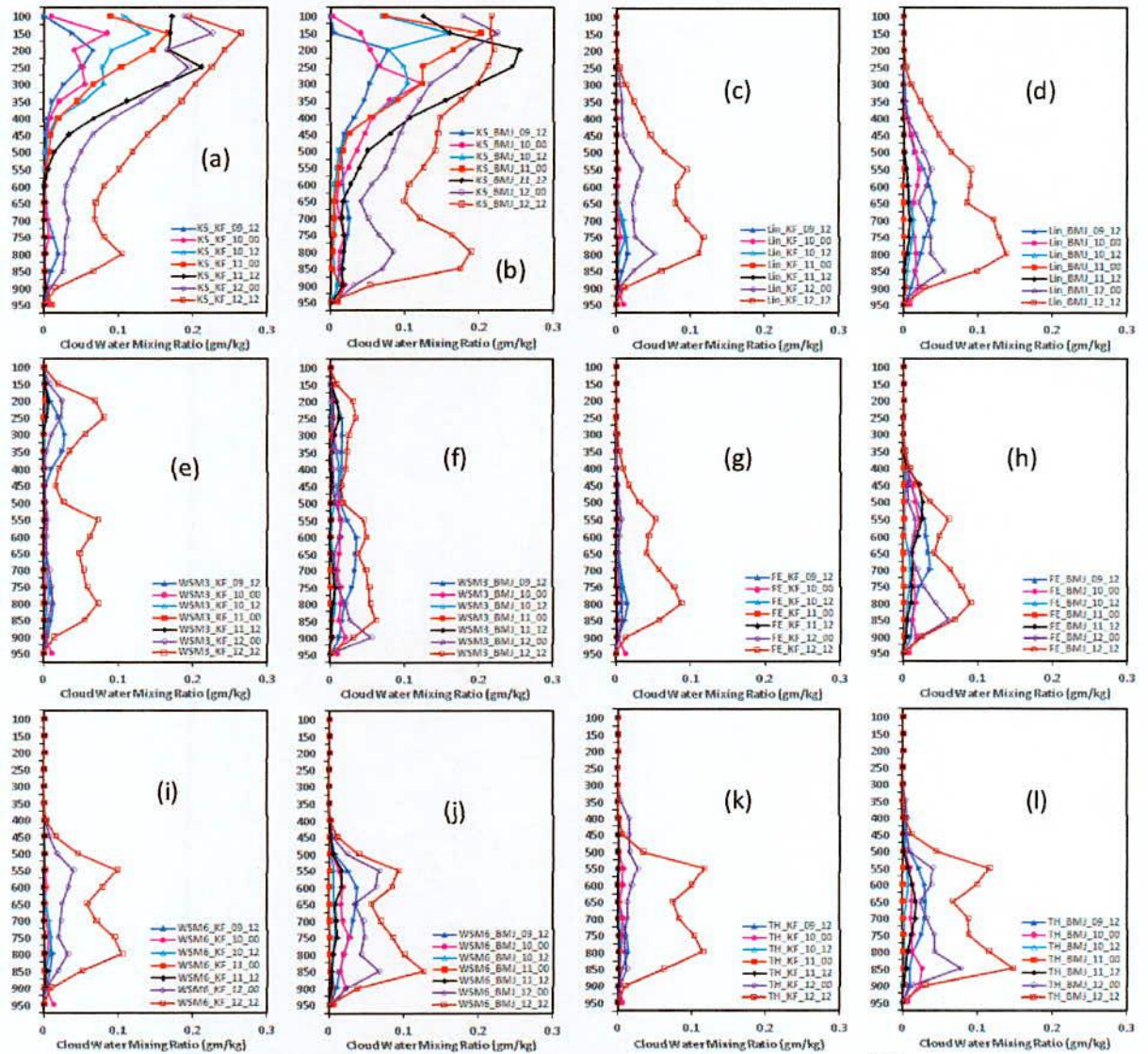
Figure 4.2.3: Simulated CWMR with the progression of time using different MP schemes coupling with KF and BMJ schemes of TC 'Phailin' at region D2.

The CWMR has increased up to 1200 UTC of 12 October in region D2 i.e. after the landfall also. Kessler scheme has simulated maximum CWMR and Ferrier scheme has simulated minimum CWMR at mid troposphere.
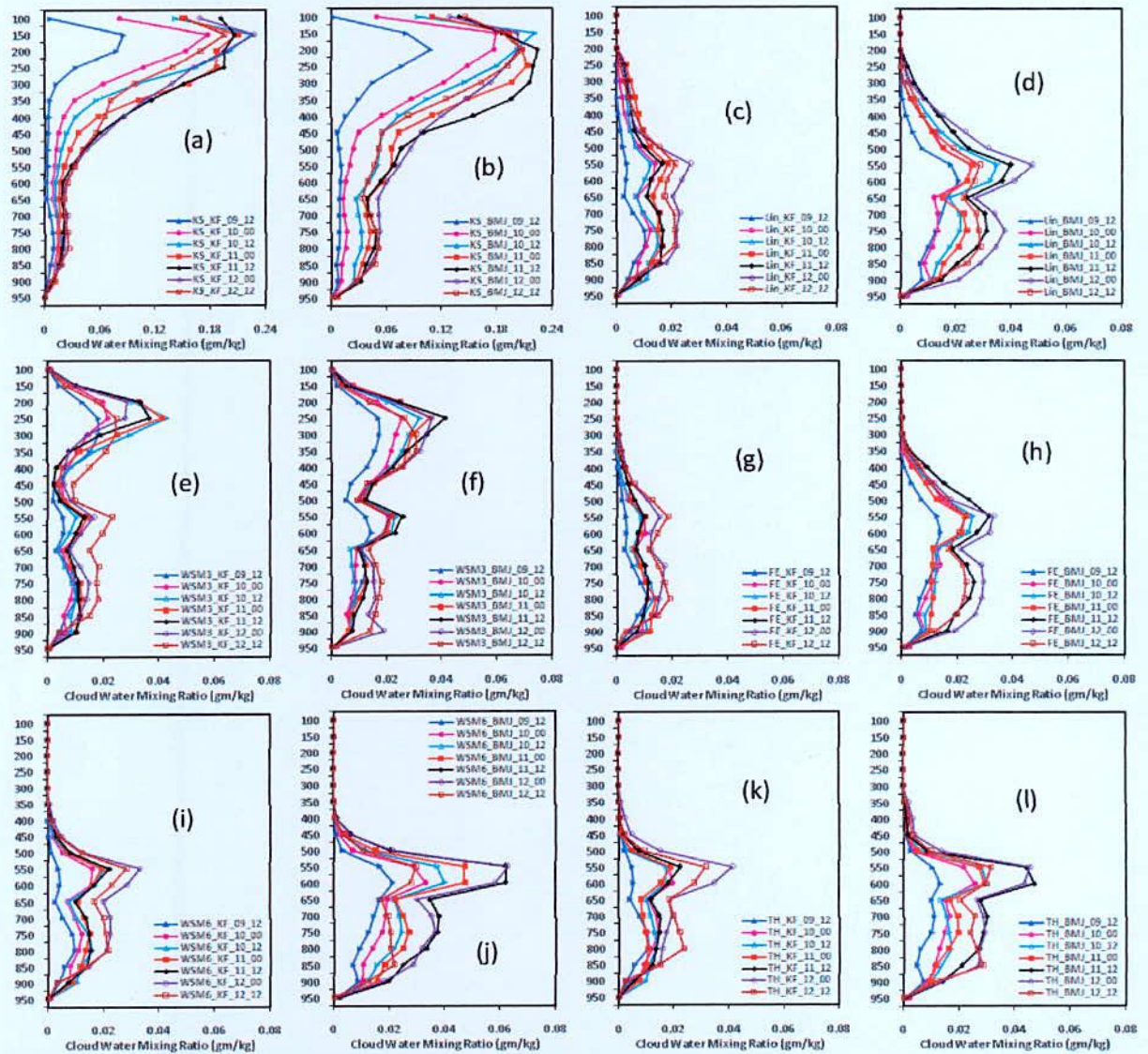
Figure 4.2.4: Simulated CWMR with the progression of time using different MP schemes coupling with KF and BMJ schemes of TC 'Phailin' at region D4.

Vertical profiles of area averaged CWMR (gm/kg) at different times 0000 UTC of 10, 11, 12 and 1200 UTC of 09, 10, 11 and 12 October 2013 has been analyzed in region D4 (i.e., Oceanic region) by using six different MP schemes coupling with KF and BMJ schemes and is shown in Figure 4.2.4 (a-l). Kessler and WSM3 schemes coupling with KF and BMJ schemes

have simulated CWMR up to 100 hPa. Ferrier, WSM6 and Thompson schemes coupling with KF and BMJ schemes have simulated CWMR up to 350 hPa. Lin *et al.* scheme coupling with KF and BMJ schemes has simulated CWMR up to 250 hPa. Kessler and WSM3 schemes coupling with KF and BMJ schemes have simulated two maxima of CWMR one at 800 & 150 hPa and another one at 550 & 250 hPa levels respectively. The CWMR have simulated maximum at 550 hPa levels for Lin, Ferrier, WSM6 and Thompson schemes in combination with KF and BMJ schemes. Vertical profiles of area averaged CWMR for Ferrier, WSM6 and Thompson schemes coupling with KF and BMJ schemes is almost constant and zero from 300-100 hPa level. The intensity of TC Phailin has changed continuously from CS to VSCS since 1200 UTC of 09 October to 0600 UTC of 10 October and the CWMR has increased significantly during this time at 950-400 hPa level by all MPs coupling with BMJ scheme. It has been observed that the CWMR has increased up to 0000 UTC of 12 October for all MPs coupling with KF and BMJ schemes after that the CWMR has decreased significantly in region D4. Due to the deviation of simulated track of TC Phailin towards right from the observed track the CWMR has simulated minimum out of all combinations by Ferrier-KF combination. The intensity of TC Phailin has decreased in terms of pressure fall and wind speed, the CWMR has also decreased in region D4 (i.e. Oceanic region) after 0000 UTC of 12 October. This suggests that CWMR increases with the increase in intensity of TC and over the area where the TC Phailin moves.

BMJ scheme has simulated higher CWMR than that of KF scheme in combination with different MP schemes in regions D1, D3 and D5; but their magnitude is not significant (Figure not shown) except D3. As the time progress, the TC moves towards northwest direction and the CWMR has decreased in regions D1 (Bangladesh), D3 (South India) and D5 (Myanmar). It indicates that the cyclone was not moving in this direction. Except Kessler all MPs coupling with KF and BMJ schemes have simulated small peak of CWMR at around 550 hPa but the other levels the CWMR shows minimum value in regions D1 and D5. Since almost there is no significant change of CWMR, the cyclone has not moved in those directions.

4.2.5 Rain Water Mixing Ratio

Vertical profiles of area averaged RWMR (gm/kg) at different times 0000 UTC of 10, 11, 12 and 1200 UTC of 09, 10, 11 and 12 October 2013 has been analyzed in region D2 by using six different MP schemes coupling with KF and BMJ schemes as shown in Figure 4.2.5 (a-l). Kessler and WSM3 schemes coupling with KF and BMJ schemes have simulated RWMR up to 150 hPa. All other MPs coupling with KF and BMJ schemes have simulated RWMR up to 450 hPa level. The maximum RWMR has been simulated at 400 hPa level by WSM3 scheme coupling with KF scheme. After decreasing the RWMR in region D2 on 0000 UTC of 11 October with respect to the time of 1200 UTC of 09 October for all MPs coupling with KF and BMJ schemes, the RWMR has increased up to 1200 UTC of 12 October (i.e. before landfall). Vertical profiles of area averaged profiles of RWMR for Lin, Ferrier, WSM6 and Thompson schemes coupling with KF and BMJ schemes are almost constant and zero from 450-100 hPa level. As the time progress the RWMR has increased in region D2 for all MP schemes coupling with KF and BMJ schemes as the TC Phailin moves towards region D2 i.e. in Indian coast. It indicates that RWMR increases along the direction where TC Phailin moves.

Vertical profiles of area averaged RWMR (gm/kg) at different times 0000 UTC of 10, 11, 12 and 1200 UTC of 09, 10, 11 and 12 October 2013 has been analyzed in region D4 by using six different MP schemes coupling with KF and BMJ schemes as shown in Figure 4.2.6(a-l). Kessler and WSM3 schemes has simulated RWMR up to 100 hPa level and the other MPs has simulated up to 500 hPa level coupling with KF and BMJ schemes. The maximum RWMR has been simulated at 400 hPa level by WSM3 scheme coupling with KF and BMJ scheme. The intensity of TC has changed continuously from CS to VSCS since 1200 UTC of 09 October to 0600 UTC of 10 October and the RWMR has also increased significantly during the time 0000 UTC of 12 October at 950-100 hPa and 950-500 hPa level by Kessler, WSM3 and Lin, WSM6, Thompson schemes respectively coupling with KF and BMJ schemes. The patterns of rain water profile are similar up to 500 hPa levels with Lin, FE, WSM6 and Thompson schemes coupling with KF and BMJ schemes. The RWMR decreases after 0000 UTC of 12 October by all MPs coupling with KF and BMJ schemes. Due to the significant increase of RWMR up to 0000 UTC of 12 October simulated by all MPs coupling with KF and BMJ schemes, the intensity of TC Phailin in terms of pressure fall and wind speed has

increased. In this respect, at the time of simulated MSLP has minimum and the MWS at 10 m level has maximum. The average maximum RWMR has been simulated by Kessler-BMJ, WSM3-KF, WSM3-BMJ, WSM6-BMJ and Lin-BMJ at 900, 400, 450, 700 and 650 hPa level and are 0.12, 0.24, 0.30, 0.12 and 0.12 gm/kg respectively. WSM3-BMJ combination has simulated maximum and FE-KF combination has simulated minimum area averaged RWMR from 950–500 hPa level.

Figure 4.2.5: Simulated RWMR with the progression of time using different MP schemes coupling with KF and BMJ schemes of TC 'Phailin' at region D2.

Figure 4.2.6: Simulated RWMR with the progression of time using different MP schemes coupling with KF and BMJ schemes of TC 'Phailin' at region D4.

Vertical profiles of area averaged values of RWMR for Lin, Ferrier, WSM6 and Thompson schemes coupling with KF and BMJ schemes are almost constant and zero from 450-100 hPa level. BMJ scheme has simulated higher RWMR than that of KF scheme in combination with different MP schemes in regions D1, D3 and D5 but their magnitude is not significant (Figure not shown). Lin *et al.*, Ferrier, WSM6 and Thompson schemes coupling with KF and BMJ schemes have simulated small peak of RWMR at around 650 hPa but the other level the RWMR shows zero value in regions D1, D3 and D5. The RWMR has not been simulated so

much in region D1, D3 and D5 but as the progression of time it has decreased. Since the RWMR has decreased in regions D1, D3 and D5 and cyclone has not moved in those directions. This indicates that RWMR increases with the increase in intensity of TC and over the area where the TC Phailin moves.

4.2.6   Cloud Ice Mixing Ratio

In regions D2 and D4 the vertical profiles of area averaged CIMR (gm/kg) has been simulated at different times 0000 UTC of 10, 11, 12 and 1200 UTC of 09, 10, 11 and 12 October 2013 by Lin *et al.*, WSM6 and Thompson schemes coupling with KF and BMJ schemes and are presented in Figure 4.2.7 (a-d) and 4.2.7 (e-g) respectively. Lin *et al.* and WSM6 schemes have simulated cloud ice maximum at around 250 hPa and Thompson scheme simulated maximum (about to zero value) at 150 hPa. WSM6 profile exhibits a prominent spike containing much larger CIMR values between 550 to 100 hPa and Thompson scheme has simulated less CIMR than that of other schemes. Thompson scheme in combination with KF and BMJ schemes have simulated much smaller amount of ice and concentrated at 250–100 hPa. Lin scheme has simulated cloud ice between 400–100 hPa levels. Vertical profiles of area averaged values of CIMR for Lin, WSM6 and Thompson schemes coupling with KF and BMJ schemes are almost constant and zero from 950-400, 950-600 and 950-250 hPa level respectively. The CIMR has increased significantly during 0000 UTC of 11 October to 1200 UTC of 12 October as simulated by Lin and WSM6 schemes coupling with KF and BMJ schemes in region D2.

The CIMR has increased significantly during 1200 UTC of 09 October to 1200 UTC of 11 October by Lin and WSM6 schemes coupling with KF and BMJ schemes in region D4. The CIMR has decreased after 1200 UTC of 11 October simulated by using Lin and WSM6 schemes coupling with KF and BMJ schemes in region D4. The CIMR has increased up to 1200 UTC of 11 October for Lin and WSM6 schemes coupling with KF and BMJ schemes and after that it has decreased. The TC Phailin could not intensify properly and the CIMR has decrease after 1200 UTC of 11 October 2006.

In region, D2 Lin *et al.* and WSM6 schemes have simulated cloud ice maximum at around 250 hPa and Thompson scheme simulate maximum (about to zero value) at 150 hPa levels. Lin *et*

al., WSM6 and Thompson schemes are exhibits a prominent spike containing much larger CIMR values between 400-100 hPa, 600-100 hPa and 250–100 hPa respectively. Thompson scheme has simulated less CIMR than that of other schemes. Vertical profiles of area averaged profiles of CIMR for Lin, WSM6 and Thompson schemes coupling with KF and BMJ schemes are almost constant and zero from 950-400, 950-600 and 950-250 hPa level respectively. The CIMR has also increased significantly during 0000 UTC of 11 October to 1200 UTC of 12 October for Lin and WSM6 schemes coupling with KF and BMJ schemes in region D2. It indicates that CIMR increases with the increase in intensity of TC and over the area where the TC Phailin moves.
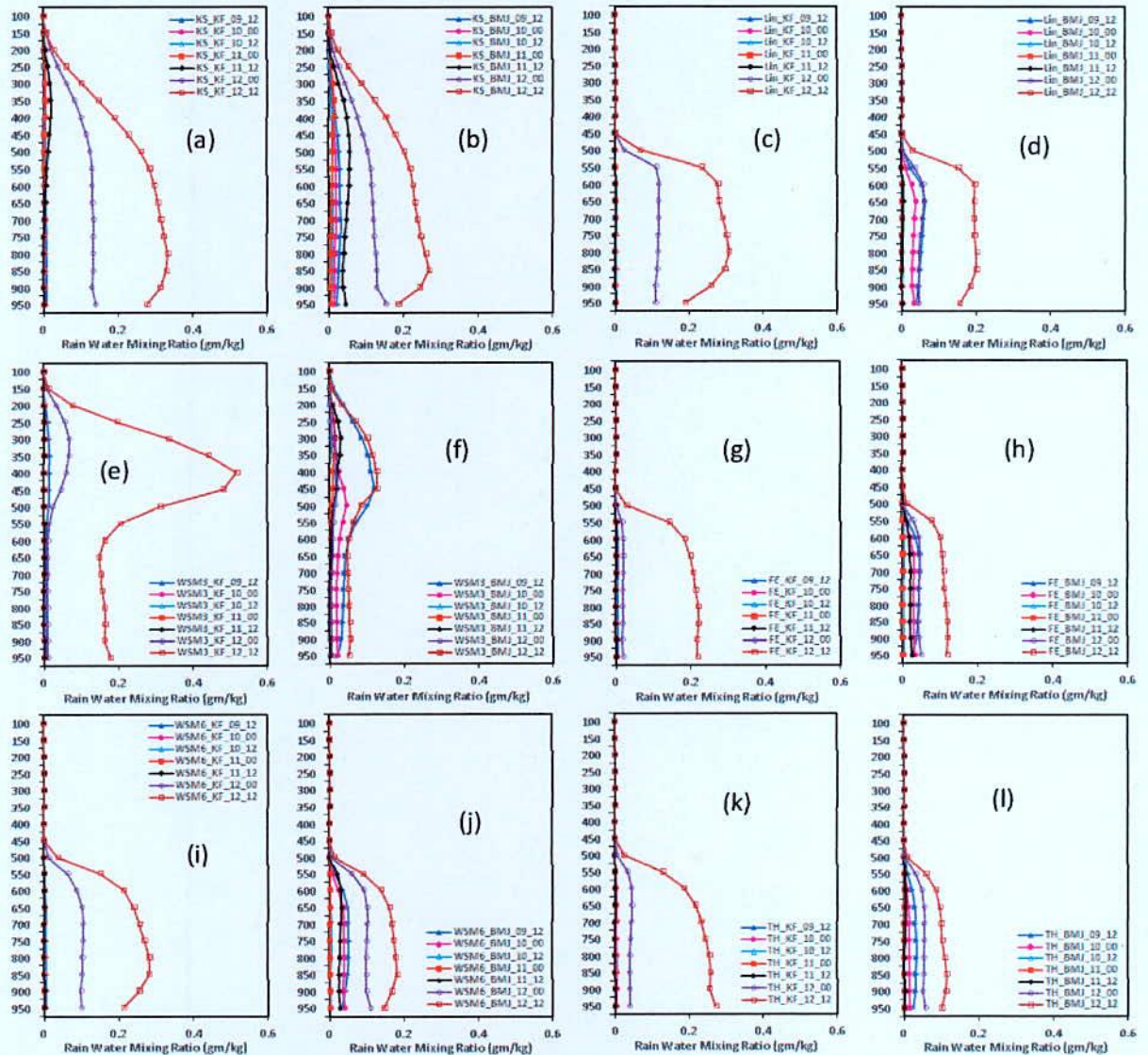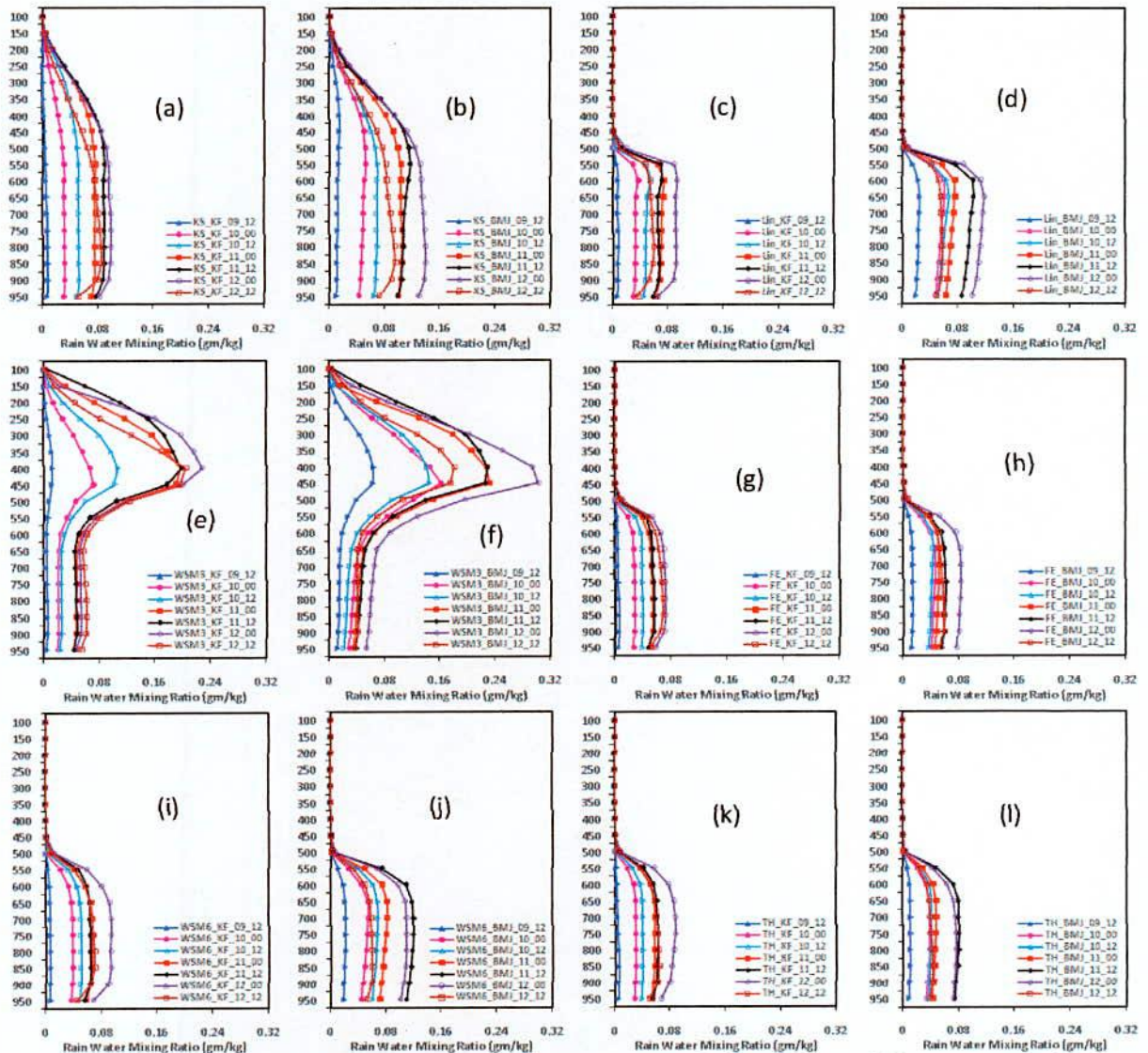

Figure 4.2.7: Simulated CIMR with the progression of time using different MP schemes coupling with KF and BMJ schemes of TC 'Phailin' at region (a-d) D2 & (e-h) D4 respectively.

The CIMR has simulated minimum in regions D1, D3 and D5 by Lin *et al.*, WSM6 and Thompson schemes coupling with KF and BMJ schemes (Figure not shown). WSM6 scheme has simulated higher CIMR than that of Lin and Thompson scheme coupling with KF and BMJ schemes in regions D1, D3 and D5. With the progression of time, the CIMR has

decreased since 1200 UTC of 09 October to 0000 UTC of 11 October after that time it has increased significantly but their magnitude are minimum in regions D1, D3 and D5 and TC Phailin moves towards region D2. It indicates that the cyclone moves in a direction where the CIMR has changed increasingly. Lin *et al.*, WSM6 and Thompson schemes coupling with KF and BMJ schemes have simulated small peak of CIMR at around 250 hPa but at the other level the CIMR shows zero value in regions D1, D3 and D5.

4.2.7 Cloud Snow Mixing Ratio

In region D2, the vertical profiles of area averaged CSMR (gm/kg) has been simulated at different times 0000 UTC of 10, 11, 12 and 1200 UTC of 09, 10, 11 and 12 October 2013 by Lin, Ferrier, WSM6 and Thompson schemes coupling with KF and BMJ schemes and are presented in Figure 4.2.8 (a-h). It is evident from the figure that the vertical structure and magnitude of these profiles vary greatly.

Figure 4.2.8: Simulated CSMR with the progression of time using different MP schemes coupling with KF and BMJ schemes of TC 'Phailin' at region D2.

Overall, the Thompson scheme coupling with KF and BMJ schemes has generated the maximum amount of snow between 650 to 100 hPa. The abundance of snow in the mid troposphere (below 400 hPa) may be due to the enhanced ice content in the upper troposphere. KF scheme has simulated greater snow than that of BMJ scheme in combination with Lin, Ferrier, WSM6 and Thompson schemes. After decreasing the CSMR in region D2 on 1200 UTC of 10 October with respect to that of 1200 UTC of 09 October by Lin, Ferrier, WSM6 and Thompson scheme coupling with KF and BMJ scheme then the CSMR has increased up to 1200 UTC of 12 October i.e. before the landfall. Vertical profiles of area averaged values of CSMR for Lin, Ferrier, WSM6 and Thompson schemes coupling with KF and BMJ schemes are almost constant and zero from surface to 650 hPa level. This indicates that the TC moves in a region where the CSMR has increased. As the time progress the CSMR has increased in region D2 for Lin, Ferrier, WSM6 and Thompson schemes coupling with KF and BMJ schemes and TC also moves towards region D2 i.e. in Indian coast. It indicates that CSMR increases where the TC Phailin moves.
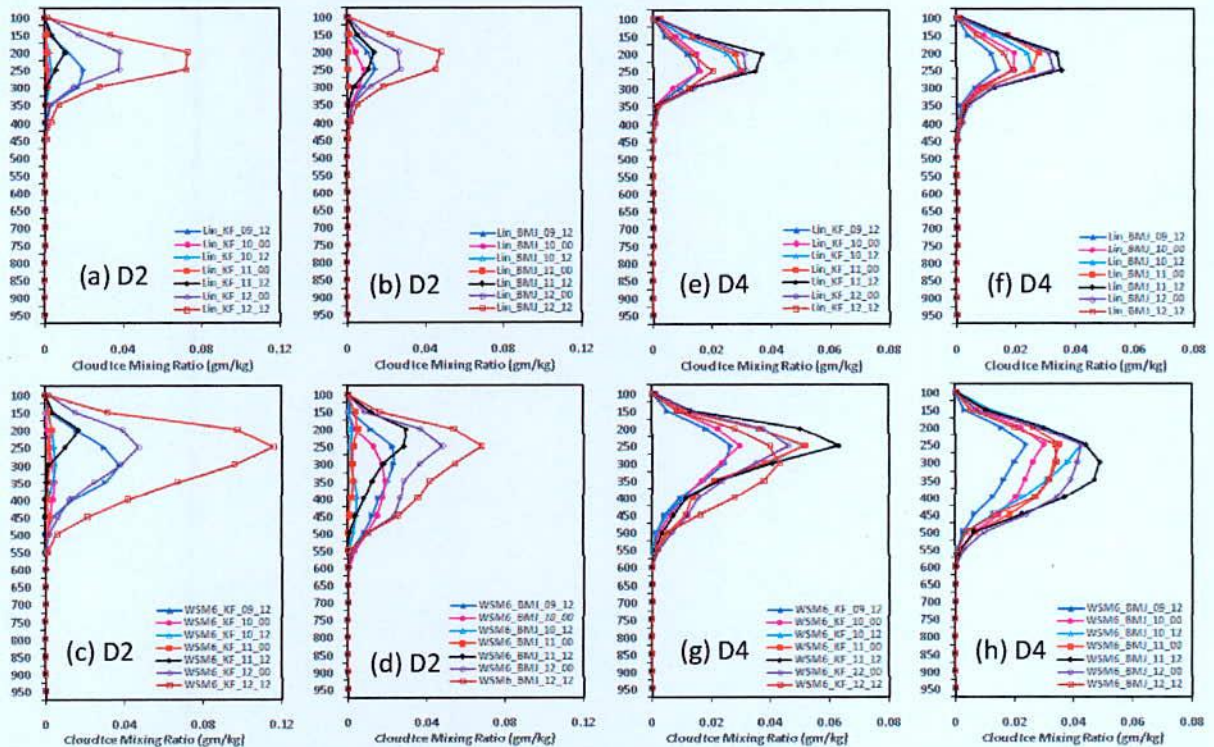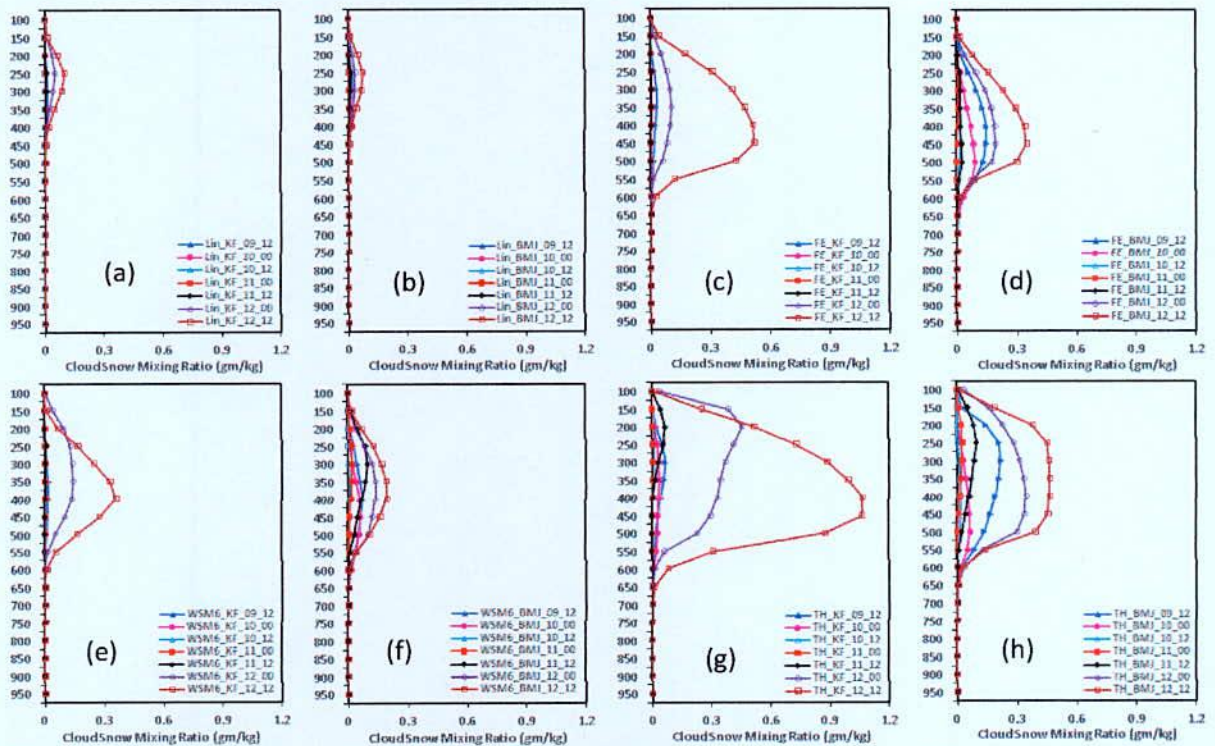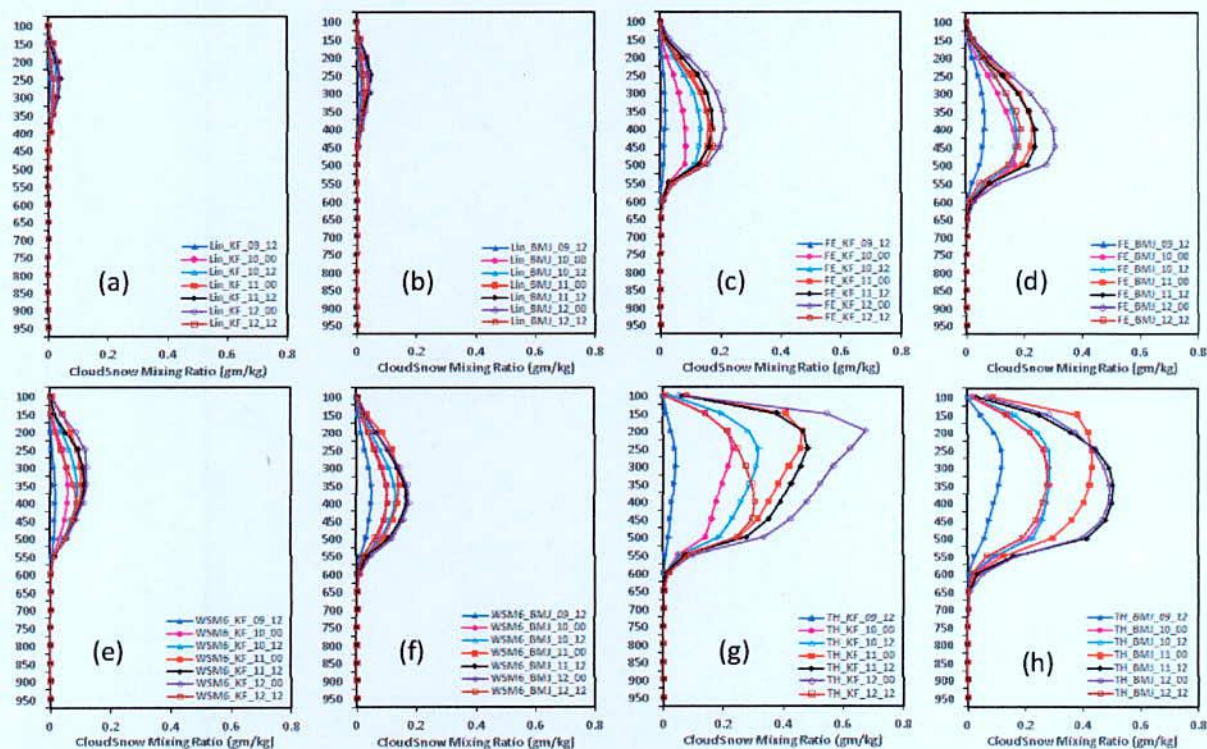

Figure 4.2.9: Simulated CSMR with the progression of time using different MP schemes coupling with KF and BMJ schemes of TC 'Phailin' at region D4.

74

In region D4, vertical profiles of area averaged CSMR (gm/kg) has been simulated at different times 0000 UTC of 10, 11, 12 and 1200 UTC of 09, 10, 11 and 12 October 2013 by Lin, Ferrier, WSM6 and Thompson schemes coupling with KF and BMJ schemes are presented in Figure 4.2.9(a-h). Ferrier, WSM6 and Thompson schemes have simulated cloud snow maximum around 350 hPa and Lin *et al.* scheme simulated maximum at 250 hPa. Overall, the Thompson scheme has generated the maximum amount of cloud snow between 650 to 100 hPa than that of other schemes. Lin *et al.* scheme has simulated minimum and about to zero cloud snow between 400 to 150 hPa levels. The abundance of snow in the mid troposphere (below 400 hPa) may be due to the enhanced ice content in the upper troposphere. Vertical profiles of area averaged values of CSMR for Ferrier, WSM6 and Thompson schemes coupling with KF and BMJ schemes are almost constant and zero at surface to 600 hPa level but at Lin scheme this is almost constant and zero up to 400 hPa level. The intensity of TC has changed continuously from CS to VSCS since 1200 UTC of 09 October to 0600 UTC of 10 October the CSMR has also increased significantly during this time by Ferrier, WSM6 and Thompson schemes coupling with KF and BMJ schemes. The patterns of cloud snow profile are similar to upper level with Ferrier, WSM6 and Thompson schemes coupling with KF and BMJ schemes. The CSMR decreases after 0000 UTC of 12 October by using Lin, Ferrier, WSM6 and Thompson schemes coupling with KF and BMJ schemes. Due to the significant increase of CSMR up to 1200 UTC of 12 October by using Lin, Ferrier, WSM6 and Thompson schemes coupling with KF and BMJ schemes the intensity of TC Phailin in terms of pressure fall and wind speed has increased. The CSMR has decreased since 1200 UTC of 12 October by all MPs coupling with KF and BMJ schemes. The TC Phailin intensifies similarly as observed by using all MPs coupling with KF and BMJ schemes so that the CSMR has increased. In this respect the simulated MSLP has minimum and MWS at 10 m level has maximum.

The CSMR has simulated for Lin *et al.*, Ferrier, WSM6 and Thompson schemes coupling with KF and BMJ schemes. BMJ scheme has simulated higher CSMR than that of KF scheme in combination with different MP schemes in regions D1, D3 and D5 but their magnitude is not significant (Figure not shown). With the progression of time, the TC moves towards region D2 and the CSMR has decreased in regions D1, D3 and D5. Lin, Ferrier, WSM6 and

75

Thompson schemes coupling with KF and BMJ schemes have simulated small peak of CSMR at around 400 hPa but at the other level the CSMR shows zero value in regions D1, D3 and D5. Since there is no change of CSMR in the mid troposphere of region D1, D3 and D5, the cyclone was not moving in those directions.

4.2.8 Cloud Graupel Mixing Ratio

In region D4, the vertical profiles of area averaged CGMR (gm/kg) at different times 1200 UTC of 09, 10, 11 and 12 October and 0000 UTC of 10, 11 and 12 October 2013 by Lin et al., WSM6 and Thompson schemes coupling with KF and BMJ schemes is presented in Figure 4.2.10 (a-d). Lin et al., WSM6 and Thompson schemes have created the maximum amount of CGMR at around 500 hPa levels. The WSM6 scheme has simulated higher CGMR and Thompson scheme has simulated lower but insignificant amount of CGMR than that of Lin et al. scheme. Graupel starts to produce at 650 hPa and sharp spike are found at 500 hPa levels in case of Lin et al. and WSM6, and then has decreased to minimum at 100 hPa. BMJ scheme coupling with all MPs has simulated larger CGMR than that of KF scheme. The intensity of TC has changed continuously from CS to VSCS since 1200 UTC of 09 October to 0600 UTC of 10 October and the CGMR has also increased significantly during this time as simulated Lin and WSM6 schemes coupling with KF and BMJ schemes. The patterns of cloud graupel profile are similar to upper level with Lin and WSM6 schemes coupling with KF and BMJ schemes. The CGMR has increased up to 0000 UTC of 12 October, 1200 UTC of 11 October by Lin-BMJ, WSM6-BMJ combinations respectfully and after that it has decreased up to 1200 UTC of 12 October. In region D4, the Thompson scheme coupling with KF and BMJ schemes cannot simulate the CGMR. As the intensity of TC Mala has increased significantly in terms of pressure fall and wind speed, the CGMR has increased up to 0000 UTC of 12 October by Lin et al. and WSM6 schemes coupling with KF and BMJ schemes.

In region D2, the vertical profiles of area averaged CGMR (gm/kg) has been simulated at different times 0000 UTC of 10, 11, 12 and 1200 UTC of 09, 10, 11 and 12 October 2013 by Lin et al., WSM6 and Thompson schemes coupling with KF and BMJ schemes are presented in Figure 4.2.10(e-h). Lin et al. and WSM6 schemes coupling with KF and BMJ schemes have simulated maximum CGMR at around 500 hPa levels. The Lin et al. and WSM6 schemes have simulated higher CGMR and Thompson scheme has simulated lower CGMR. Graupel

starts to produce at 650 hPa and sharp spike are found at 500 hPa levels in case of Lin *et al.* and WSM6 and then decreases to zero at 100 hPa. KF scheme has simulated larger CGMR than that of BMJ scheme for Lin *et al.* and WSM6 schemes in region D2. The Thompson scheme coupling with KF and BMJ schemes cannot simulate the CGMR. After decreasing the CGMR in region D2 at 0000 UTC of 11 October with respect to that of 1200 UTC of 09 October by Lin *et al.* (Fig 4.2.10(f)) and WSM6 (Fig.4.2.10 (h)) schemes coupling with BMJ scheme then the CGMR has increased up to 1200 UTC of 12 October i.e. before the landfall also. Vertical profiles of area averaged values of CGMR for Lin *et al.* and WSM6 schemes coupling with KF and BMJ schemes are almost constant and are zero from 950-650 hPa level. The intensity of TC has changed continuously from CS to VSCS since 1200 UTC of 09 October to 0600 UTC of 10 October and the CGMR has also increased significantly during this time by Lin and WSM6 schemes coupling with KF and BMJ schemes.

Figure 4.2.10: Simulated CGMR with the progression of time using different MP schemes coupling with KF and BMJ schemes of TC 'Phailin' at region (a-d) D4 and (e-h) D2 respectively.

77

As the time progress with respect to VSCS category of the TC Phailin, the CGMR has increased in region D2 for Lin *et al.* and WSM6 schemes coupling with KF and BMJ schemes when the TC moves towards region D2 (i.e. in Indian coast). It indicates that CGMR increases with the increase in intensity of TC and over the area where the TC moves. The simulated CGMR has been not significant for Lin, WSM6 and Thompson schemes coupling with KF scheme in regions D1, D3 and D5. BMJ scheme has simulated higher CGMR than that of KF scheme in combination with Lin, WSM6 and Thompson schemes in regions D1, D3 and D5 but the amount is not significant (Figure not shown). With the progression of time, the simulated CGMR has becomes minimum in regions D1, D3 and D5 and the TC moves towards region D2 where the CGMR has increased. Lin, WSM6 and Thompson schemes coupling with KF and BMJ schemes have simulated small peak of CGMR at around 650 to 200 hPa but at the other level, the CGMR has not shown any value in regions D1, D3 and D5. Since almost there is no change of CGMR, the cyclone has not moved in those directions.

4.2.9 Water Vapor Mixing Ratio

The vertical profiles of area averaged WVMR (gm/kg) has been analyzed at different times 0000 UTC of 10, 11, 12 and 1200 UTC of 09, 10, 11 and 12 October 2013 in region D2 by using six different MP schemes coupling with KF and BMJ schemes as shown in Figure 4.2.11 (a-l). The patterns of WVMR are similar up to 200 hPa levels with all MPs coupling with KF and BMJ schemes. The simulated WVMR have maximum at the surface and has decreased continuously with height for all MPs coupling with KF and BMJ schemes. The simulated WVMR is approximately equal for all MPs schemes coupling with KF and BMJ schemes. Vertical profiles of area averaged values of WVMR for all MP schemes coupling with KF and BMJ schemes are almost constant and are zero from 200-100 hPa level. The intensity of TC has changed continuously from CS to VSCS since 1200 UTC of 09 October to 0600 UTC of 10 October and the WVMR has decreased significantly at all levels during this time in region D2. It is found that the WVMR has increased significantly in region D2 since 0000 UTC of 11 October to 1200 UTC of 12 October as the TC moves towards region D2. This increase is prominent from 900 – 400 hPa level. This indicates that the WVMR increases where the TC moves in a region.
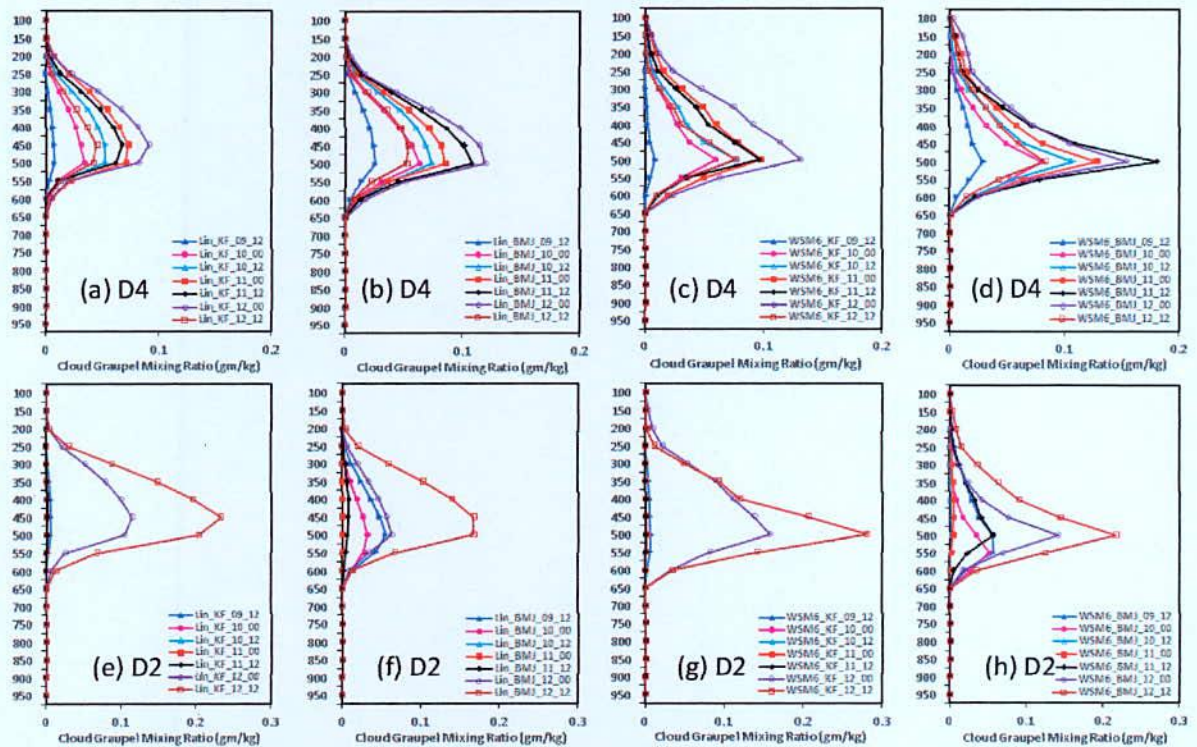
Figure 4.2.11: Simulated WVMR with the progression of time using different MP schemes coupling with KF and BMJ schemes of TC 'Phailin' at region D2.

Vertical profiles of area averaged WVMR (gm/kg) at different times 0000 UTC of 10, 11, 12 and 1200 UTC of 09, 10, 11 and 12 October 2013 has been analyzed in region D4 by using six different MP schemes coupling with KF and BMJ schemes as shown in Figure 4.2.12 (a-l). The WVMR is similar up to 200 hPa levels with all MPs coupling with KF and BMJ schemes. The simulated WVMR has maximum at the surface and has decreased continuously with height for all MPs coupling with KF and BMJ schemes. The simulated WVMR is approximately equal for all MPs coupling with KF and BMJ schemes. It has been observed

79

that the simulated WVMR is almost constant but with the progression of time, the WVMR simulated by all MPs coupling with KF and BMJ schemes has increased significantly up to 0000 UTC of 12 October in region D4.

Figure 4.2.12: Simulated WVMR with the progression of time using different MP schemes coupling with KF and BMJ schemes of TC 'Phailin' at region D4.

Since the WVMR has increased, the intensity of TC has also increased significantly for different MP schemes in combination with KF and BMJ schemes of TC Phailin in region D4. It has been seen that in the Oceanic region i.e. region D4, the WVMR has not changed significantly during the progression of time. With all MPs coupling with KF and BMJ

80

schemes, the WVMR has decreased in regions D1 and D3 since 1200 UTC of 09 October to 0000 UTC of 11 October; after that it has increased up to 1200 UTC of 12 October but the WVMR has increased in region D5 up to 1200 UTC of 12 October 2013. The WVMR is similar up to 250 hPa levels with all MPs coupling with KF and BMJ schemes in regions D1, D3 and D5. The simulated WVMR has maximum at the surface (around 10 gm/kg) and has decreased continuously with height for all MPs coupling with KF and BMJ schemes. With the progression of time, the TC moves towards northwest direction and the WVMR has no significant variation (Figure not shown) in regions D1, D3 and D5, so the cyclone has not moved in those directions.

4.2.10 Relative Humidity

The vertical profiles of area averaged RH (%) in region D2 at different times 0000 UTC of 10, 11, 12 and 1200 UTC of 09, 10, 11 and 12 October 2013 have been presented in Figure 4.2.13(a-l) for six different MP schemes coupling with KF and BMJ schemes by using 0000 UTC of 09 October initial condition. The simulated RH exceeds 80% from surface to 450 hPa levels for Lin et al., WSM3, FE, WSM6 and Thompson schemes coupling with CP schemes. KS scheme coupling with KF and BMJ schemes has simulated more than 90% RH at upper level. It is observed that the RH increases continuously in region D2 for all MPs coupling with KF and BMJ schemes from 0000 UTC of 11 October to 1200 UTC of 12 October i.e. before landfall of TC Phailin. This suggested that the RH increases in region D2 and TC also has crossed in this region.

The vertical profiles of area averaged RH (%) in region D4 at different times 0000 UTC of 10, 11, 12 and 1200 UTC of 09, 10, 11 and 12 October 2013 have been presented in Figure 4.2.14(a-l) for six different MP schemes coupling with KF and BMJ schemes by using 0000 UTC of 09 October initial condition. The simulated RH ranges from 80 to 100% from surface to 100 hPa levels for Kessler scheme coupling with CP schemes. The simulated RH exceeds 80% from surface to 400 hPa levels for Lin *et al.*, WSM3, FE, WSM6 and Thompson schemes coupling with CP schemes. The RH increased continuously in region D4 from starting time up to 0000 UTC of 12 October after that it has decreased.
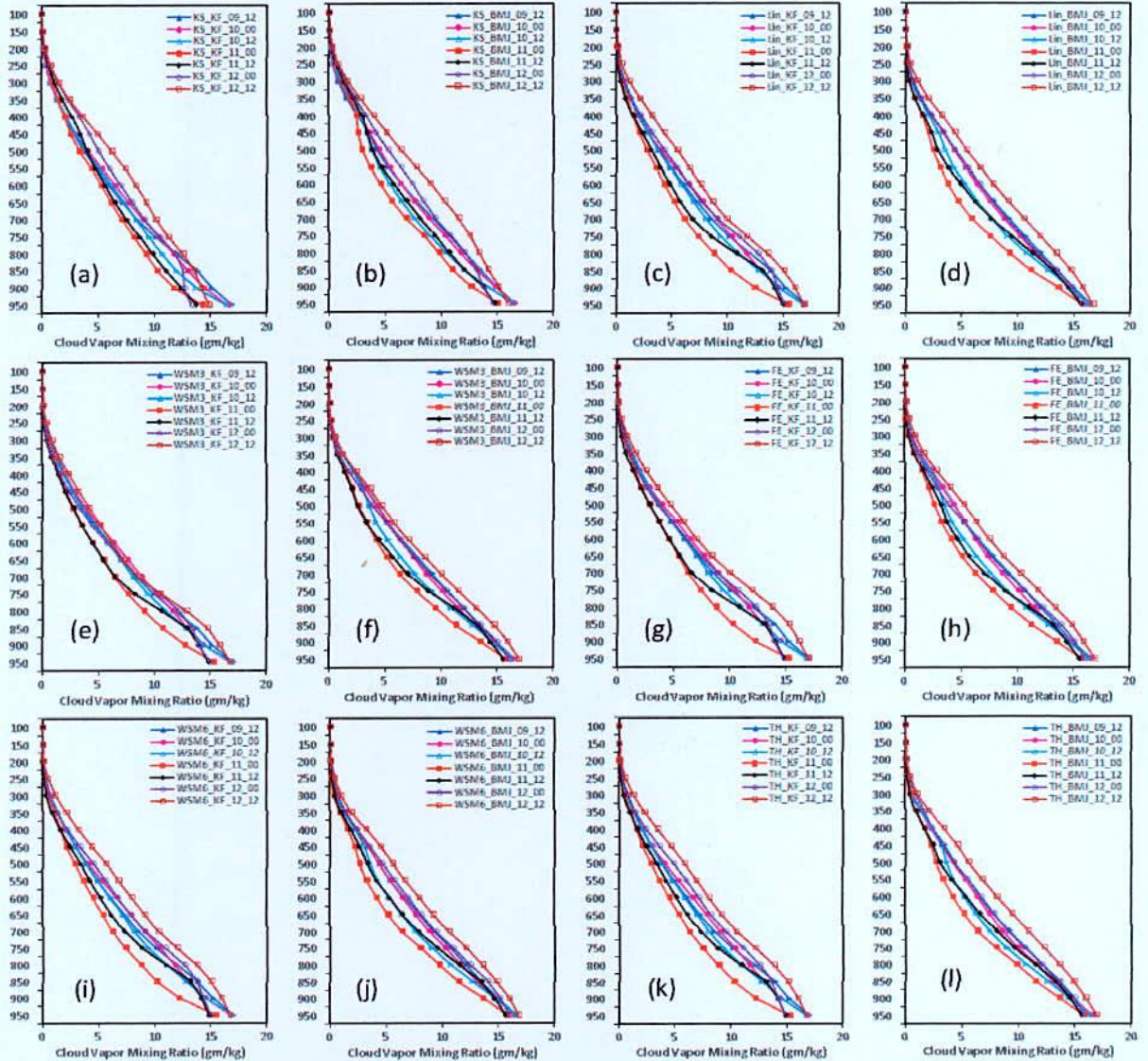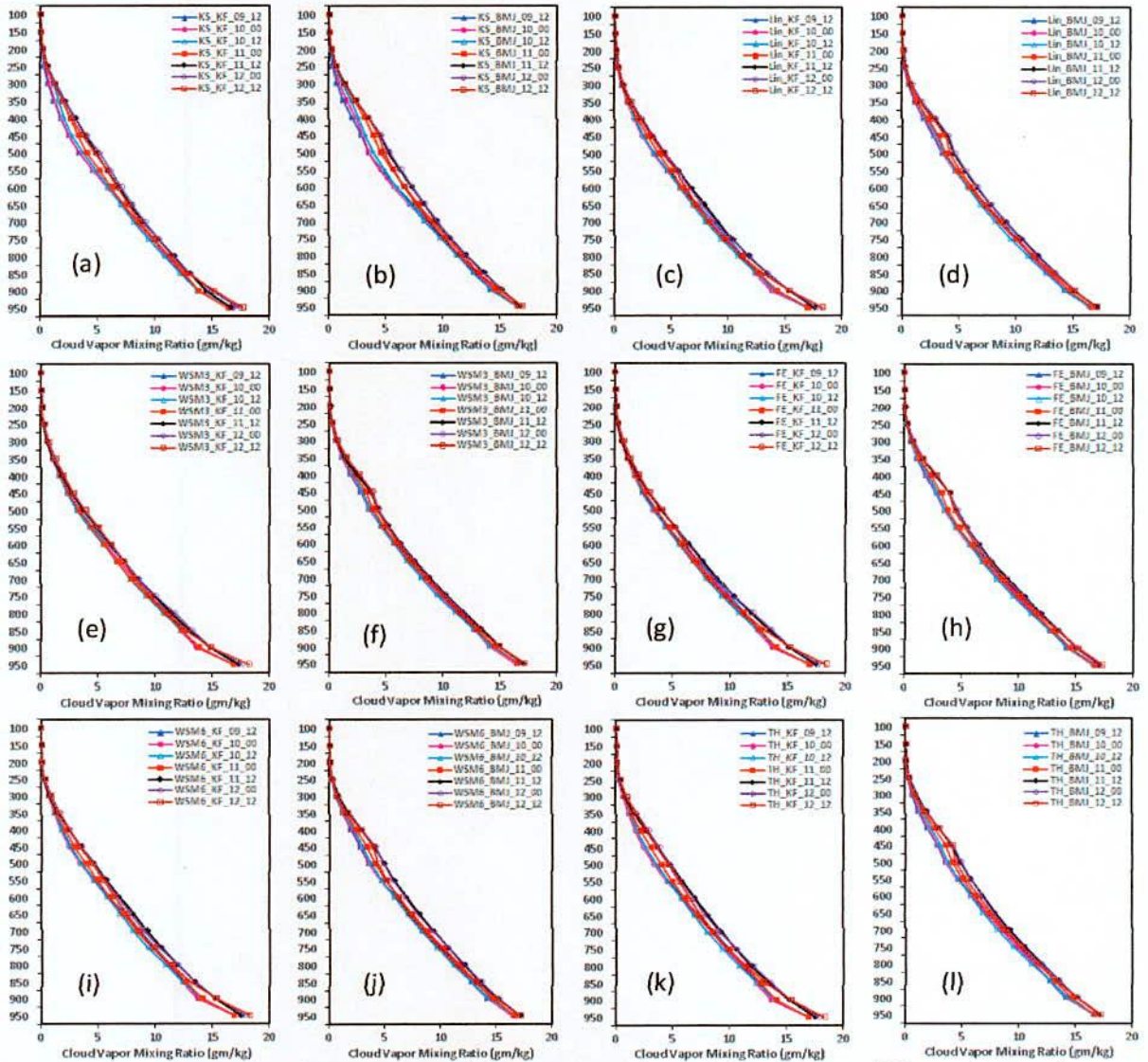
Figure 4.2.13: Simulated RH at region D2 with the progression of time using different MP schemes coupling with KF and BMJ schemes of TC 'Phailin'.

The simulated RH has been maximum (above 80%) at the upper level (100 hPa) for Kessler scheme coupling with KF and BMJ schemes in region D1, D3 and D5 but it is below 80% at surface to mid troposphere for all MPs coupling with KF and BMJ schemes (Fig. not shown). In region D3, the RH (%) has decreased with respect to the initial time of model run for six different MPs coupling with KF and BMJ schemes. In region D5, the RH (%) has increased up to 1200 UTC of 12 October 2013 at surface to mid level and it has decreased at upper level for six different MPs coupling with KF and BMJ schemes with initial conditions at 0000 UTC of

09 October but the amount of RH (%) is below 80%. As the time progresses, the TC moves towards northwest in the Bay of Bengal and the simulated RH (%) has become minimum in region D1 (Bangladesh), D3 (SE India) and D5 (Myanmar). The cyclone has not moved in D1, D3 and D5 and the RH have also decreased in those directions. It indicates that there is positive correlation with the movement of TC and RH. The relative humidity starts to increase earlier over the region when the TC Phailin moves in that direction.
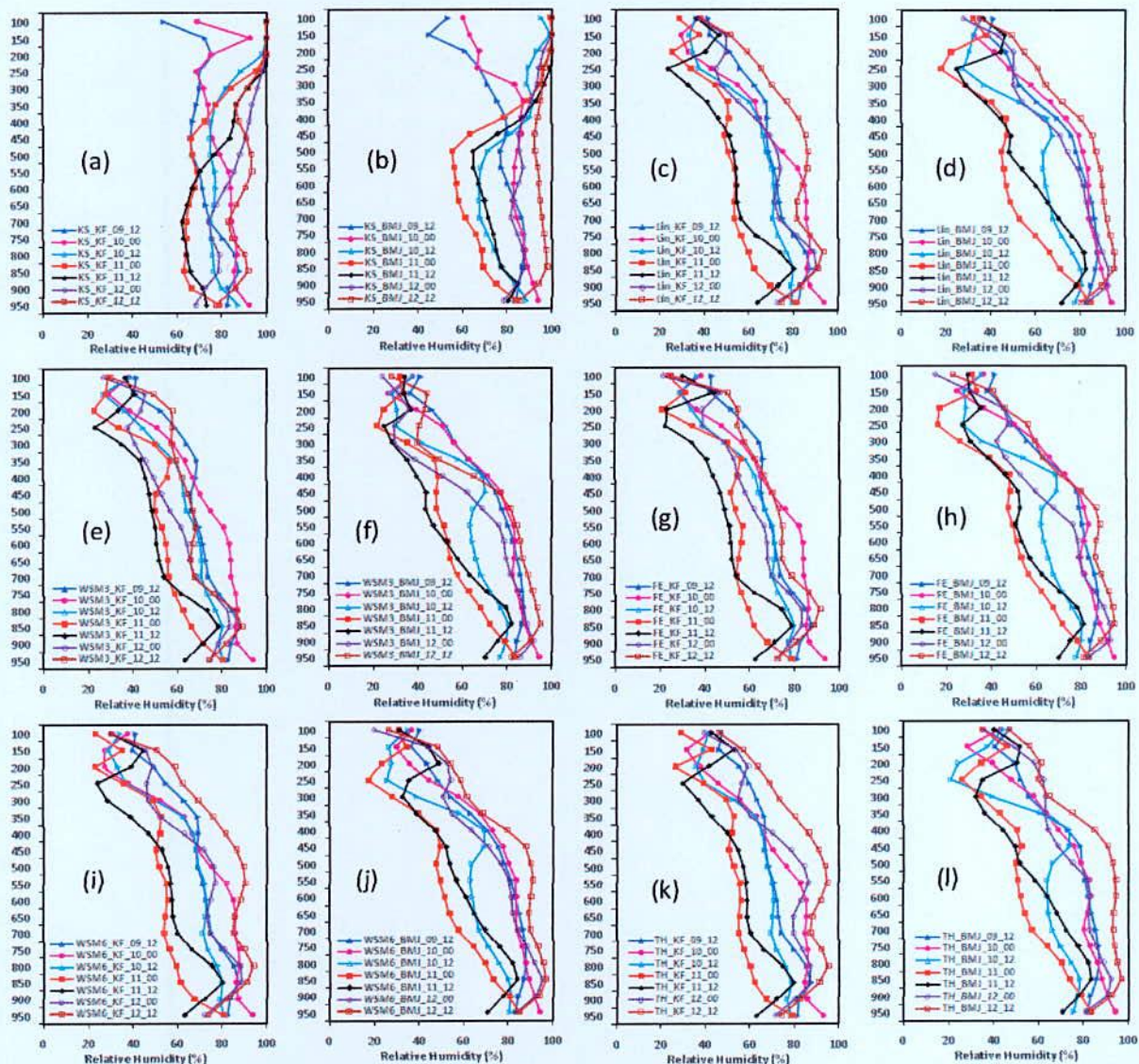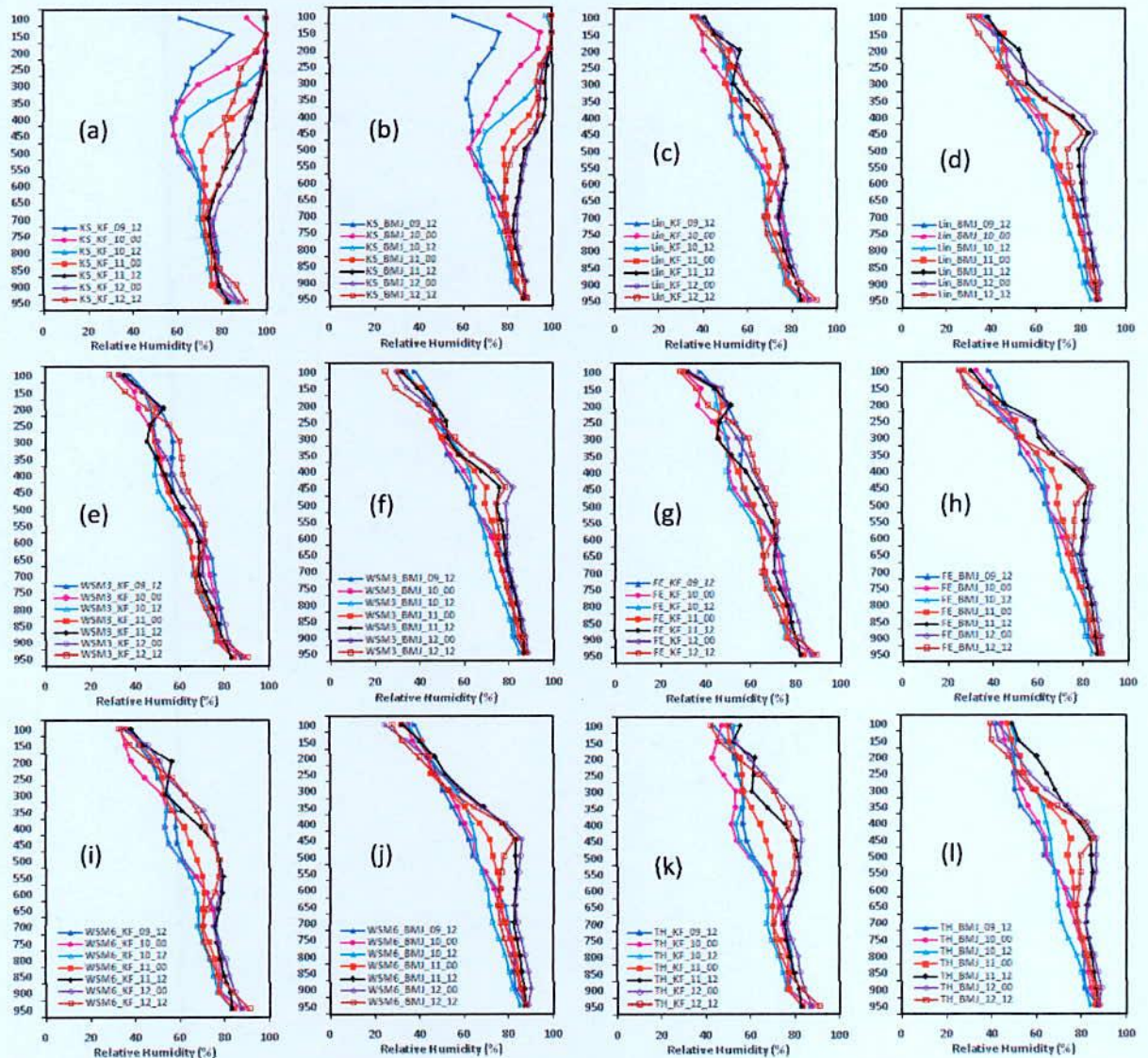

Figure 4.2.14: Simulated RH at region D4 with the progression of time using different MPs coupling with KF and BMJ schemes of TC 'Phailin'.

4.2.11 Vorticity

The vertical profiles of space averaged (starting from 1200 UTC of 09 October to 1200 UTC of 12 October 2013) vorticity in region D2 for six MP schemes coupling with KF and BMJ schemes are presented in Figure 4.2.15(a-l). The vorticity has increased significantly at 0000 UTC of 11 October to 1200 UTC of 12 October 2013 (i.e. before landfall) for all MP schemes coupling with KF and BMJ schemes. The positive vorticity has been simulated from surface to 100 hPa by all MPs coupling with KF and BMJ schemes at 0000 & 1200 UTC of 12 October 2013 which indicates the cyclonic circulation exists before crossing the region D2. The negative vorticity has been simulated from surface to 100 hPa by all MPs coupling with KF and BMJ schemes at 1200 UTC of 10 October to 1200 UTC of 11 October 2013 and this indicates the anticyclonic flow there. The WRF model simulated vorticity has been found positive and has increased significantly at 0000 to 1200 UTC of 12 October 2013 for all MP schemes in coupling with BMJ scheme. All through the simulation, Thompson-KF and Kessler-BMJ have simulated maximum averaged vorticity and WSM3-KF and WSM3-BMJ combinations have simulated minimum averaged vorticity during the period. But the general tendency of all the figures, the vorticity has increased with respect to initial value. As the time progresses, the TC moves northwestward direction in the Bay of Bengal and also the vorticity increased in region D2 and TC Phailin moves in that direction. It indicates that there is positive correlation with the movement of TC and positive vorticity. It has observed that the vorticity has increased in a direction where the TC Phailin moves.

The time varying vertical profiles of space averaged vorticity ($\times 10^{-5}$/s) simulated in region D4 by six different MPs coupling with KF and BMJ schemes are presented in Figure 4.2.16(a-l). The vorticity has increased continuously during 1200 UTC of 09 October to 0000 UTC of 12 October for all MPs coupling with KF and BMJ schemes. The positive vorticity has been simulated at surface to 300 hPa and negative vorticity at 300-100 hPa levels for all MPs coupling with KF and BMJ schemes. After 0000 UTC of 12 October the vorticity has decreased significantly for all MPs coupling with KF and BMJ schemes. The intensity of TC has turned continuously from CS to VSCS since 1200 UTC of 09 October to 0600 UTC of 10 October the vorticity has also increased significantly during this time by all MPs coupling with KF scheme.

Figure 4.2.15: WRF Model simulated vorticity in region D2 with the progression of time using different MPs coupling with KF and BMJ schemes of TC 'Phailin'.

The positive vorticity has been simulated at 1200 UTC of 09 October to 0000 UTC of 11 October and negative at 1200 UTC of 11 October to 1200 UTC of 12 October from surface to 100 hPa level for all MPs coupling with KF and BMJ schemes in region D1 (Figure not shown).For all MPs coupling with KF and BMJ schemes, the vorticity has decreased continuously at 1200 UTC of 09 October to 1200 UTC of 12 October in region D1. The simulated vorticity has been positive from surface to mid troposphere and negative from mid to upper troposphere for all MPs coupling with KF and BMJ schemes in region D3 (Figure not

shown). The vorticity has increased at 0000 UTC of 11 October to 1200 UTC of 12 October in region D3 for all MPs coupling with KF and BMJ schemes. The simulated vorticity has been almost negative for all MPs coupling with KF and BMJ schemes in region D5 (Figure not shown). All MPs coupling with KF and BMJ schemes have simulated single peak of vorticity at around 400 hPa in region D5. With the progression of time, the TC moves towards region D2 and the vorticity has decreased continuously in region D5.
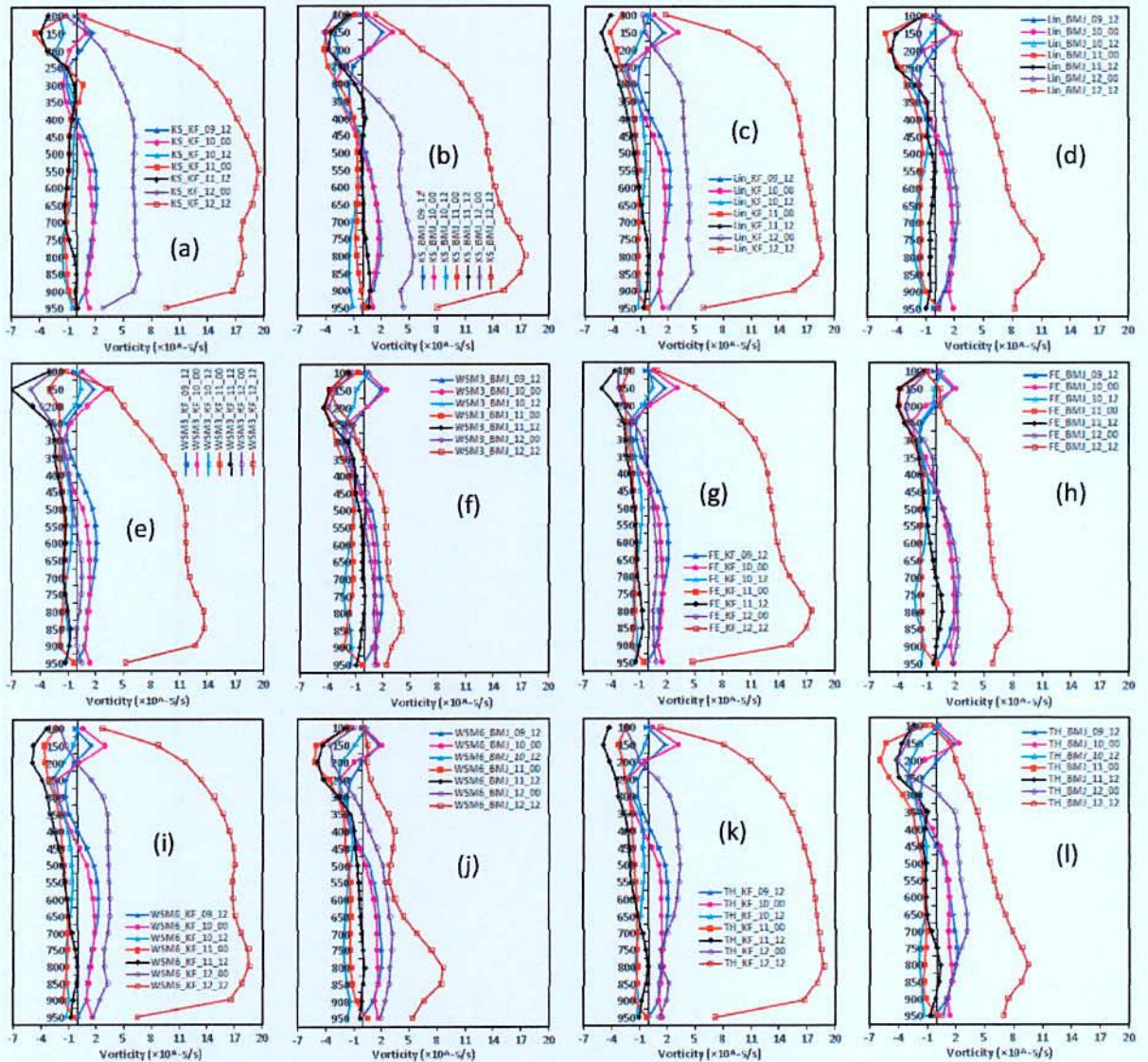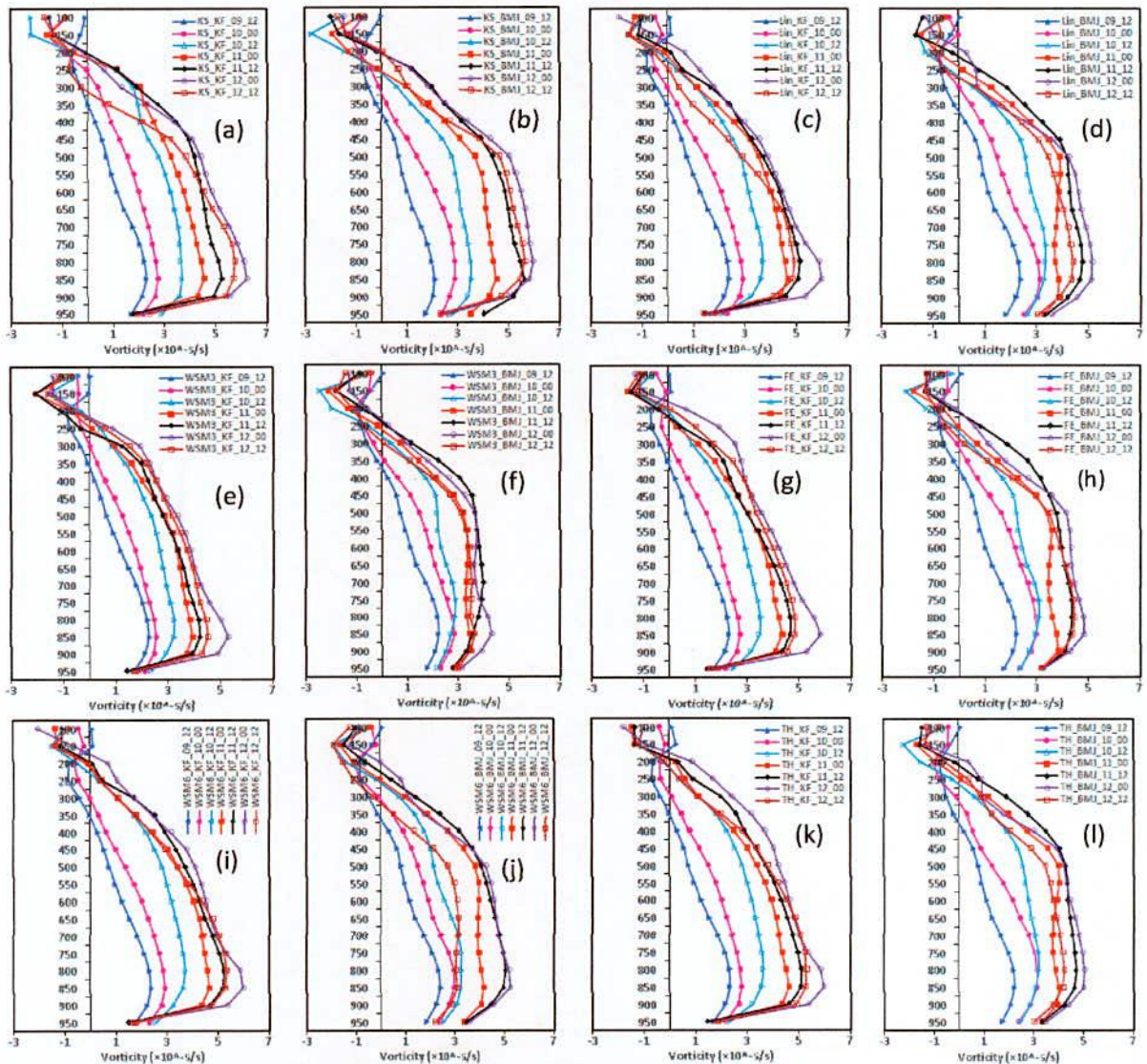

Figure 4.2.16: Simulated vorticity in region D4 with the progression of time using different MPs coupling with KF and BMJ schemes of TC 'Phailin'.

4.3 Tropical Cyclone Sidr

4.3.1 Synoptic situation of Tropical Cyclone Sidr

A low pressure area formed over southeast of the Andaman Islands with a weak low-level circulation near the Nicobar Islands on 9 November 2007. It moved north-northwesterly direction initially and intensified into a well-marked low over the same area. India Meteorological Department (IMD) designated the system as Depression. Depression over the southeast Bay of Bengal and adjoining Andaman Sea and lay centered at 0900 UTC of 11 November 2007 near 10°N and 92°E about 200 km south–southwest of Port Blair and the system is likely to intensify further and move in a west north westerly direction. The depression moved further north northwest and transformed to deep depression (DD) and lay centered 10.5°N and 91.5°E at 1800 UTC of the same day. The system further intensified into cyclonic storm as on 0300 UTC of 12 November and severe cyclonic storm (SCS) as on 1200 UTC of the same day and lay centered at 11.5 N and 90 E and move northerly direction. The system attained into a very severe cyclonic storm (VSCS) with the central MSLP of 986 hPa, the MWS of 33 m/s and the central location at about 11.5°N and 90.0°E at around 1800 UTC of 12 November. The VSCS 'Sidr' moved in the same direction and intensified further and at 0300 UTC of 15 November its central MSLP lowered to 944.0 hPa, the MWS increased to 58.8 m/s when its central location was at about 18°N and 89°E. Then, the VSCS 'Sidr' moved continuously north wards finally crossed Bangladesh coast at around 1600 UTC of 15 November 2007. After landfall, the system weakened slowly by giving precipitation over Bangladesh coast. The IMD, JTWC and WRF model simulated tracks are depicted in Figure 4.3.2 (a-d).

4.3.2 Intensity of TC Sidr

3-hourly minimum sea level pressure (MSLP) and associated maximum wind speed (ms^{-1}) at 10 m level have been simulated using different MP schemes coupling with CP schemes and are presented in Figure 4.3.1. The simulated intensity in terms of MSLP for six different MP schemes in combination with KF scheme is much higher than that of BMJ scheme with the initial conditions at 0000 UTC of 11 and 12 November. IMD observed intensity (944 hPa, 58.8 m s^{-1}) is much lower than that of JTWC intensity (918 hPa, 71.5 m s^{-1}).

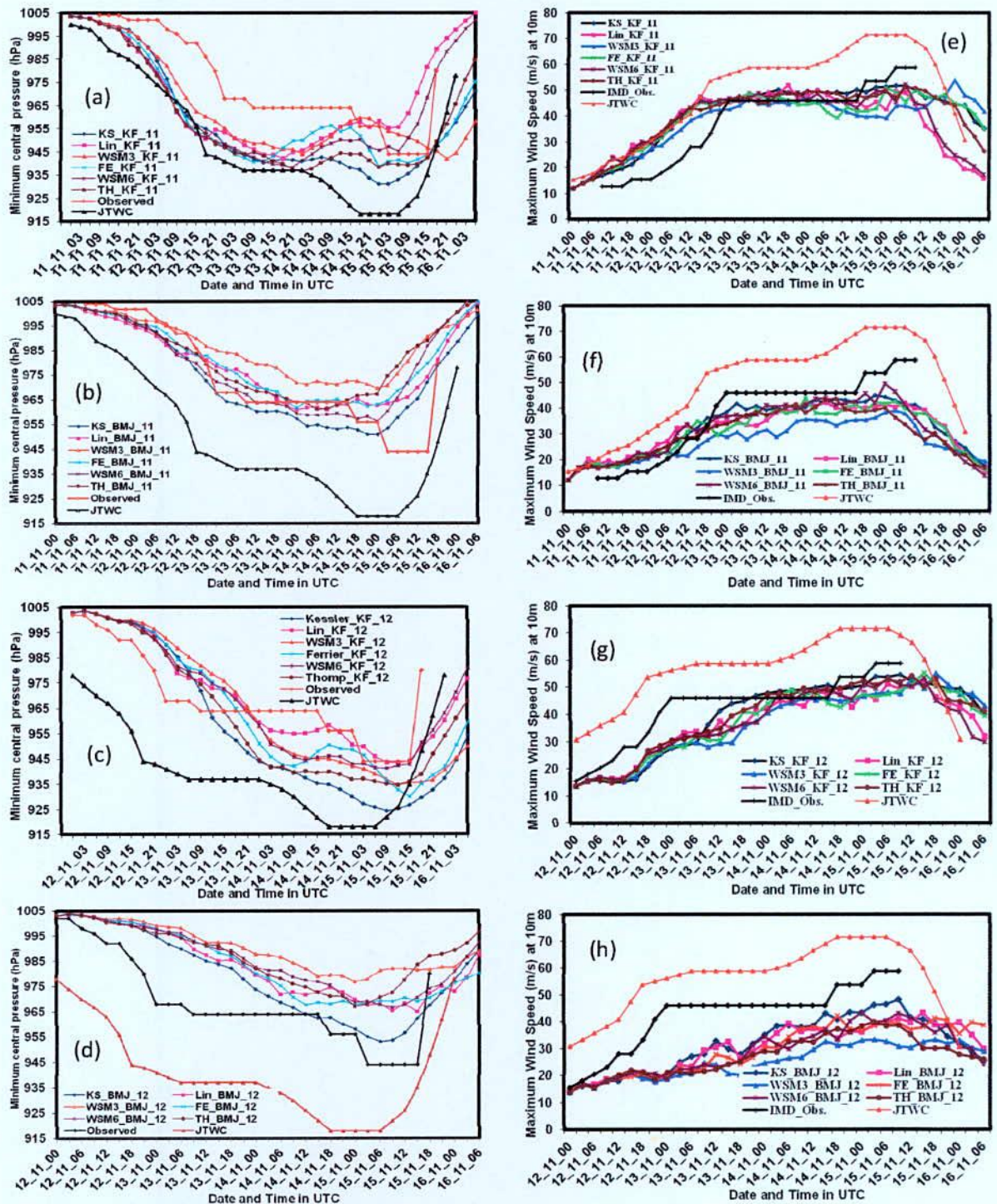Figure 4.3.1: Model simulated (a-d) CSLP (hPa) and (e-h) maximum sustained wind at 10 m level of TC Sidr using six different MP schemes coupling with KF and BMJ schemes with initial conditions at 0000 UTC of 11 and 12 November 2007.

The simulated pressure fall with the initial conditions at 0000 UTC of 11 and 12 November Lin *et al.* scheme in combination with KF scheme are close to IMD observed results but lower than JTWC observed results. The simulated MSLP for all other MP schemes in combination with KF scheme lies between IMD and JTWC observed results with the initial conditions 0000 UTC of 11 and 12 November. The pressure drop and wind speed simulated with the initial conditions of 0000 UTC of 11 & 12 November for all MP schemes in combination with BMJ scheme are much lower than that of IMD and JTWC observed pressure and maximum wind speed. The wind speed simulated at 10 m level for all MP schemes coupling with KF scheme with the initial condition of 0000 UTC of 11 and 12 November is lower than that of JTWC observed wind speed and matched with IMD observed wind speed all through the simulation except maximum wind, which is less than that of IMD observed wind. BMJ scheme coupling with all MP schemes has simulated wind speed at 10 m level, which is much lower than that of IMD and JTWC observed wind with the initial conditions at 0000 UTC of 11 and 12 November.

4.3.3 Track of TC Sidr

The observed and simulated track for the period of 120-h and 96-h of TC Sidr for different MP schemes are displayed in Fig.4.3.2 (a-d). The track forecasts have shown reasonably accurate for different experiments i.e., up to the landfall time (landfall time of 1800 UTC of 15 November 2007). For all combination of MP and CP schemes, the model has captured the north-northwestward movement with the initial conditions at 0000 UTC of 11 and 12 November 2007. The significant deviations in tracks are observed among different microphysical schemes in combination with CP scheme with the initial conditions of 0000 UTC of 11 and 12 November. WSM3 and Kessler schemes in combination with KF and BMJ schemes has provided most deviated track with the initial conditions of 0000 UTC of 11 November and deviated towards left from the actual track of IMD and JTWC. At the time of landfall, Lin *et al.* and WSM6 schemes in combination with KF scheme and Lin *et al.*, Ferrier, WSM6 and Thompson schemes in combination with BMJ schemes have simulated less deviated track with the initial conditions of 0000 UTC of 11 November. The simulated tracks for all six MP schemes coupling with KF schemes have deviated significantly towards west from the original track with the initial conditions of 0000 UTC of 12 November. At the time of

landfall, the track deviation has minimum for Lin-BMJ and TH-BMJ combinations with the initial conditions at 0000 UTC of 12 November. There is no landfall of TC Sidr up to the simulation time for WSM3 scheme in combination with KF and BMJ schemes with the initial conditions of 0000 UTC of 11 and 12 November 2007.
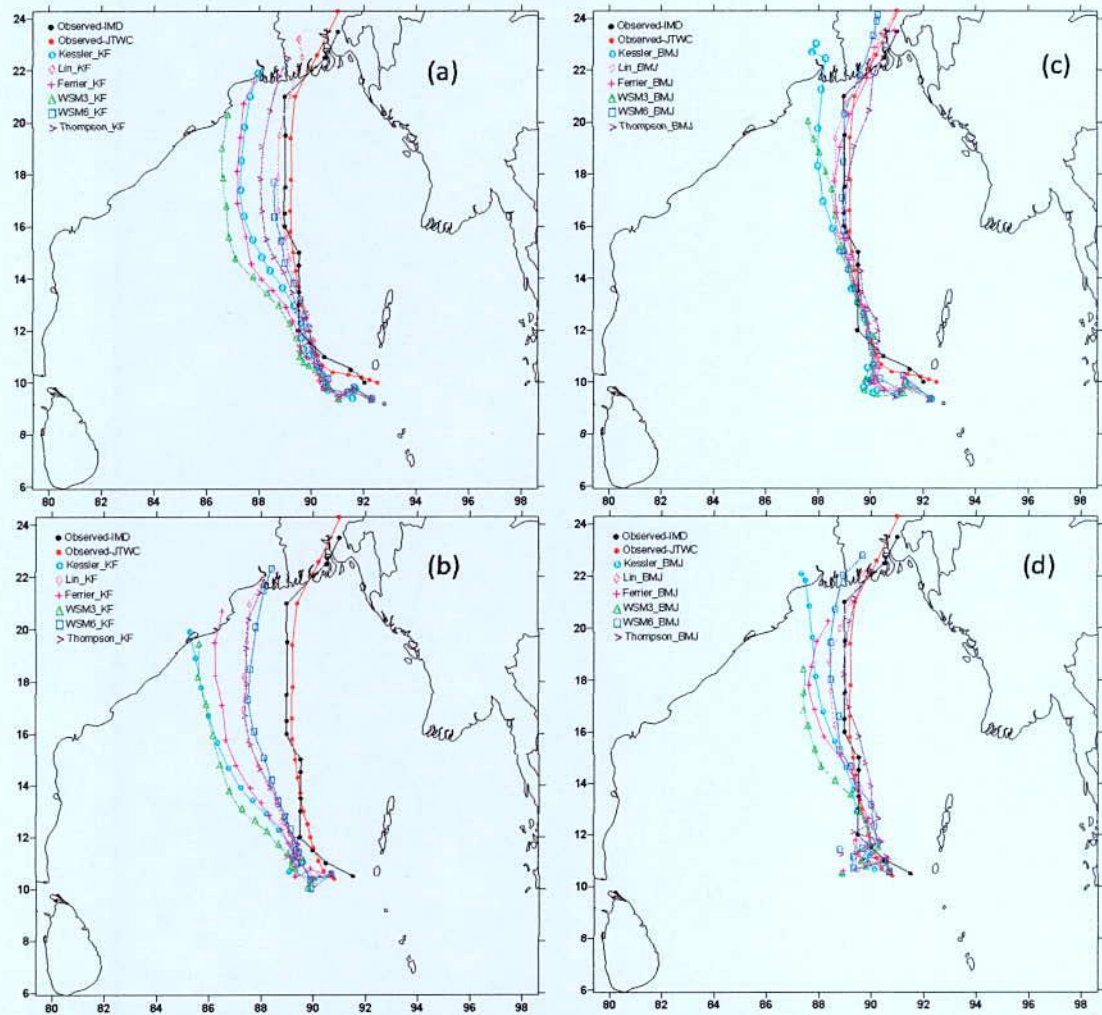
Figure 4.3.2: IMD and JTWC observed and simulated track of tropical cyclone 'Sidr' using six different MP schemes coupling with (a-b) KF scheme and (c-d) BMJ scheme with the initial conditions of 0000 UTC of 11 and 12 November 2007.

The landfall time has almost matched for all MP schemes in combination with BMJ scheme and Lin *et al.* and WSM6 schemes in combination with KF scheme for the initial conditions of 0000 UTC 11 November. The other combinations show landfall time delayed by 5-15h with the initial conditions of 0000 UTC 11 November. The simulated landfall time by using six

different MP schemes coupling with KF scheme are 0300UTC16, 1500UTC15, 0600UTC16, 0600UTC16, 1500UTC15 and 0000UTC16 respectively but when coupling with BMJ scheme, the times of landfall are 1400UTC15, 1500UTC15, no landfall, 1800UTC15, 1400UTC15 and 1600UTC15 respectively. The landfall time has delayed further with the initial conditions of 0000 UTC 12 November. No landfall of TC Sidr up to 0600 UTC of 16 November for WSM3-KF, WSM3-BMJ, Thompson-KF and Ferrier-BMJ combinations with the 0000 UTC of 12 November initial condition. Simulated landfall times by using Kessler, Lin *et al.*, Ferrier and WSM6 schemes coupling with KF scheme are 0600UTC16, 0600UTC16, 0600UTC16, and 0000UTC16 respectively. But when Kessler, Lin *et al.*, WSM6 and Thompson schemes are coupled with BMJ scheme, the landfall times are 0000UTC16, 0600UTC16, 0000UTC16 and 0600UTC16 respectively.

4.3.4 Cloud Water Mixing Ratio

The vertical profiles of area averaged CWMR (gm/kg) has been analyzed in region D1 by using six different MP schemes coupling with KF and BMJ schemes at different times 0000 UTC of 14, 15, 16 and 1200 UTC of 14 and 15 November 2007 as shown in Figure 4.3.3 (a-l). Kessler and WSM3 schemes coupling with KF and BMJ schemes have simulated CWMR up to 100 hPa. The other MPs like as Lin *et al.* and Ferrier, WSM6 and Thompson schemes coupling with KF and BMJ schemes have simulated CWMR up to 300, and 400 hPa levels respectively. The CWMR have simulated maximum at 900–500 hPa level for Lin, Ferrier, WSM6 and Thompson schemes in combination with KF and BMJ schemes. Vertical profiles of area averaged values of CWMR for Lin, Ferrier, WSM6 and Thompson schemes coupling with KF and BMJ schemes are almost constant and are zero from 350-100 hPa level. The CWMR has increased continuously up to the landfall time in region D1 on 0000 UTC of 16 November i.e. also after the landfall with respect to the time of 0000 UTC of 14 November for Lin-KF, Lin-BMJ, WSM3-KF, Ferrier-BMJ, WSM6-KF, WSM6-BMJ and Thompson-BMJ combinations. The intensity of TC has changed continuously from CS to SCS and VSCS since 0300 UTC of 12 November to 1200 UTC of 12 November and 1600 UTC of 15 November and the CWMR has also increased significantly during this time. It is observed that the CWMR has increased in region D1 and also the TC Sidr moves towards in that region. This indicates that the CWMR increases in a region towards which the TC moves.
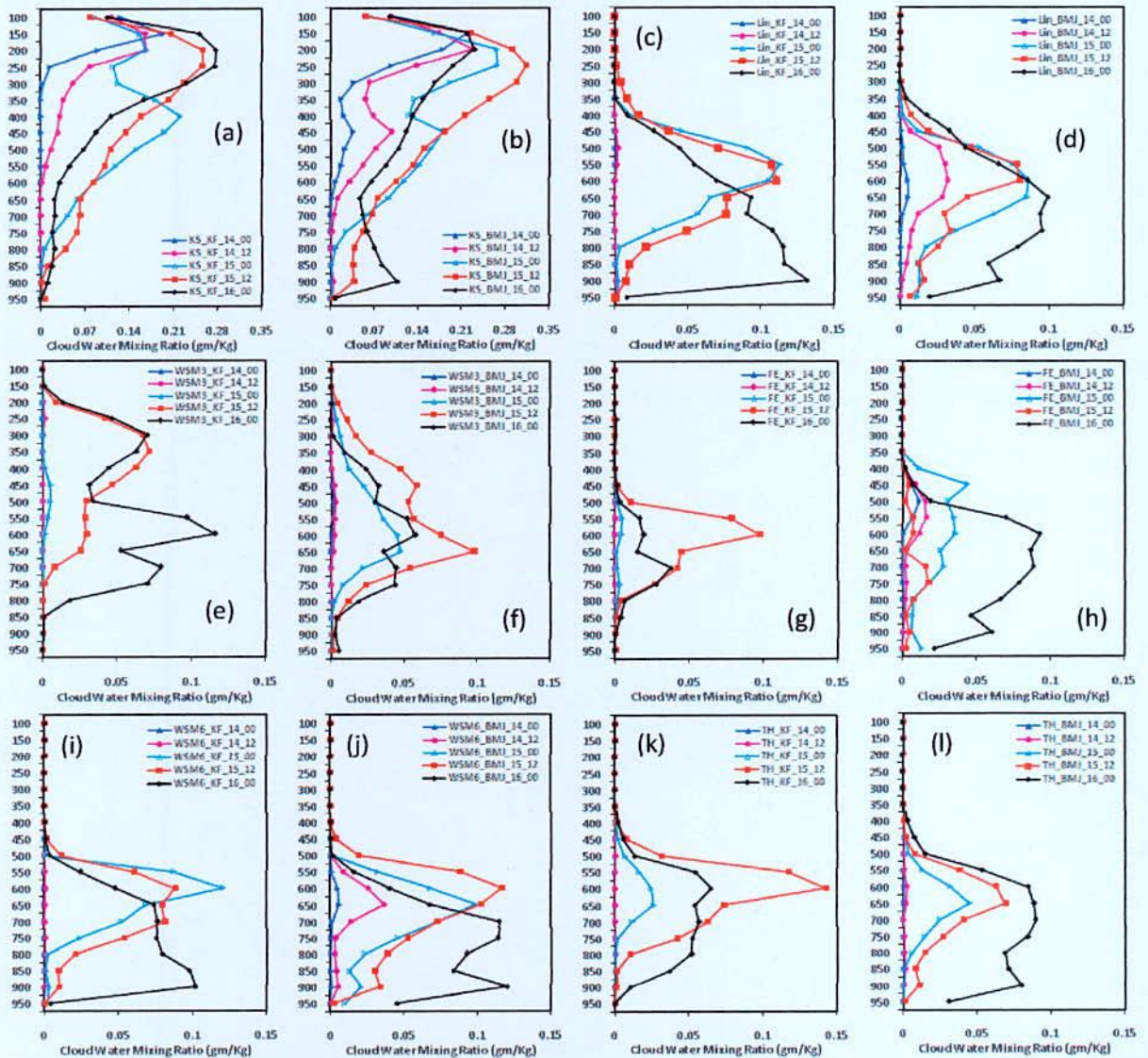
Figure 4.3.3: Simulated CWMR with the progression of time using different MP schemes coupling with KF and BMJ schemes of TC 'Sidr' at region D1.

The vertical profiles of area averaged CWMR (gm/kg) at different times such as 0000 UTC of 12, 13, 14, 15, 16 and 1200 UTC of 11, 12, 13, 14 and 15 November 2007 has been analyzed in region D4 by using six different MP schemes coupling with KF and BMJ schemes as shown in Figure 4.3.4(a-l). Kessler and WSM3 schemes coupling with KF and BMJ schemes have simulated CWMR up to 100 hPa. Lin *et al.*, Ferrier, WSM6 and Thompson schemes coupling with KF and BMJ schemes have simulated CWMR up to 200, 300, 400 and 400 hPa levels.

Kessler and WSM3 schemes coupling with KF and BMJ schemes have simulated two maxima of CWMR one at 200 & 250 and another one at 550 hPa level respectively.
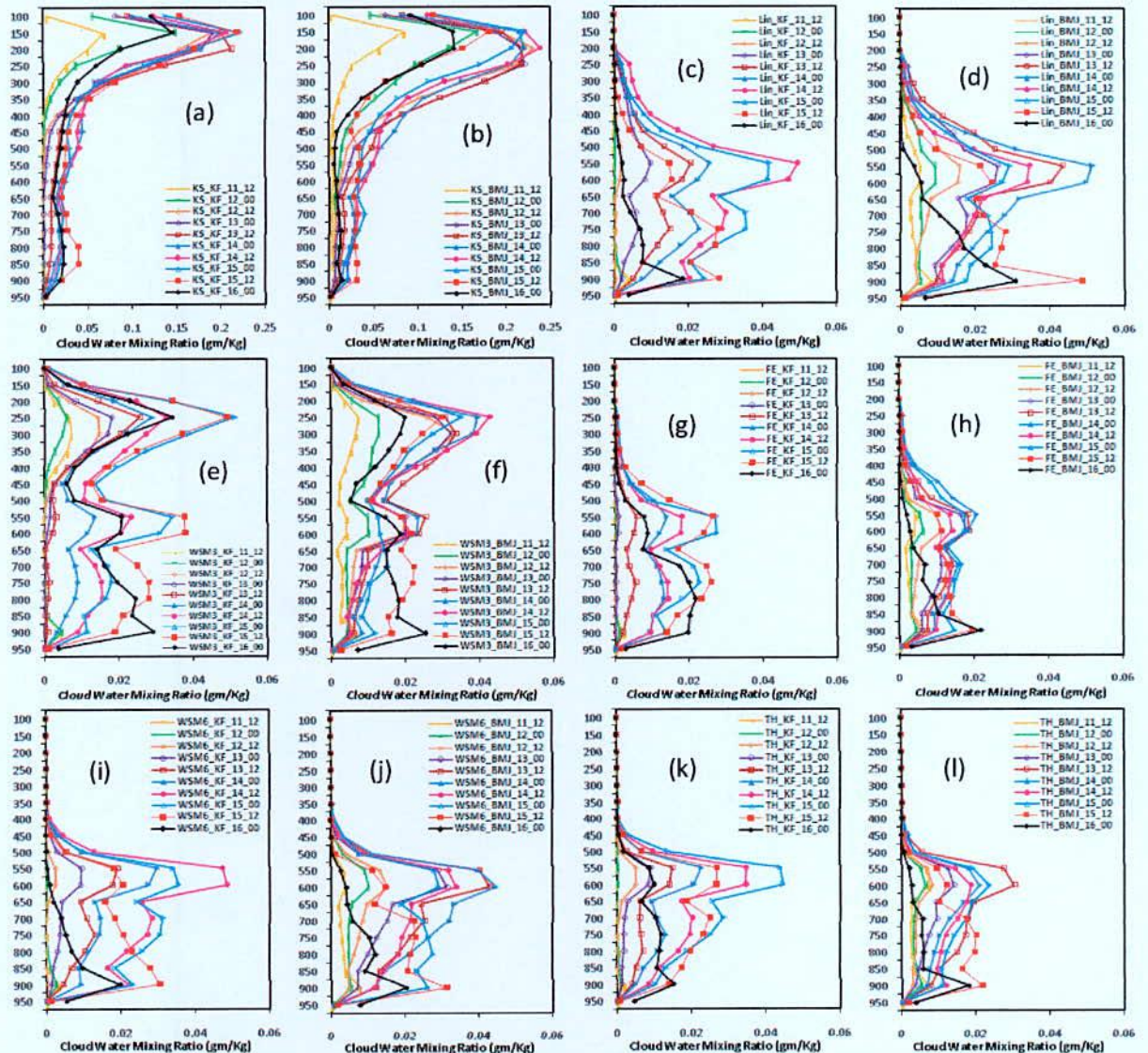
Figure 4.3.4: Simulated CWMR with the progression of time using different MP schemes coupling with KF and BMJ schemes of TC 'Sidr' at region D4.

The simulated CWMR has maximum at 650–550 hPa level for Lin, Ferrier, WSM6 and Thompson schemes in combination with KF and BMJ schemes. Vertical profiles of area averaged CWMR for all MPs coupling with KF and BMJ schemes are almost constant and CWMR is zero from 250-100 hPa. The intensity of TC has changed continuously from CS to SCS and VSCS since 0300 UTC of 12 November to 1200 UTC of 12 November and 1600

93

UTC of 15 November and the CWMR has also increased significantly during this time. The CWMR has decreased after 1200 UTC of 15 November as seen by using Kessler-KF, WSM3-KF, WSM3-BMJ, Ferrier-KF, Ferrier-BMJ and Thompson-BMJ combinations and decreases after 1200 UTC of 14 November by using Kessler-BMJ, Lin-KF, Lin-BMJ, WSM6-KF, WSM6-BMJ and Thompson-KF combinations. The CWMR has decreased since 0000 UTC of 15 November by Kessler-KF, Lin-KF, Lin-BMJ WSM6-KF, WSM6-BMJ and Thompson-KF combinations. Since the CWMR has not increased sufficiently and the intensity of TC has also not increased significantly for different MPs in combination with KF and BMJ schemes of TC Sidr. As Kessler-KF combination has simulated minimum CWMR out of all combinations and the track of the cyclone deviated towards right from the observed track.

BMJ scheme has simulated much higher CWMR than that of KF scheme in combination with different MPs in regions D2, D3 and D5 but its magnitude is not significant (Figure not shown). As the time progresses, the TC moves towards north in the BoB and also the CWMR has decreased in region D3 and D5 and the simulated CWMR is minimum in region D3. It indicates that the cyclone has not moved in those directions. Except Kessler, all MPs coupling with KF and BMJ schemes have simulated small peak of CWMR at around 750 hPa levels but at the other level the CWMR shows zero value in regions D2 and D5. BMJ scheme has simulated higher CWMR than that of KF scheme in combination with different MPs in regions D3 and D5, and KF scheme has simulated higher CWMR than that of BMJ scheme in combination with different MPs in region D2, but its magnitude is not significant (Figure not shown). Since the intensity of TC has not increased in those directions where the vertical profiles of CWMR has not increased.

4.3.5 Rain Water Mixing Ratio

Vertical profiles of area averaged RWMR (gm/kg) have been analyzed in region D1 by using six different MP schemes coupling with KF and BMJ schemes at 0000 UTC of 12, 13, 14, 15, 16 and 1200 UTC of 11, 12, 13, 14 and 15 November 2007 as shown in Figure 4.3.5 (a-l). Kessler, WSM3 and Lin, Ferrier, WSM6 and Thompson schemes coupling with KF and BMJ schemes have simulated RWMR up to 150, 200 and 500 hPa respectively. The maximum RWMR has been simulated at 750 hPa level by WSM6-BMJ combination. The RWMR has

increased in region D1 since 0000 UTC of 14 to 1200 UTC of 15 November 2007 after that it has decreased at 0000 UTC of 16 November for all MPs coupling with KF and BMJ schemes. The RWMR simulated for Lin, Ferrier, WSM6 and Thompson schemes coupling with KF and BMJ schemes is almost constant and zero from 500 to100 hPa level. The RWMR has also increased in region D1 after the landfall by Kessler-KF, Lin-BMJ, Ferrier-BMJ, Thompson-KF and Thompson-BMJ combinations.
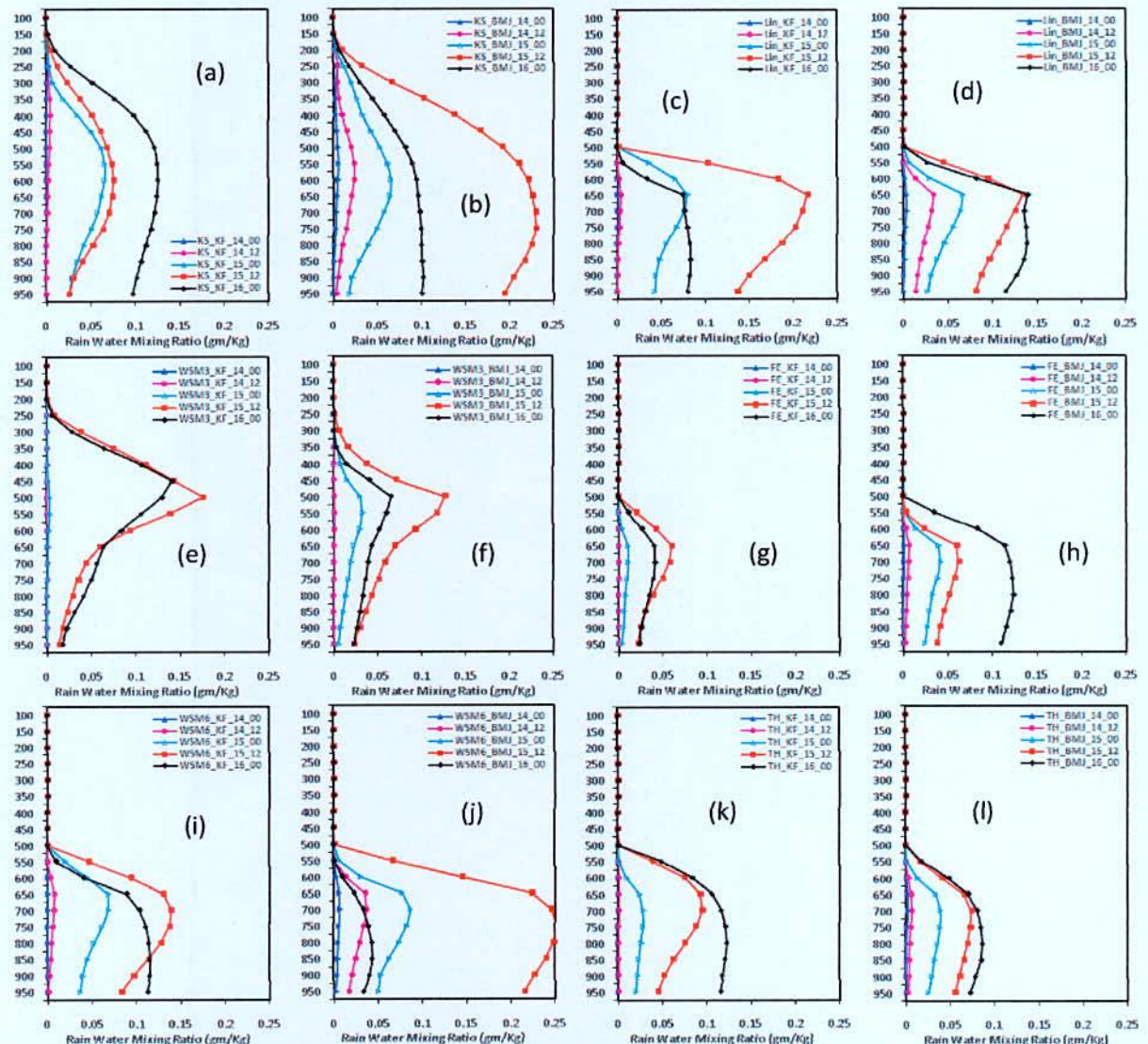

Figure 4.3.5: Simulated RWMR in region D1 with the progression of time using different MP schemes coupling with KF and BMJ schemes of TC 'Sidr'.

As the time progresses, the RWMR has increased in region D1 for all MPs coupling with KF and BMJ schemes and the TC Sidr moves towards region D1 i.e. in Bangladesh coast. It indicates that the RWMR increases with the advancement of the TC Sidr.

The vertical profiles of area averaged RWMR (gm/kg) has been analyzed in region D4 by using six different MP schemes coupling with KF and BMJ schemes at 0000 UTC of 12, 13, 14, 15, 16 and 1200 UTC of 11, 12, 13, 14 and 15 November 2007 and are shown in Figure 4.3.6 (a-l). Kessler and WSM3 schemes has simulated RWMR up to 150 and 100 hPa respectively and the other MPs has simulated up to 500 hPa level coupling with KF and BMJ schemes. The maximum RWMR has been simulated at 450 hPa level by WSM3 scheme coupling with KF and BMJ scheme. The intensity of TC has changed continuously from CS to SCS and VSCS since 0300 UTC of 12 November to 1200 UTC of 12 November and 1600 UTC of 15 November and the RWMR has also increased significantly during this time. The patterns of rain water profile are similar up to 500 hPa levels with Lin, FE, WSM6 and Thompson schemes coupling with KF and BMJ schemes. The RWMR has decreased after 0000 UTC of 15 November by using KS-KF, WSM3-KF and Kessler-BMJ combinations and after 1200 UTC of 14 November by using Lin-KF, WSM6-KF and Thompson-KF combinations and after 0000 UTC of 14 November by using Lin-BMJ, WSM3-BMJ, Ferrier-BMJ and WSM6-BMJ combinations. Due to the significant increase of RWMR up to 1200 UTC of 14 November as simulated by all MPs coupling with KF and BMJ schemes, the intensity of the TC Sidr in terms of pressure fall and wind speed has increased significantly. TC Sidr could not intensify using Lin-KF, Lin-BMJ, WSM3-BMJ, Ferrier-BMJ, WSM6-KF, WSM6-BMJ, Thompson-KF and Thompson-BMJ combinations similarly as observed. Due to this reason the RWMR has decreasing tendencies in region D4. The average maximum RWMR has been simulated by Kessler-BMJ, WSM3-KF, WSM3-BMJ, WSM6-BMJ and Lin-BMJ at 750, 400, 400, 700 and 650 hPa levels and are 0.11, 0.22, 0.21, 0.10 and 0.11 gm/kg respectively. WSM3-KF combination has simulated maximum and Thompson-BMJ combination has simulated minimum area averaged RWMR. Vertical profiles of area averaged profiles of RWMR for Lin, Ferrier,WSM6 and Thompson schemes coupling with KF and BMJ schemes are almost constant and RWMR is zero from 500 to100 hPa level.

BMJ scheme has simulated higher RWMR than that of KF scheme in regions D3 and D5 but KF scheme has simulated higher RWMR than that of BMJ scheme in region D2 in combination with different MPs but its magnitude is not significant (Figure not shown). The vertical profiles of RWMR have not simulated properly in regions D2, D3 and D5 but with the progression of time it has decreased. Since the RWMR has decreased in regions D2, D3 and D5 and cyclone has not moved in those directions, it indicates that the RWMR depends on direction of movement of TC.
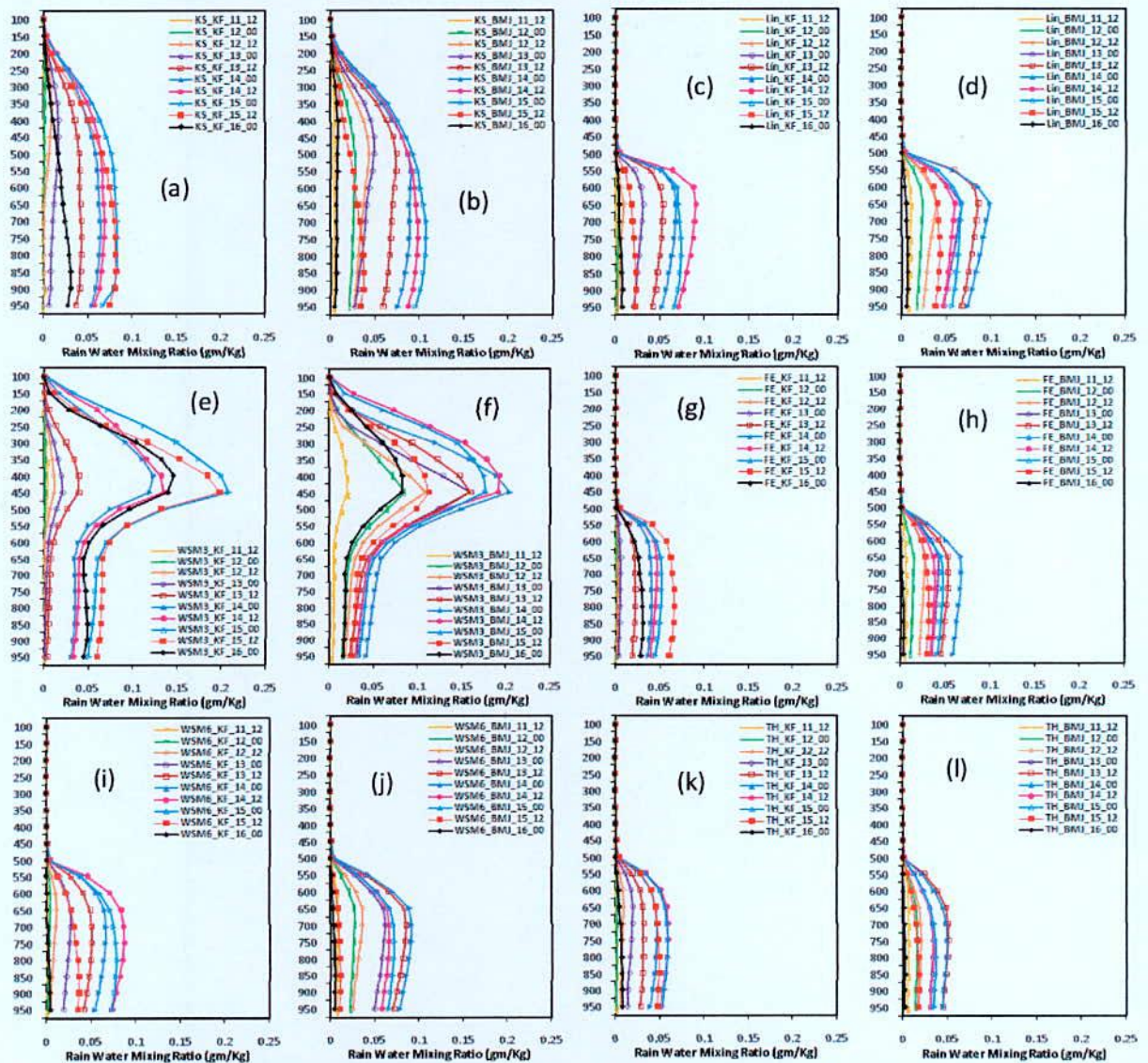

Figure 4.3.6: Simulated RWMR in region D4 with the progression of time using different MP schemes coupling with KF and BMJ schemes of TC 'Sidr'.

4.3.6   Cloud Ice Mixing Ratio

In regions D4 and D1, the vertical profiles of area averaged CIMR (gm/kg) have been simulated by Lin *et al.*, WSM6 and Thompson schemes coupling with KF and BMJ schemes at 0000 UTC of 12, 13, 14, 15, 16 and 1200 UTC of 11, 12, 13, 14 and 15 November 2007 and are presented in Figure 4.3.7 (a-d) and Figure 4.3.7 (e-g) respectively. In Figure 4.3.7 (a-d), in region D4 the Lin *et al.* and WSM6 schemes have simulated maximum cloud ice at around 250 hPa and Thompson scheme has simulated no significant amount of CIMR. WSM6 profile exhibits a prominent spike containing much larger CIMR values between 550 to 100 hPa and Thompson scheme has simulated less CIMR than that of other schemes. Thompson scheme in combination with KF and BMJ schemes have simulated much smaller amount of ice and concentrated at 250–100 hPa. Lin *et al.* scheme has simulated cloud ice between 450–100 hPa levels. Vertical profiles of area averaged CIMR for Lin, WSM6 and Thompson schemes coupling with KF and BMJ schemes are almost constant and CIMR is found zero at 950-450, 950-600 and 950-250 hPa levels respectively. As the intensity of TC has increased continuously from CS to VSCS, the CIMR has also increased significantly since 1200 UTC of 11 November to 1200 UTC of 14 November as seen by using Lin, WSM6 and Thompson schemes coupling with KF and BMJ schemes. The CIMR decreases after 1200 UTC of 14 November by using Lin, WSM6 and Thompson schemes coupling with KF and BMJ schemes. Lin *et al.* and WSM6 schemes have simulated maximum cloud ice at around 250 hPa and Thompson scheme has simulated maximum CIMR at 150 hPa levels. Lin *et al.*, WSM6 and Thompson schemes exhibit a prominent spike containing much larger CIMR values at 350-100, 600-100 and 300–100 hPa levels respectively.

Thompson scheme has simulated less but insignificant amount of CIMR than that of other schemes. The CIMR has increased since 0000 UTC of 14 November to 1200 UTC of 15 November for Lin, WSM6 and Thompson schemes coupling with KF and BMJ schemes and after that it has decreased at 0000 UTC of 16 November (i.e. at the time of landfall). Due to the movement of TC Sidr in region D1, the CIMR has increased in that direction. It indicates that CIMR increases with the increase in intensity of TC and over the area where the TC Sidr moves.

The CIMR has minimum simulated in regions D2, D3 and D5 by Lin *et al.*, WSM6 and Thompson schemes coupling with KF and BMJ schemes (Figure not shown). WSM6 scheme has simulated higher CIMR than that of Lin and Thompson scheme coupling with KF and BMJ schemes in regions D2, D3 and D5. With the progression of time, the CIMR has decreased in regions D2, D3 and D5 and TC Sidr does not move in those regions also. It indicates that the CIMR has increased over the region in the direction in which cyclone moves.

Figure 4.3.7: Simulated CIMR at region (a-d) D4 & (e-h) D1 with the progression of time using different MP schemes coupling with KF and BMJ schemes of TC 'Sidr'.

4.3.7 Cloud Snow Mixing Ratio

In region D1, the vertical profiles of area averaged CSMR (gm/kg) have been simulated by Lin, Ferrier, WSM6 and Thompson schemes coupling with KF and BMJ schemes at 0000 UTC of 14, 15, 16 and 1200 UTC of 14 and 15 November 2007 and are presented in Figure 4.3.8 (a-h). It is evident from the figure that the vertical structure and magnitude of these profiles vary greatly. Overall, the Thompson scheme has generated the maximum amount of snow between 700 to 100 hPa. The abundance of snow in the mid troposphere (below 400

hPa) may be due to the enhanced ice content in the upper troposphere. The CSMR has increased up to 1200 UTC of 15 November i.e. before the landfall and decreased at 0000 UTC of 16 November by all MPs coupling with BMJ scheme. As the intensity of TC Sidr in terms of pressure fall and wind speed has increased, there is significant increase of CSMR up to 1200 UTC of 15 November as simulated by Lin, Ferrier, WSM6 and Thompson schemes coupling with KF and BMJ schemes. Vertical profiles of area averaged CSMR for Lin, Ferrier, WSM6 and Thompson schemes coupling with KF and BMJ schemes are almost constant and CSMR is zero from surface to 650 hPa levels. As the time progresses, the CSMR has increased in region D1 for Lin, Ferrier, WSM6 and Thompson schemes coupling with KF and BMJ schemes when the TC Sidr moves towards region D1 i.e. in Bangladesh coast.

Figure 4.3.8: Simulated CSMR with the progression of time using different MP schemes coupling with KF and BMJ schemes of TC 'Sidr' at region D1.

In region D4, the vertical profiles of area averaged CSMR (gm/kg) have been simulated by Lin, Ferrier, WSM6 and Thompson schemes coupling with KF and BMJ schemes at 1200 UTC of 11, 12, 13, 14, 15 and 0000 UTC of 12, 13, 14, 15 and 16 November 2007 and are presented in Figure 4.3.9 (a-h). It is evident from the figure that the vertical structure and
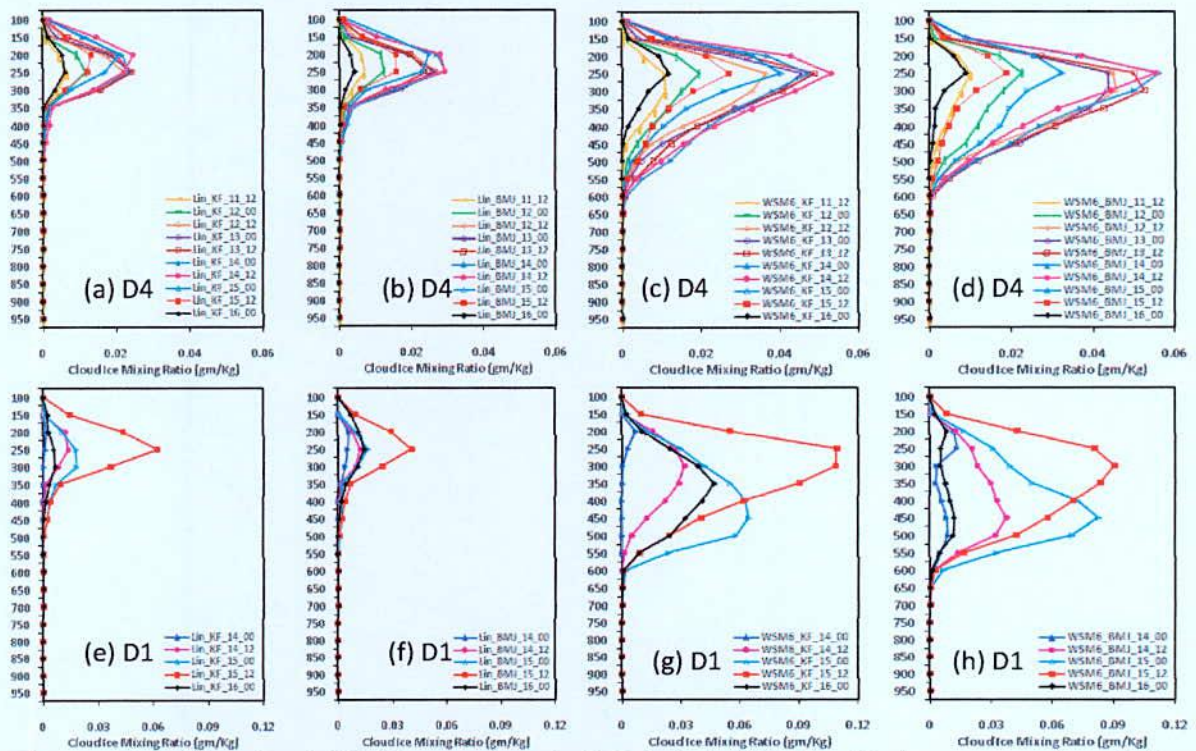
100

Figure 4.3.9: Simulated CSMR with the progression of time using different MP schemes coupling with KF and BMJ schemes of TC 'Sidr' at region D4.

The intensity of TC has changed continuously from CS to VSCS since 0300 UTC of 12 November to 1200 UTC of 12 November and 1600 UTC of 15 November and the CSMR has also increased significantly during this time by Lin *et al.*, Ferrier, WSM6 and Thompson schemes coupling with KF and BMJ schemes. The patterns of cloud snow profile are similar to upper level with Lin *et al.*, Ferrier, WSM6 and Thompson schemes coupling with KF and BMJ schemes. The CSMR has decreased after 1200 UTC of 14 November as obtained by using Lin-KF, Ferrier-KF, WSM6-KF and Thompson-KF combinations and has decreased after 0000 UTC of 14 November by using Lin-BMJ, Ferrier-BMJ, WSM6-BMJ and Thompson-BMJ combinations.

In regions D2, D3 and D5 the minimum CSMR has simulated for Lin, Ferrier, WSM6 and Thompson schemes coupling with KF and BMJ schemes. KF scheme has simulated higher (lower) CSMR than that of BMJ scheme in regions D2, D3 and D5 but its magnitude is not

significant (Figure not shown). With the progression of time, the TC moves towards region D1 (i.e. Bangladesh coast) and the CSMR has decreased in regions D2, D3 and D5.

4.3.8 Cloud Graupel Mixing Ratio

The vertical profiles of area averaged CGMR (gm/kg) have been simulated in region D4 by Lin *et al.*, WSM6 and Thompson schemes coupling with KF and BMJ schemes at 1200 UTC of 11, 12, 13, 14, 15 and 0000 UTC of 12, 13, 14, 15 and 16 November 2007 and are presented in Figure 4.3.10 (a-d). Lin *et al.*, WSM6 and Thompson schemes have simulated maximum CGMR at around 500 hPa levels and BMJ scheme has simulated larger CGMR than that of KF scheme. The Lin and WSM6 scheme have simulated higher CGMR and Thompson scheme has simulated lower CGMR. The WSM6 scheme has simulated higher CGMR and Thompson scheme has simulated lower CGMR than that of Lin *et al.* schemes. Graupel starts to produce at 650 hPa and sharp spike are found at 500 hPa levels in case of Lin *et al.* and WSM6 and then decreases to zero at 100 hPa.
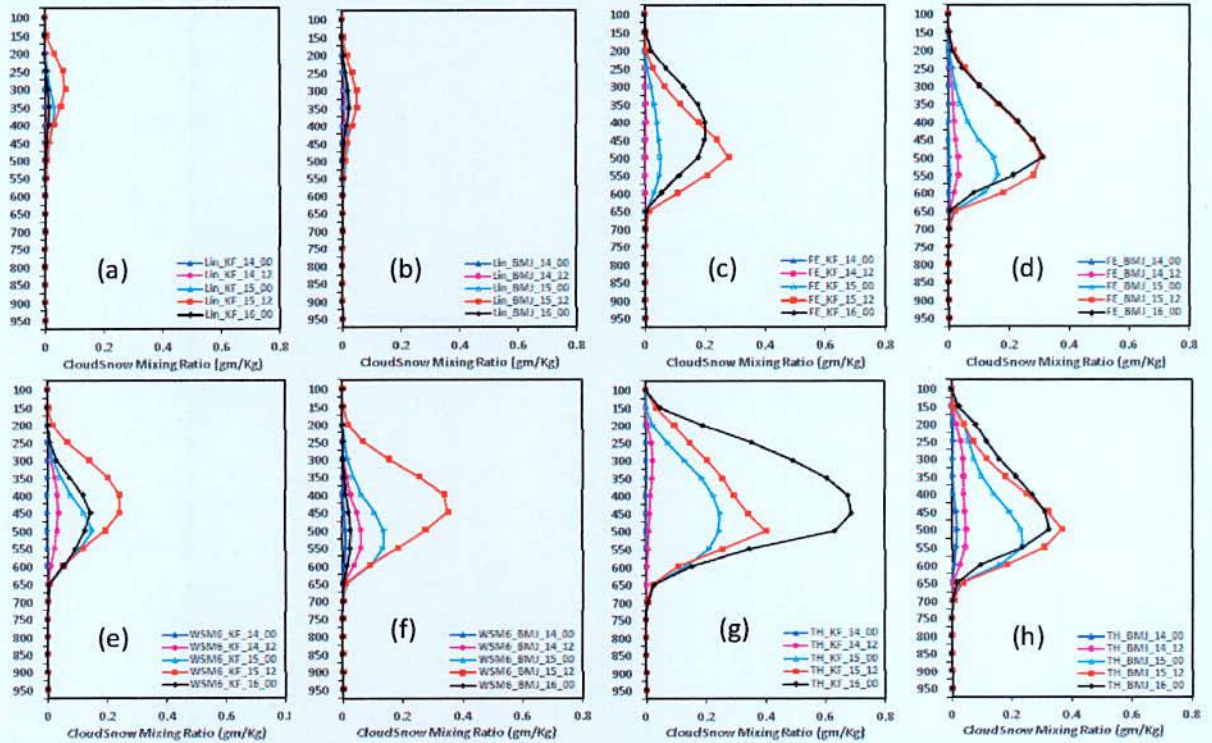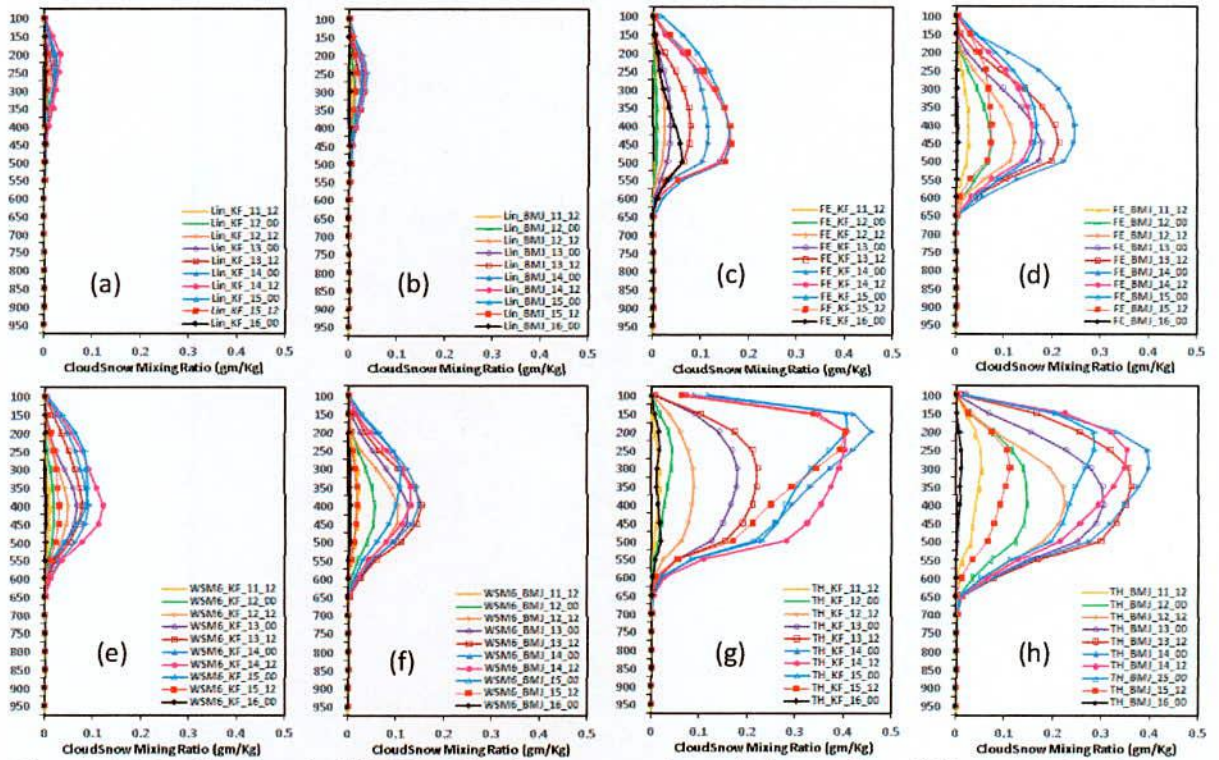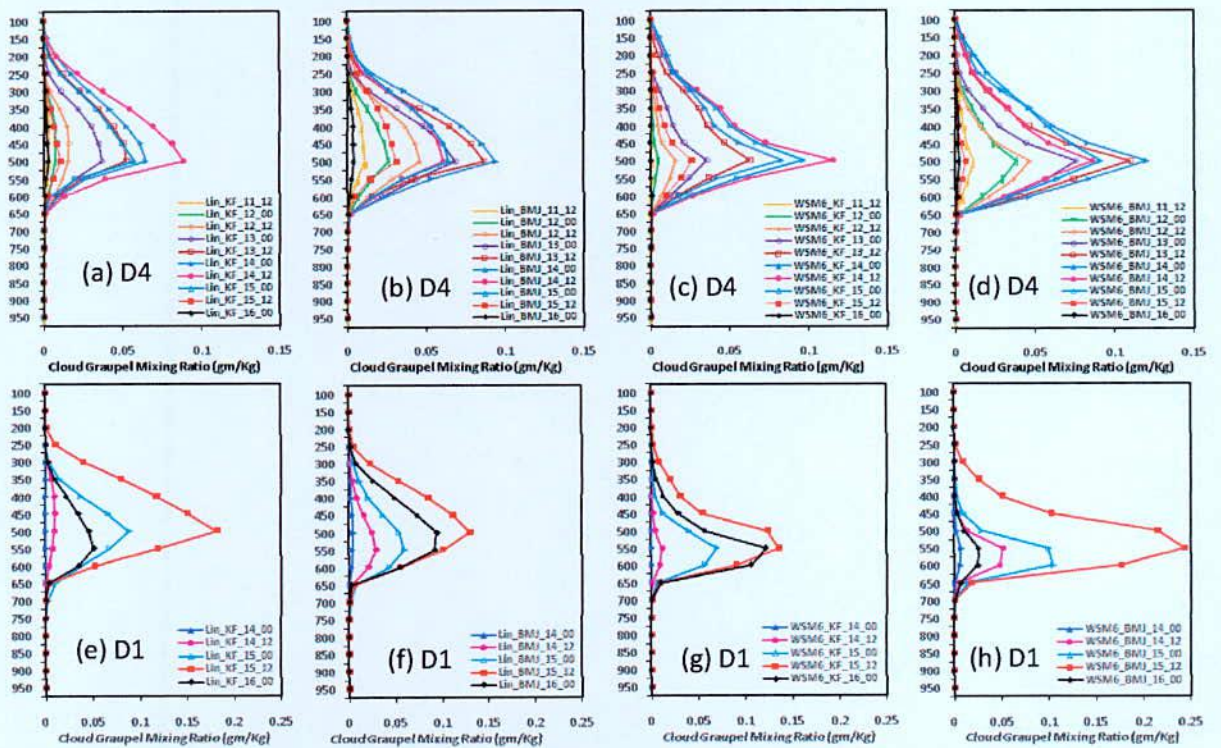

Figure 4.3.10: Simulated CGMR with the progression of time using different MP schemes coupling with KF and BMJ schemes of TC 'Sidr' at region (a-d) D1 & (e-h) D4.

The intensity of TC has changed continuously from CS to SCS and VSCS since 0300 UTC of 12 November to 1200 UTC of 12 November and 1600 UTC of 15 November, and the CGMR has also increased significantly up to 1200 UTC of 14 November by Lin-KF, WSM6-KF combinations and the CGMR has also increased significantly up to 0000 UTC of 14 November by Lin-KF, WSM6-KF combinations. The patterns of cloud graupel profile are similar at upper level for Lin, WSM6 and Thompson schemes coupling with KF and BMJ schemes. The CGMR has increased up to 1200 UTC of 14 November and 0000 UTC of 14 November and after that it has decreased by Lin and WSM6 schemes coupling with KF and BMJ schemes respectively. TC Sidr could not intensify similarly as observed by Lin, WSM6 and Thompson schemes coupling with KF and BMJ schemes due to this CGMR decrease earlier since 1200 UTC of 14 November.

The vertical profiles of area averaged CGMR (gm/kg) have been simulated in region D1 at 0000 UTC of 14, 15, 16 November and 1200 UTC of 14, 15 November 2007 by Lin et al., WSM6 and Thompson schemes coupling with KF and BMJ schemes and are presented in Figure 4.3.10 (e-h). Lin et al. and WSM6 schemes have simulated maximum CGMR at around 550 hPa levels. The Lin and WSM6 scheme has simulated higher CGMR and Thompson scheme has simulated lower but insignificant amount of CGMR. Graupel starts to produce at 700 hPa and sharp spike has found at 500 and 550 hPa levels in case of Lin et al. and WSM6 schemes respectively and then decreases to minimum at 200 hPa. KF scheme has simulated larger (smaller) CGMR than that of BMJ scheme for Lin et al. (WSM6) scheme. The CGMR has increased in region D1 on 1200 UTC of 15 with respect to that of 0000 UTC of 14 November by Lin et al. and WSM6 coupling with KF and BMJ schemes. As the time progresses, the CGMR has increased in region D1 (i.e. Bangladesh region) for Lin et al. and WSM6 schemes coupling with KF and BMJ schemes and also the TC Mala moves towards this region. This indicates that the CGMR has increased in the region where the TC Sidr moves.

In regions D2, D3 and D5, the CGMR has simulated minimum for Lin, WSM6 and Thompson schemes coupling with KF and BMJ schemes. KF scheme has simulated higher CGMR than that of BMJ scheme in combination with Lin, WSM6 and Thompson schemes in regions D2, D3 and lower in region D5 but its magnitude is not significant (Figure not shown). With the

progression of time, the TC moves towards region D1 and the CGMR has decreased in regions D2, D3 and D5. Since almost there is no change of CGMR the cyclone has not moved in those directions.

4.3.9   Cloud Water Vapor Mixing Ratio

The vertical profiles of area averaged WVMR (gm/kg) have been analyzed at different times 0000 UTC of 14, 15, 16 and 1200 UTC of 14 and 15 November 2007 in region D1 by using six different MP schemes coupling with KF and BMJ schemes and are shown in Figure 4.3.11 (a-l). The patterns of WVMR are different up to 200 hPa levels with all MPs coupling with KF and BMJ schemes. The maximum WVMR have been simulated at the surface and WVMR has decreased continuously with height for all MPs coupling with KF and BMJ schemes. The simulated WVMR is approximately equal for all MPs schemes. Vertical profiles of area averaged WVMR for all MPs coupling with KF and BMJ schemes are almost constant and WVMR is zero from 200-100 hPa level. The intensity of TC has changed continuously from CS to SCS and VSCS since 0300 UTC of 12 November to 1200 UTC of 12 November and 1600 UTC of 15 November and the WVMR has also increased significantly during this time. It is observed that the WVMR has increased in region D1 up to 1200 UTC of 15 November 2007 i.e. also before the landfall with respect to that of 0000 UTC of 14 November as the TC moves towards in that region. This indicates that the WVMR has increased in the region where the TC moves.

The vertical profiles of area averaged WVMR (gm/kg) at different times 1200 UTC of 11, 12, 13, 14,15 and 0000 UTC of 12, 13, 14, 15 and 16 November 2007 have been analyzed in region D4 by using six different MP schemes coupling with KF and BMJ schemes and are shown in Figure 4.3.12 (a-l). The WVMR is similar up to 200 hPa levels with all MP schemes coupling with KF and BMJ schemes. The simulated WVMR has maximum at the surface and decreases continuously with height for all MPs coupling with KF and BMJ schemes. The simulated WVMR is approximately equal for all MPs schemes. It has been observed from figure that the simulated WVMR is almost constant but after the time at 0000 UTC of 15 November by all MPs coupling with KF and BMJ schemes the WVMR has decreased significantly in region D4. The WVMR has increased sufficiently with time and the intensity

of TC has increased significantly for different MPs in combination with KF and BMJ schemes of TC Sidr. It indicates that WVMR increases with the increase in intensity of TC and over the area where the TC Sidr moves.

Figure 4.3.11: Simulated WVMR in region D1 with the progression of time using different MP schemes coupling with KF and BMJ schemes of TC 'Sidr'.

The values of WVMR are similar up to 200 hPa levels with all MPs coupling with KF and BMJ schemes in regions D3 and D5. The simulated WVMR has maximum at the surface (around 10 gm/kg) and decreases continuously with height for all MPs coupling with KF and BMJ schemes. In region D3, the WVMR has been simulated up to 700 hPa levels and is

approximately equal for all MPs schemes coupling with KF and BMJ schemes. But with respect to time variation, it has been observed that in region D2 the WVMR has small variation up to mid level but its magnitude is not significant (Figure not shown) by all MPs coupling with KF and BMJ schemes. Since in regions D3 and D5 almost there is no change or variation of WVMR, it indicates that the cyclone has not moved in those directions.
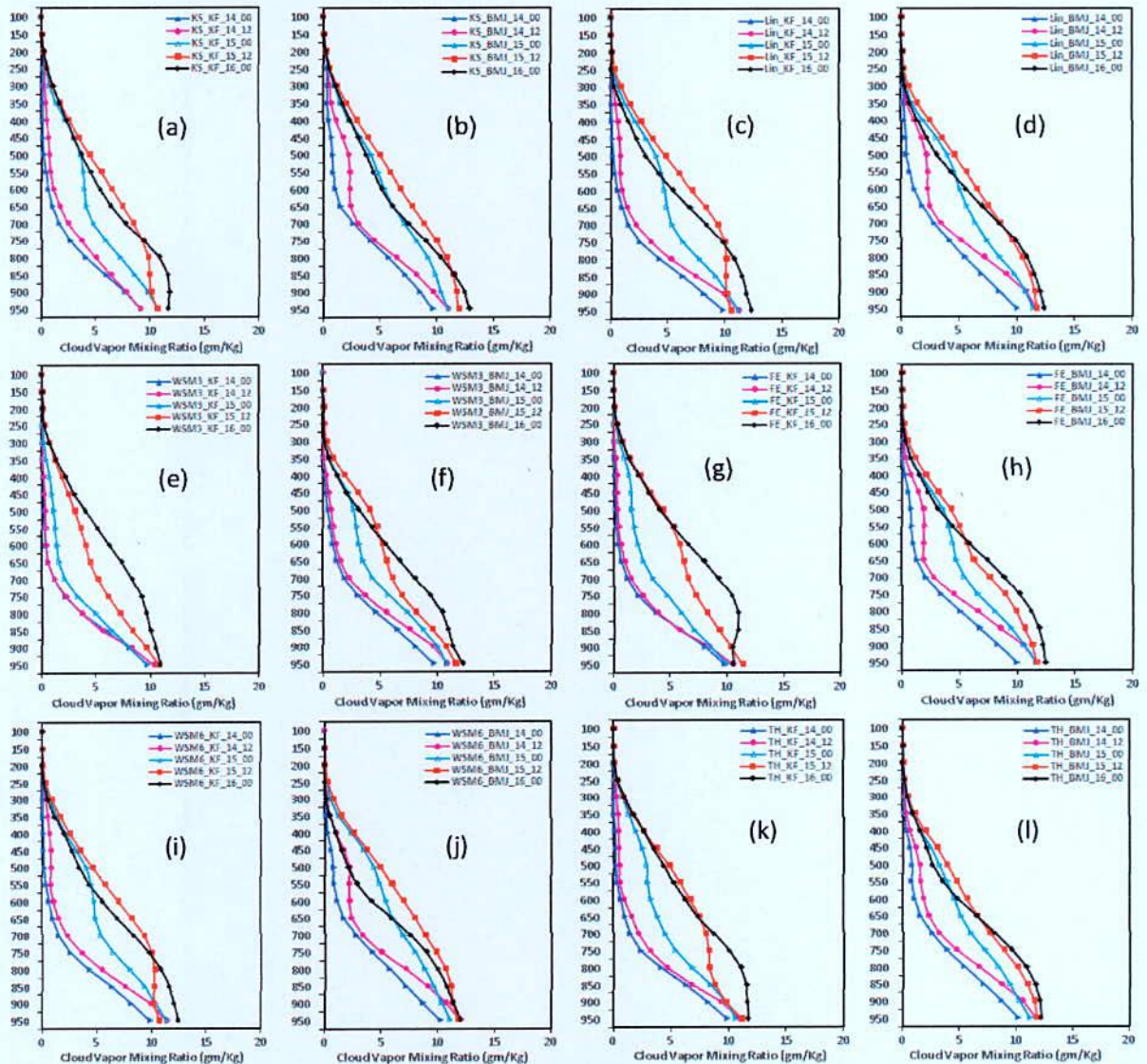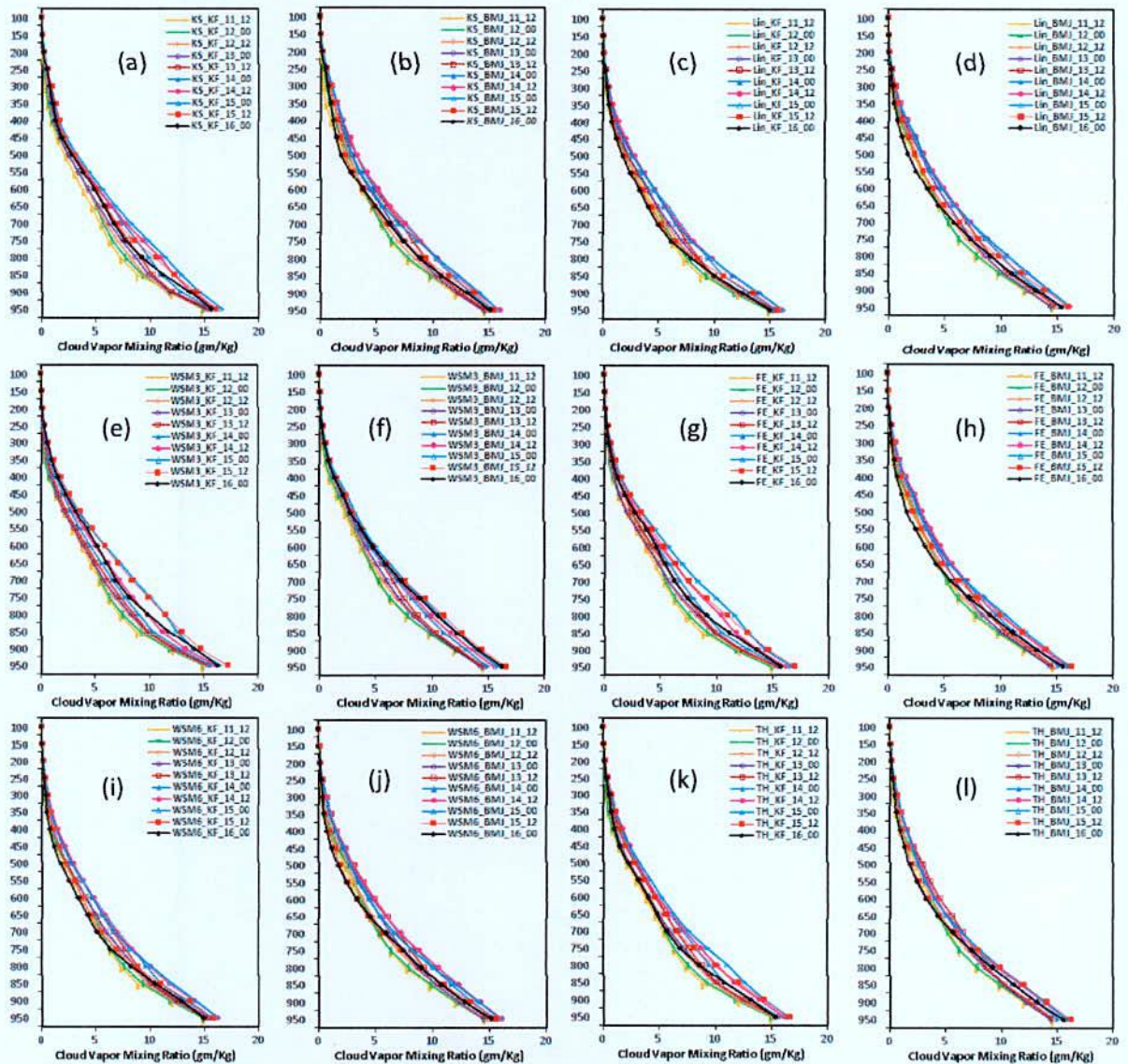

Figure 4.3.12: Simulated WVMR in region D4 with the progression of time using different MP schemes coupling with KF and BMJ schemes of TC 'Sidr'.

4.3.10 Relative Humidity

In region D1, the vertical profiles of area averaged RH (%) have been simulated at different times 0000 UTC of 14, 15, 16 and 1200 UTC of 14 and 15 November 2007 for six different MPs coupling with KF and BMJ schemes with 0000 UTC of 14 November 2007 initial conditions and are shown in Figure 4.3.13(a-l). The simulated RH exceeds 80% from surface to 400 hPa levels for all MPs coupling with CP schemes on 15 and 16 November 2007. The area averaged sharp peak of RH has been found before crossing the land of Bangladesh for all MPs coupling with CP schemes on 0000 and 1200 UTC of 15 November 2007. KS scheme coupling with KF and BMJ schemes has simulated more than 90% RH from 350 to 150 hPa level. From figure, it is observed that the simulated RH increased continuously in region D1 from 0000 UTC of 14 November to 1200 UTC of 15 November. The RH also has increased in region D1 (i.e. Bangladesh) after landfall of TC Sidr in the lower troposphere and it has decreased sharply in the upper troposphere. This suggests that the RH continuously has increased in region D1 and also TC Sidr crossed in this region.

In region D4, the vertical profiles of area averaged RH (%) have been presented at different times 1200 UTC of 11, 12, 13, 14, 15 and 0000 UTC of 12, 13, 14, 15 and 16 November 2007 for six different MPs coupling with KF and BMJ schemes with 0000 UTC of 11 November 2007 initial conditions in Figure 4.3.14 (a-l). The simulated RH ranges from 80% to 100% from surface to 100 hPa levels for Kessler scheme coupling with CP schemes. The simulated RH exceeds 80% at surface for all MPs coupling with CP schemes. The area averaged RH has decreased from surface to 350 hPa level and again increased and has maximum at 250 hPa level for all MPs coupling with CP schemes. From figure, it is observed that the simulated area averaged RH has decreased continuously in region D4 from 0000 UTC of 15 November 2007. The vertical structures of RH for all MPs coupling with CPs are almost the same except Kessler scheme.

The simulated RH is maximum (above 80%) at the upper level (100 hPa) of Kessler scheme coupling with KF and BMJ schemes in regions D2, D3 and D5 but the simulated RH is below 80% at surface to mid level for all MPs coupling with KF and BMJ schemes (Figure not shown). In regions D2 and D3 the RH has decreased with respect to height for six different

107

MPs coupling with KF and BMJ schemes. In region D5, the RH has decreased at surface to mid level for six different MPs coupling with KF and BMJ schemes. With the time progression, the TC moves towards the region D1 and the simulated RH is minimum in regions D2, D3 and D5. It indicates that the cyclone has not moved in those directions.

Figure 4.3.13: Simulated RH at region D1 with the progression of time using different MP schemes coupling with KF and BMJ schemes of TC 'Sidr'.

Figure 4.3.14: Simulated RH at region D4 with the progression of time using different MP schemes coupling with KF and BMJ schemes of TC 'Sidr'.

4.3.11 Vorticity

The vertical profiles of area averaged (starting from 0000 UTC of 14 November to 0000 UTC of 16 November 2007) vorticity in region D1 for six MPs coupling with KF and BMJ schemes are presented in Figure 4.3.15(a-l). The vorticity has been decreased from 0000 UTC of 14 November to 1200 UTC of 15 November and increased afterwards. The vorticity has decreased from 0000 UTC of 14 November to 0000 UTC of 16 November 2007 for WSM3 scheme coupling with KF and BMJ schemes and Ferrier-KF combination.
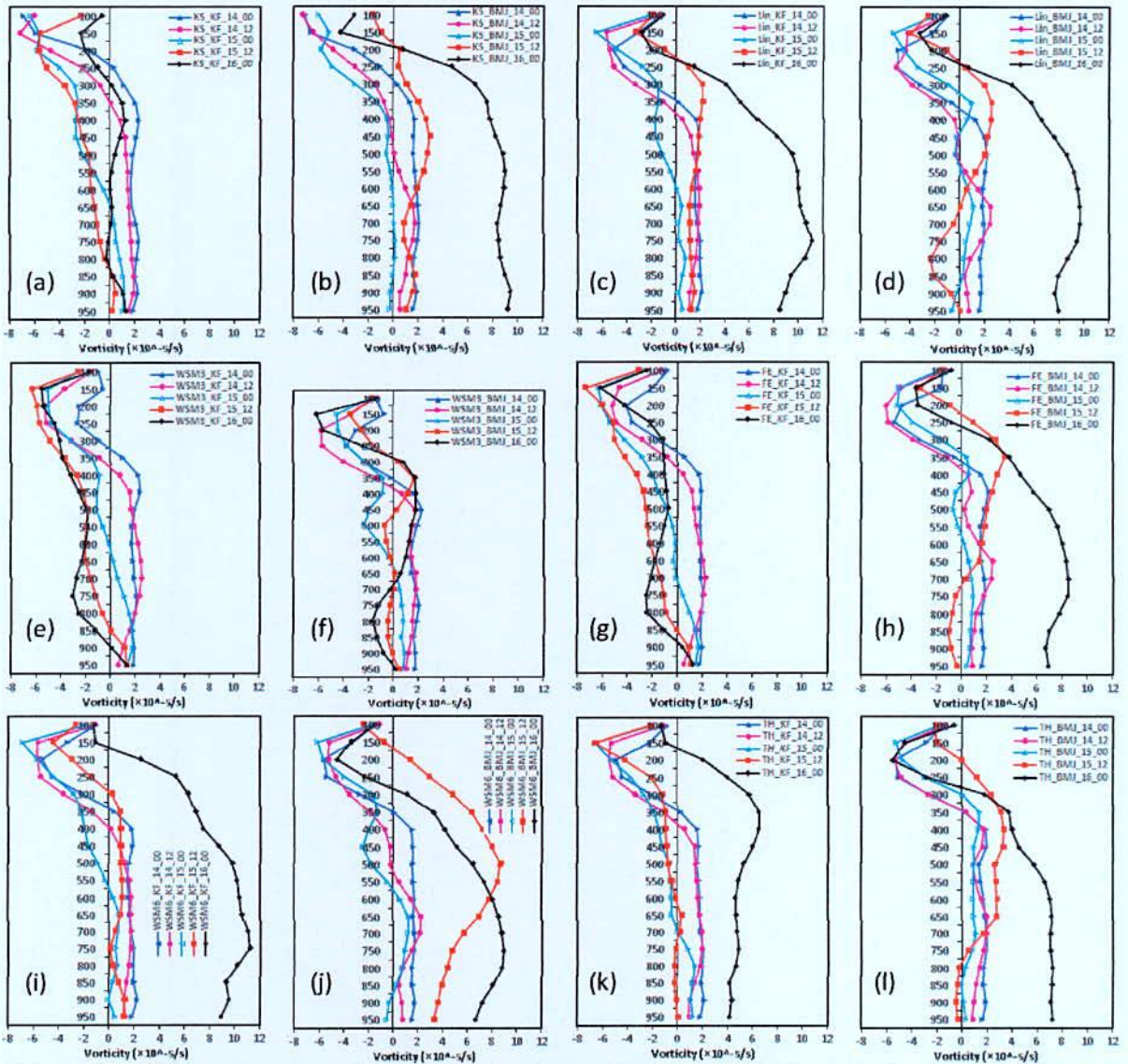
Figure 4.3.15: Simulated vorticity at region D1 with the progression of time using different MP schemes coupling with KF and BMJ schemes of TC 'Sidr'.

All through the simulation WSM6-KF & Kessler-BMJ has simulated maximum averaged vorticity and Ferrier-KF & WSM3-BMJ has simulated minimum averaged vorticity during the period. The characteristics of all the combinations are that the simulated vorticity shows negative at the upper level i.e. at around 300-100 hPa level, which indicates divergence observed at the upper level. The positive vorticity has been simulated from surface to 100 hPa levels at 0000 UTC of 15 November by all MPs (except WSM3-KF, WSM3-BMJ and FE-KF

combinations) coupling with KF and BMJ schemes that indicates the cyclonic circulation has changed with respect to the vorticity.
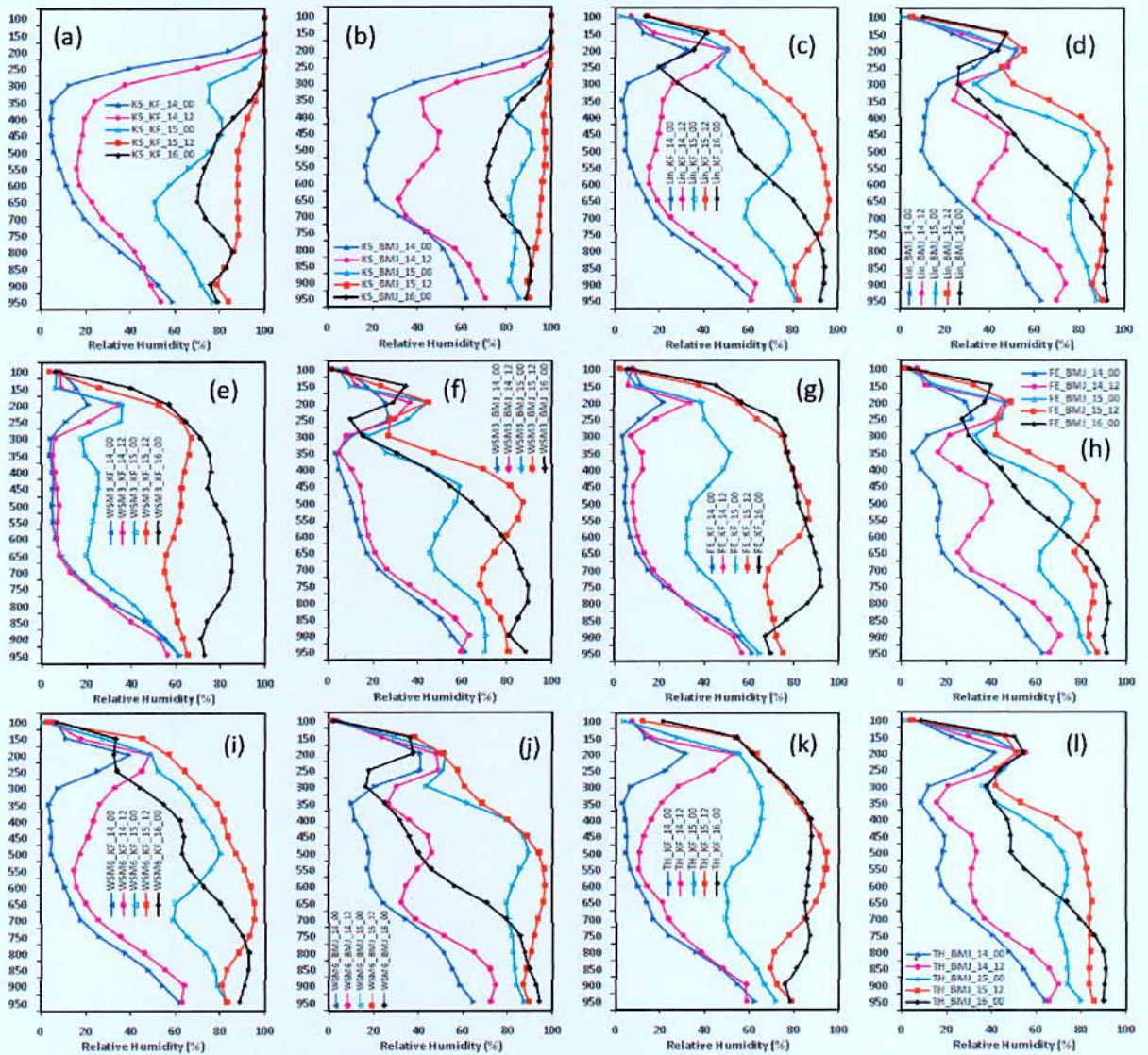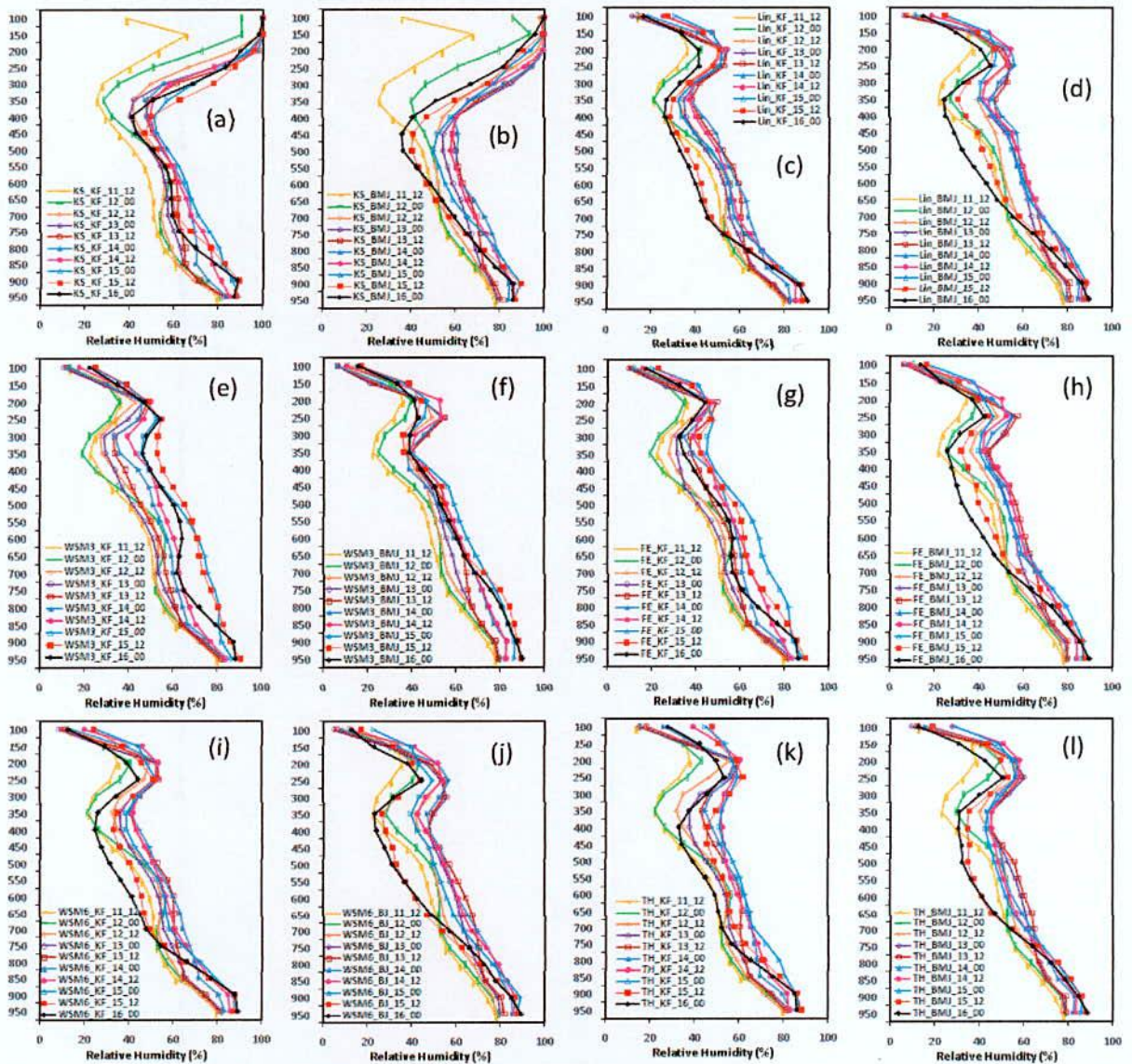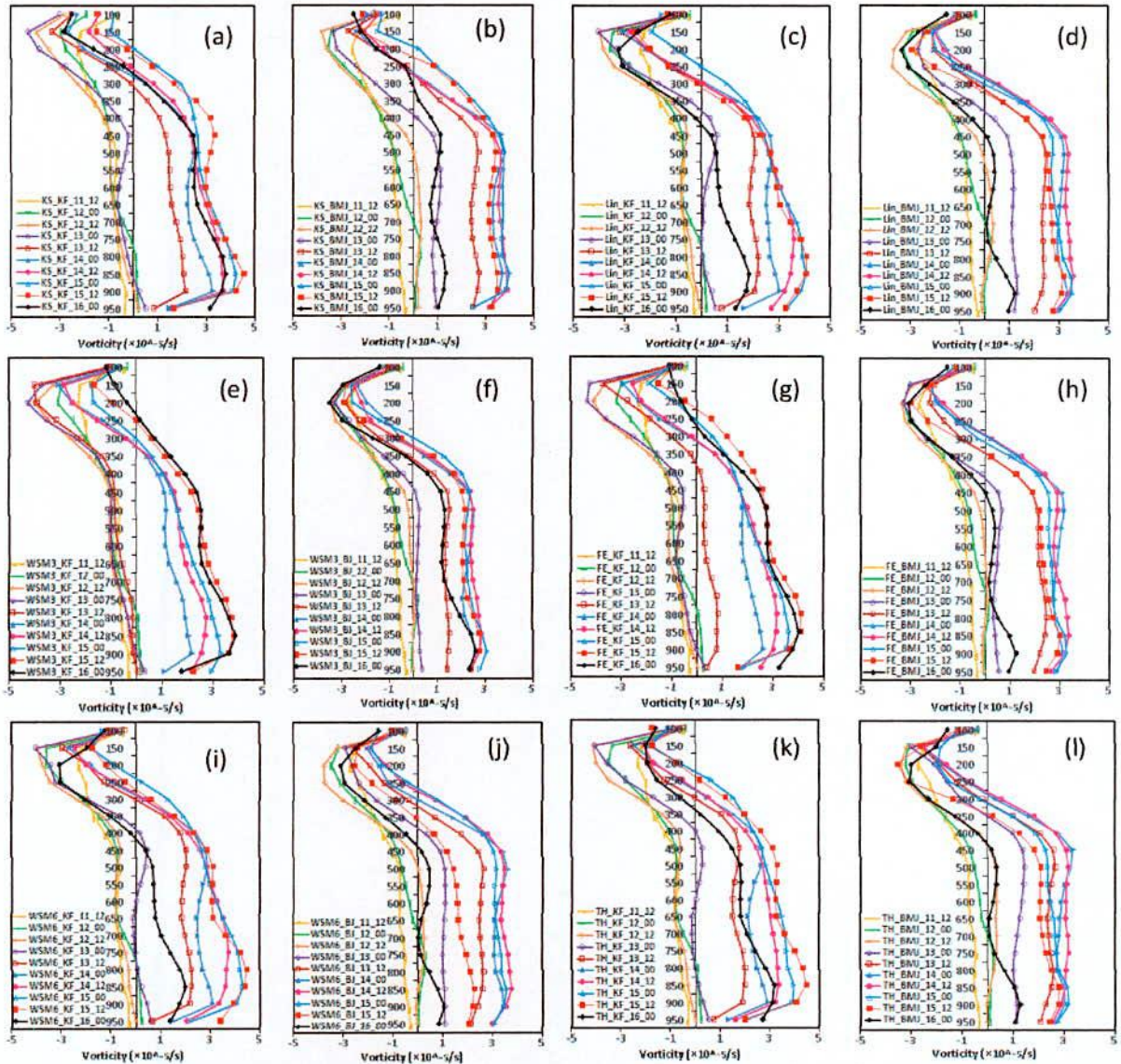

Figure 4.3.16: Simulated vorticity at region D4 with the progression of time using different MP schemes coupling with KF and BMJ schemes of TC 'Sidr'.

In region D4, time variation of vertical profiles of space averaged vorticity ($\times10^{-5}$/s) simulated by six different MPs coupling with KF and BMJ schemes are presented in Figure 4.3.16 (a-l). For KF combination, the vorticity increases continuously during 1200 UTC of 11 November to 1200 UTC of 15 November and then decreases significantly afterwards. For BMJ combination, the space averaged vorticity has increased continuously during 1200 UTC of 11

November to 1200 UTC of 14 November 2007 and after that the vorticity has decreased significantly. All through the simulation, WSM3-BMJ combination has simulated minimum averaged vorticity and Kessler-BMJ has simulated maximum averaged vorticity during the period. The vorticity has minimum and negative from mid to 100 hPa levels at 1200 UTC of 11 November to 1200 UTC of 12 November 2007 by all MPs coupling with KF and BMJ schemes. The positive vorticity has been simulated after 1200 UTC of 12 November to 0000 UTC of 16 November for all MPs (except WSM3-KF) coupling with KF and BMJ schemes. The simulated vorticity is negative from 300 to 100 hPa for all MPs coupling with KF and BMJ schemes. The intensity of TC has turned continuously from CS to VSCS since 0300 UTC of 12 November to 1600 UTC of 15 November 2007 and the vorticity has also increased significantly during this time by all MPs coupling with KF and BMJ schemes.

The vorticity has been simulated almost negative and simulated same pattern for all MPs coupling with KF and BMJ schemes in regions D3 and D5 but in region D2 the vorticity has been simulated more and it varies greatly (Figure not shown). All MPs coupling with KF and BMJ schemes have simulated single peak of vorticity at around 750 hPa in region D3. With the progress of time, the TC moves towards region D1 and the vorticity has almost decreased in lower level in regions D3 and D5. It indicates that the cyclone has not moved in those directions.

Chapter V

Summary and Conclusions

In this research WRF-ARW model has been used to simulate the tropical cyclone Mala (2006), Sidr (2007) and Phailin (2013), which formed in the Bay of Bengal and crossed the coast of Myanmar, Bangladesh and India. To examine the sensitivity of the simulations of six different microphysical schemes (Kessler, Lin, WSM3, Ferrier, WSM6 and Thompson) and two different cumulus parameterization schemes (Kain-Fritsch and Betts-Miller-Janjic) have been considered with two different initial conditions. The initial conditions have been considered 0000 UTC of 26 and 27 April 2006 for TC Mala, 0000 UTC of 8 and 9 October 2013 for TC Phailin and 0000 UTC of 11 and 12 November 2007 for TC Sidr. The different periods for different cyclones were characterized by the formation of tropical cyclones until dissipation. The model domain has been divided into different regions D1 (22-26°N and 87-93°E), D2 (18-22°N and 81-87°E), D3 (14-18°N and 78-84°E), D4 (12-22°N and 84-94°E) and D5 (17-22°N and 94-97°E). In this research, the MSLP, maximum wind at 10 m level, track of tropical cyclones, CWMR, CIMR, CGMR, CSMR, RWMR, CVMR, RH and Vorticity have been analyzed. Simulated track and intensity have also been compared with the IMD and JTWC observed results. The study has shown large variations of hydrometeors among the six microphysical schemes. For all three analyzed tropical cyclones, the IMD observed intensity has been much lower than that of JTWC intensity in terms of pressure fall and 10 m level sustained wind.

It has been found that the area averaged RH increased continuously since the formation up to one day before the landfall and starting to decrease from 24 hours before landfall in region D4 of TC Mala, Sidr and Phailin for all MPs coupling with CPs. The simulated area averaged RH has increased continuously before landfall in region D5 of TC Mala, D2 of TC Phailin and D1 of TC Sidr for all MPs coupling with CPs. The simulated area averaged RH has been found more than 90% from 850 to mid troposphere on 28 and 29 April 2006 for Mala, on 11 and 12 October 2013 for Phailin and on 14 and 15 November 2007 for Sidr. The area averaged RH has found minimum and decreased in a region where the cyclones was not moving, which suggest that the RH increased in a region where the tropical cyclone moves.

The production of area averaged RWMR between 950 and 500 hPa levels depends on MPs (except Kessler and WSM3 scheme) as well as CPs. The simulated area averaged RWMR has maximum value at the lower troposphere. The patterns of rain water profiles are similar up to 550 hPa level for all MPs coupling with CPs. It has been found that the area averaged RWMR has increased continuously since the formation of Depression up to one day before the landfall and starting to decrease from 12-18 hours before landfall in region D4 (i.e., oceanic region) of TC Mala, Sidr and Phailin for all MPs coupling with CPs. The simulated area averaged RWMR has increased continuously before landfall in region D5 of TC Mala, D2 of TC Phailin and D1 of TC Sidr for all MPs coupling with CPs. The area averaged RWMR has been found minimum and decreased in regions where the cyclones were not crossed. The simulated pattern of area averaged CWMR is similar to that of RWMR for all the cyclones. It has increased in a region where the TC has crossed and has decreased all other regions where the cyclones have not moved. The area averaged WVMR has almost constant for all cyclones in the Oceanic region and increased in a region where all the TC has crossed. In other regions, the area averaged WVMR has been found almost constant.

The CIMR, CGMR and CSMR have increased in region D4 for TC Mala, Sidr and Phailin. It also increased in region D1 for TC Sidr, D5 for TC Mala and D2 for TC Phailin. The CIMR has increased at daylight and decreased at nocturnal for TC Mala in region D5. The CIMR, CSMR and CGMR have not changed in other regions for all the cyclones. The CIMR, CSMR and CGMR have also increased significantly during the landfall time by Lin and WSM6 schemes coupling with CPs in region D2 (Phailin), D5 (Mala) and D1 (Sidr).

A significant positive vorticity has simulated at around 950–250 hPa levels and increased up to 12 hours before crossing the land over the region D4 for all MPs coupling with CPs for the TCs. Although the area averaged maximum positive vorticity in crossing region for the given TCs are found to be 2×10^{-4}/s (Mala) by Ferrier-KF, 1.9×10^{-4}/s (Phailin) by Kessler-KF and 1.1×10^{-4}/s (Sidr) by WSM6-KF at lower troposphere both at landfall time and minimum negative vorticity along the line simulated by Lin–KF are -10×10^{-5}/s (Mala at 0000 UTC of 29 April), by WSM3-KF were -7×10^{-5}/s (Phailin at 1200 UTC of 11 October) and Kessler-KF were -7×10^{-5}/s (Sidr at 1200 UTC of 14 November) only at upper troposphere. The

vorticity has been found to be negative in the upper troposphere for all cyclones in region D4 i.e. anticyclonic circulation exists at upper levels.

It has been found that for different microphysics in combination with BMJ scheme the cloud hydrometeors has decreased earlier than that of KF scheme for all the cyclones. The intensity of tropical cyclone could not intensify properly by using BMJ combinations as simulated by KF combination or as observed, so that the hydrometeors decrease earlier for these combinations. Area averaged vertical profiles of cloud hydrometeors i.e., cloud water, rain water, water vapor, snow, ice and graupel mixing ratio and RH and vorticity can be affected by the MPs and CPs. This suggests that the track and intensity of the studied TCs have impact on hydrometeors.

References:

Akhter M. A. E., 2010: Impact of chosen microphysics on tropical cyclone prediction: a case study, Journal of Engineering Science, 02, 75-81.

Alam M. M., 2013: Impact of cloud microphysics and cumulus parameterization on the simulation of Tropical Cyclone in the pre monsoon season over the North Indian Ocean, SMRC Report No. 48.

Anthes R.A., 1982: Tropical cyclones: their evolution, structure and effects. Meteorological monographs. Am Meterol Soc Boston 593, 19(41):208

Arpe K., Hollingsworth A., Tracton M. S., Lorenc A. C., Uppala S. and Kallberg P., 1985: The response of numerical weather prediction systems on the FGGE level IIb data. Part 2: Forecast verifications and implications for predictability. Quart. J. Roy. Meteor. Soc., 111, 67-101.

Bhaskar Rao D. V. and Hari Prasad D., and Srinivas D., 2009: Impact of horizontal resolution and the advantages of the nested domains approach in the prediction of tropical cyclone intensification and movement. J. Geophys. Res., 114, D11106, 1-24.

Bhaskar Rao D. V. and Hari Prasad D., 2007: Sensitivity of tropical cyclone intensication to boundary layer and convective processes. Nat. Hazards, 41, 429-445.

Bhaskar Rao D. V. and Hari Prasad D., 2006: Numerical prediction of the Orissa super cyclone (1999): Sensitivity to the parameterization of convection, boundary layer and explicit moisture processes. Mausam, 57, 61-78.

Cacciamani C., Cesari D., Grazzini F., Paccagnella T. and Pantone M., 2000: Numerical simulation of intense precipitation events south of the Alps: Sensitivity to initial conditions and horizontal resolution. Meteor. Atmos. Phys., 72,147-159.

Davis C. and Bosart L.F., 2002: Numerical Simulations of the Genesis of Hurricane Diana (1984). Part II: Sensitivity of Track and Intensity Prediction. Mon. Wea. Rev., 130, 1100–1124.

Deshpande M., Pattanaik S. and Salvekar P. S., 2010: Impact of physical parameterization schemes on numerical simulation of super cyclone Gonu. Nat. Hazards, 55, 211-231.

Deshpande M., Pattanaik S. and Salvekar P. S., 2012: Impact of cloud parameterization on the numerical simulation of a super cyclone. Ann. Geophys., 30, 775-795.

Dudhia J., 1989: Numerical study of convection observed during the winter monsoon experiment using a mesoscale two-dimensional models, J. Atmos. Sci., 46, 3077-3107.

Efstathiou G. A., Zoumakis N. M., Melas D. and Kassomenos P., 2012 : Impact of precipitating ice on the simulation of heavy rainfall event with advanced research WRF using two bulk microphysical schemes. Asia-Pac. J. Atmos. Sci., 48, 357-368.

Efstathiou G. A., Zoumakis N. M., Melas D. and Kassomenos P., 2013: Sensitivity of WRF to boundary layer parameterizations in simulating a heavy rainfall event using different microphysical schemes. Effect on large-scale processes. Atmos. Res., 132-133, 125-143, http://dx.doi.org/10.1016/j.atmosres. 2013.05.004.

Ferrier B. S., Tao W.K. and Simpson J., 1995: A double moment multiple phase four-class bulk ice scheme, Part II: Simulations of convective storms in different large-scale environments and comparisons with other bulk parameterizations. J. Atmos. Sci., 52, 1001-1033.

Fovell R. G. and Su H., 2007: Impact of cloud microphysics on hurricane track forecasts. Geophys. Res. Lett., 34, L24810.

Gray W. M. 2000: General characteristics of tropical cyclones. In: Pielke R Jr, Pielke R Sr (eds) Storms, vol. 1, Routledge, 11 New Fetter Lane, London EC4P4EE: 145-163

Grell, G. A. and D. Devenyi, 2002: A generalized approach to parameterizing convection combining ensemble and data assimilation techniques. Geophys. Res. Lett., 29, 14, Article 1693.

Hong S. Y., Dudhia J. and Chen S.H., 2004: A Revised Approach to Ice Microphysical Processes for the Bulk Parameterization of Clouds and Precipitation, Mon. Wea. Rev., 132, 103-120.

Hong S.Y., Noh Y. and Dudhia J., 2006: A new vertical diffusion package with an explicit treatment of entrainment processes. Mon. Wea. Rev., 134, 2318-2341.

India Meteorological Department, Cyclone Manual (IMD, Delhi), 2003.

Janjic Z. I., 2000: Comments on 'Developments and evaluation of a convection scheme for use in climate models'. J. Atmos. Sci., 57, 3686.

Janjic Z. I., 1994: The step-mountain eta coordinate model: Further developments of the convection, viscous sublayer, and turbulence closure schemes. Mon. Weather Rev., 122, 926-945.

117

Kanase R. D., Mukhopadhyay P. and Salvekar P. S. 2014: Understanding the role of cloud and convective process in simulating the weaker cyclones over Indian Seas. Pure Appl Geophys. doi:10.1007/s00024-014-0996-3

Kain J. S., 2004: The Kain-Fritsch convective parameterization: An update. J. Appl. Meteor., 43, 170-181.Lin, Y.-L., R.D. Farley, and H. D. Orville, 1983: Bulk parameterization of the snow field in a cloud model. J. Climate Appl. Meteor., 22, 1065-1092.

Kain J. S. and Fritsch J. M., 1993: Convective parameterization for mesoscale models: the Kain-Fritsch scheme. The representation of cumulus convection in numerical models, Meteo. Monogr, No. 46 Amer. Meteor. Soc., 165 – 170.

Kain J. S. and Fritsch J. M., 1990: A one-dimensional entraining/detraining plume model and its application in convective parameterization. J. Atmos. Sci., 47, 2684-2702.

Kessler E. 1969: On the distribution and continuity of water substance in atmospheric circulations. Meteor. Monogr., No. 32, Amer. Meteor. Soc., 84pp.

Kirk J. R., 2003: Comparing the dynamical development of two mesoscale convective vortices, Mon. Wea. Rev., 131, 862–890

Kuo Y. H. and Reed R. J., 1988: Numerical simulation of an explosively deepening cyclone in the eastern Pacific. Mon. Wea. Rev., 116, 2081-2105.

Li X. and Pu Z., 2008: Sensitivity of numerical simulation of early rapid intensification of Hurricane Emily (2005) to cloud microphysical and planetary boundary layer parameterizations. Mon. Wea. Rev., 136, 4819-4838.

Lin Y. L., Farley R. D. and Orville H. D., 1983: Bulk parameterization of the snow field in a cloud model. J. Climate Appl. Meteor., 22, 1065-1092.

Lord S. J., Willoughby H. E. and Piotrowicz J. M., 1984: Role of a parameterized ice-phase microphysics in an axisymmetric, non-hydrostatic tropical cyclone model. J. Atmos. Sci., 41, 2736-2748.

Lorenz E. N., 1963: Deterministic nonperiodic flow. J. Atmos. Sci., 20, 130-141.

McCumber M., Tao W.K. and Simpson J., Penc R., and Soong S.T., 1991: Comparison of ice-phase microphysical parameterization schemes using numerical simulations of tropical convection. J. Appl. Meteorol., 30, 985-1004.

Mellor G. L. and Yamada T., 1982: Development of a turbulence closure model for geophysical fluid problems. Rev. Geophys. Space Physics, 20, 851-875.

Mlawer E. J., Taubman S. J., Brown P.D., Lacono M. J. and Clough S. A., 1997: Radiative transfer for inhomogeneous atmosphere: RRTM, a validated correlated-k model for the longwave. J. Geophys. Res., 102(D14), 16663-16682.

Mohanty U. C., Osuri K. K., Routray A., Mohapatra M. and Pattanayak S., 2010: Simulation of bay of Bengal tropical cyclones with WRF model: Impact of initial and boundary conditions. Mar. Geod., 33, 294-314.

Mukhopadhyay P., Taraphdar S. and Goswami B. N., 2011: Influence of moist processes on track and intensity forecast of cyclones over the north Indian Ocean. J. Geophys. Res., D05116, doi:10.1029/2010- JD014700.

Osuri K. K., Mohanty U. C., Routray A., Kulkarni M. A. and Mohapatra M., 2012: Customization of WRF-ARW model with Physical parameterization schemes for the simulation of tropical cyclones over North Indian Ocean. Nat. Hazards, 63, 1337-1359.

Osuri K. K., Mohanty U. C., Routray A., Mohapatra M. and Nivogi D., 2013: A real-time track prediction of tropical cyclones over the North Indian Ocean using the ARW model. J. Appl. Meteor. Climatol., 52, 2476- 2492.

Pattnaik S. and Krishnamurti T. N., 2007: Impact of cloud microphysical processes on hurricane intensity, part 2: Sensitivity experiments. Meteorol Atmos Phys 97, 126-147.

Pattanayak S. and Mohanty U. C., 2008: A comparative study on performance of MM5 and WRF models in simulation of tropical cyclones over Indian seas. Curr. Sci. India, 95, 923-936.

Pattanaik D. R. and Rama Rao Y. V., 2009: Track prediction of very severe cyclone 'Nargis' using high resolution weather research forecasting (WRF) model. J. Earth Syst. Sci., 118, 4, 309-329.

Pielke R. A. and Coauthors, 2006: A new paradigm for parameterizations in numerical weather prediction and other atmospheric models. Natl. Wea. Digest, 30, 93-99.

Radhika D., Kanase and Salvekar P. S., 2015: Effect of Physical Parameterization Schemes on Track and Intensity of Cyclone LAILA Using WRF Model. Asia-Pac. J. Atmos. Sci., 51(3), 205-227, 2015.

Raju P. V. S., Potty J. and Mohanty U. C., 2011: Sensitivity of physical parameterizations on prediction of tropical cyclone Nargis over the Bay of Bengal using WRF model. Meteor. Atmos. Phys., 113,125-137.

Rao D. and Prasad D., 2007: Sensitivity of tropical cyclone intensification to boundary layer and convective process; Natural Hazards 41(3) 429-445.

Rosenfeld D., Khain A., Lynn B. and Woodley W.L., 2007: Simulation of hurricane response to suppression of warm rain by sub-micron aerosols. Atmos. Chem. Phys., 7, 3411-3424.

Sanders F., 1987: Skill of NMC operational models in prediction of explosive cyclogenesis. Wea. Forecasting, 2, 322-336.

Srinivas C., Venkatesan R., Bhaskar Rao D. and Hari Prasad D., 2007: Numerical simulation of Andhra severe cyclone (2003): Model sensitivity to the boundary layer and convection parameterization; Pure Appl. Geophys. 164(8-9) 1465-1487.

Srinivas C. V., Bhaskar Rao D. V., Yesubabu V., Baskarana R. and Venkatraman B., 2013: Tropical cyclone predictions over the Bay of Bengal using the high-resolution Advanced Research Weather Research and Forecasting (ARW) model. Quart. J. Roy. Meteor. Soc., 139, 1810-1825.

Srinivas D. and Bhaskar Rao D. V., 2014: Implications of vortex initialization and model spin-up in tropical cyclone prediction using Advanced Research Weather Research and Forecasting Model. Nat. Hazards, 73, 1043-1062.

Srinivas C. V., Venkatesan R., Yesubabu V. and Nagaraju C., 2010: Impact of assimilation of conventional and satellite meteorological observations on the numerical simulation of a Bay of Bengal tropical cyclone of Nov 2008 near Tamilnadu using WRF model. Meteor. Atmos. Phys., 110, 19-44.

Tao W. K. and Coauthors, 2003: Microphysics, radiation and surface processes in the Goddard Cumulus Ensemble (GEC) model. Meteor. Atmos. Phys., 82, 97-137.

Tao W. K., Simpson J., Lang S., McCumber M., Adler R. and Penc R., 1990: An algorithm to estimate the heating budget from vertical hydrometeor profiles. J. Appl. Meteor., 29, 1232-1244.

Tao W., Shi J., Chen S., Lang S., Lin P., Hong S., Lidard C.P. and Hou A., 2011: The impact of microphysical schemes on hurricane intensity and track. Asia-Pac. J. Atmos. Sci. 47, 1-16.

Trivedi D. K., Mukhopadhyay P. and Vaidya S. S., 2006: Impact of physical parameterization schemes on the numerical simulation of Orissa super cyclone (1999). Mausam, 57, 97-110.

Trivedi D. K., Sanjay J. and Singh S. S., 2002: Numerical simulation of a super cyclonic storm, Orissa 1999: Impact of initial conditions. Meteor. Appl., 9, 367-376.

Wang Y., 2001a: An Explicit Simulation of Tropical Cyclones with a Triply Nested Movable Mesh Primitive Equation Model: TCM3. Part 2: Model refinements and sensitivity to cloud microphysics parameterization. Mon. Wea. Rev., 130, 3022–3036.

Wang Y., 2001b: An Explicit Simulation of Tropical Cyclones with a Triply Nested Movable Mesh Primitive Equation Model - TCM3. Part 1: Model Description and Control Experiment. Mon. Wea. Rev., 129, 1370–1394.

Wang Y., 1999: A triply nested movable mesh tropical cyclone model – TCM3. BMRC Research Rep 74, 81.

White B., Paegle J., Steenburgh W. J., Horel J. D., Swanson R. T., Cook L.K., Onton D. J. and Miles J. G., 1999: Short-term forecast validation of six models. Wea. Forecasting, 14, 84-108.

Willoughby H. E., Jin H.L., Lord S. J. and Piotrowicz J. M., 1984: Hurricane structure and evolution as simulated by an axisymmetric non-hydrostatic model. J. Atmos. Sci., 41, 1169-1186.

Wu X., Hall W. D., Grabowski W. W., Moncrieff M. W., Collins W. D. and Kiehl J. T., 1999: Long-term behaviour of cloud systems in TOGA COARE and their interactions with radiative and surface processes. Part II: Effects of ice microphysics on cloud-radiation interaction. J. Atmos. Sci., 56, 3177-3195.

Yesubabu V., Srinivas C. V., Ramakrishna S. S. V. S. and Hariprasad K. B. R. R., 2014: Impact of period and timescale of FDDA analysis nudging on the numerical simulation of tropical cyclones in the Bay of Bengal. Nat. Hazards, 74, 2109-2128.

Zhu T. and Zhang D.L., 2006: Numerical Simulation of Hurricane Bonnie (1998). Part II: Sensitivity to Varying Cloud Microphysical Processes. J. Atmos. Sci., 63, 109–126.